Department of the Navy
Bureau of Ships
Contract Nonr-220(12)

EXPERIMENTAL INVESTIGATIONS OF THREE-DIMENSIONAL EFFECTS ON CAVITATING HYDROFOILS

by

R. W. Kermeen

This research was carried out under the Bureau of Ships
Fundamental Hydromechanics Research Program
Project SR-0090101, David Taylor Model Basin

Engineering Division
California Institute of Technology
Pasadena, California

Report No. 47-14
September, 1960

Approved:
M.S. Plesset

ABSTRACT

An investigation in the High Speed Water Tunnel of the hydrodynamic characteristics of a family of three-dimensional sharp-edged hydrofoils is described. Four rectangular planform, 6 degree wedge profiles with aspect ratios of 4.0, 2.0, 1.0 and 0.5 were tested over a range of cavitation numbers from noncavitating to fully cavitating flow. The effects of aspect ratio on the flow and cavity configurations and on the lift, drag and pitching moment are discussed. Where data were available the results have been compared with the two-dimensional case.

TABLE OF CONTENTS

LIST OF FIGURES

LIST OF FIGURES (cont'd)

LIST OF FIGURES (cont'd)

INTRODUCTION

The use of water tunnels as a valuable tool in the study of the hydrodynamics of hydrofoils has been established and a considerable body of data has been accumulated. To date hydrofoil testing in water tunnels has been almost entirely limited to two-dimensional profiles and the testing of finite aspect hydrofoils has been left to towing tanks. Many advantages accrue to water tunnel testing such as duration of test run, ease of observation, elimination of surface effects and surface-piercing struts, and easy and rapid control of cavitation number and other parameters. Testing of three-dimensional reflection plane mounted airfoils has long been a testing technique in low-speed wind tunnels and has been adopted to hydrofoil testing in the experiments described below.

The tests described in this report were designed to provide data on the effects of aspect ratio on the force and cavitation characteristics of rectangular plan-form hydrofoils. Thin, wedge profiles were chosen to obtain separation and cavitation from the leading edge. These profiles are of particular interest because considerable experimental and theoretical data exist on flat plate airfoils and hydrofoils including the results of tests in the High Speed Water Tunnel on two-dimensional wedge hydrofoils.

No attempt has been made to correlate the result with existing theory. This report consists primarily of a presentation of the measured data and a discussion of observations made during the experiments.

HYDROFOILS

Four wedge-shaped hydrofoils with aspect ratios of 0.5, 1.0, 2.0 and 4.0 were used in these experiments. The lower surfaces of the hydrofoils provide flat plate profiles in full cavity flow while the wedge shape gives the necessary strength to the models. The hydrofoils have 6 degree apex angles and rectangular plan form with sharp, unbroken edges. The hydrofoil models are shown in Fig. 1 and the principal dimensions are given in Table I. All surfaces of the models were ground smooth to final dimensions. Due to the small apex angle and the difficulty in obtaining a sharp, straight leading edge in the finishing operation, the final chord

lengths deviated somewhat from the specified dimensions, as noted in the table. The models were machined from 416 stainless steel and are made integral with a rectangular block for mounting on the force balance spindle. Each model has a single pressure tap, 1/6 inch diameter, located at the center in the upper surface. The pressure tap, used for measuring cavity pressure, is connected to 1/16-inch diameter brass tubing which passes through the hydrofoil mounting block.

APPARATUS AND TEST PROCEDURE

1. Apparatus

A reflection plane setup was installed in the 14-inch diameter test section of the High Speed Water Tunnel (Ref. 1). The reflection plane consisted of a vertical flat plate set one-half the distance from the tunnel wall to the test section axis. The plate, 12 inches high by 20 inches long, was faired to a simple circular arc nozzle casting and a 23-1/4 inch long, 3-1/2 degree diffuser section. The nozzle casting has a 25-7/16 inch radius circular arc profile hand-faired at the downstream juncture with the flat plate to eliminate the discontinuity in curvature. No fairing was used between the nozzle section and the circular test section wall. The flat diffuser section extended into the water tunnel diffuser and was terminated in an abrupt step. This type of section had proven successful in the two-dimensional water tunnel hydrofoil tests (Ref. 2), and it was felt that attempts to completely diffuse the flow without separation would be unsuccessful with such an unsymmetrical flow configuration. With this setup, separation occurred at a fixed and stable position. The reflection plate assembly is shown in Fig. 2. Figure 3 shows a view looking downstream of the plate setup in the tunnel test section. The test section window and the aspect ratio 2 hydrofoil can be seen in this figure. A description of the flow calibration tests and the results are given in Appendix A.

The hydrofoils were mounted on a 5.00-inch diameter disk attached to the balance spindle and set flush with the reflection plate. A small radial clearance gap was provided between the spindle disk and the flat plate. The hydrofoils were mounted with the midchord point of the lower wedge surface coincident with the spindle disk centerline. With this setup,

the hydrofoil was rotated about the midchord point to change attack angle and the pitching moment was measured about this axis. A 3-5/16 inch diameter by 4-inch long hollow cylindrical spindle supported the hydrofoil and mounting disk. The space around the spindle was sealed from the remainder of the space behind the reflection plane by a pressure shield so that the pressure around the spindle, mounting disk, and force balance seal was the same as in the test section. Though the hydrofoils were tested only at angles of attack up to 30 degrees, the spindle and model could be rotated through 360 degrees. The pressure tap on the hydrofoil upper surface was connected to a manometer outside the test section by means of 1/16-inch diameter Tygon tubing passing through a hole in the side of the hollow spindle, through the pressure shield and through the tunnel wall. A water trap was provided in this pressure line to permit purging of water from the tubing before making cavity pressure measurements.

With this arrangement, forces were measured on both the hydrofoil and the spindle disk. In order to determine these tare forces on the spindle disk, selected force tests were repeated with the hydrofoils mounted on a streamlined strut from the opposite side of the test section from the reflection plane. The strut was mounted on a contoured plate installed in the test section window frame. The angle of attack of the hydrofoil could be varied from outside the tunnel with this image setup. The hydrofoil was positioned so that the free tip was within approximately 0.002 inches of the spindle disk. In these tests the forces and moments were measured on the spindle disk alone and these data were applied as corrections to the forces and moments measured with the hydrofoil-disk combination. Details of the tare calibration tests and correction procedures are given in Ref. 2.

The three component force balance, force gages and data recording systems are described in Refs. 2 and 3.

2. Test Procedure

Force measurements were made on each hydrofoil in noncavitating flow for a range of attack angles to 30 degrees at a velocity of 30 fps. The force characteristics in cavitating flow were determined in tests in which the angle of attack and velocity were held constant and the cavitation number varied from noncavitating to full cavity flow. The tests were made at

hydrofoil angles of attack of 0 to 30 degrees. The runs were made at a tunnel velocity of 30 fps except for the aspect ratio 4.0 hydrofoil, which, due to its thin section was tested at 25 and 20 fps at high attack angles. Variations of coefficients with Reynolds number were investigated with the aspect ratio 2.0 hydrofoil at an angle of attack of 8 degrees at velocities of 20 to 50 fps giving Reynolds numbers of 5.0×10^5 to 1.25×10^6.

In the cavitation tests the cavitation number was varied by changing test section pressure while holding the velocity constant. At each test point, the lift, drag and pitching moment gage readings were photographically recorded and the velocity and test section pressure were read on manometers. Photographs were taken of the cavitating hydrofoil by means of a camera mounted above the test section. Two photographs were taken at each cavitation number tested. At small cavitation numbers, for which the cavity on the hydrofoil upper surface extended beyond the pressure tap, measurements were also made of cavity pressure.

3. Data Reduction

The force and cavitation data were reduced to dimensionless coefficients as follows:

$$\text{Lift coefficient, } C_L = \frac{\text{Lift}}{\rho/2\, V^2 S},$$

$$\text{Drag coefficient, } C_D = \frac{\text{Drag}}{\rho/2\, V^2 S},$$

$$\text{Moment Coefficient, (about leading edge) } C_M = \frac{\text{Moment}}{\rho/2\, V^2 Sc},$$

$$\text{Cavitation number, } \sigma_v = \frac{P_o - P_v}{\rho/2\, V^2},$$

$$\text{Cavitation number, } \sigma_k = \frac{P_o - P_c}{\rho/2\, V^2},$$

$$\text{Reynolds number, } R_e = \frac{Vc}{\nu},$$

$$\text{Aspect Ratio, } AR = \frac{2b}{c} = \frac{2S}{c^2},$$

where

V = velocity of undisturbed flow, ft/sec,
ρ = density of water at the temperature of the run, slugs/ft^3,
S = hydrofoil plan area, ft^2,
c = hydrofoil chord, ft,
b = hydrofoil half-span, ft,
P_o = pressure of undisturbed flow, lb/ft^2,
P_v = vapor pressure of fresh water at the temperature of the run, lb/ft^2,
P_c = measured cavity pressure, lb/ft^2,
ν = kinematic viscosity of fresh water at the temperature of the run, ft^2/sec.

The angle of attack, α, is defined as the angle between the free stream direction and the lower, flat plate surface of the hydrofoils (Fig. 4). The attack angle for the wedge profile is obtained by adding the wedge half angle, 3 degrees, to the flat plate angle of attack.

A sample of ten force data points were photographically recorded on 35 mm film at each test point. The data were read from the film, averaged and punched on tape, and coefficients were calculated by a Burroughs 205 digital computer. Corrections for balance pressure sensitivity, temperature drift, and transfer of moments from the spindle axis to the hydrofoil leading edge were programmed on the computer. Corrections for the forces on the spindle disk were applied to the reduced coefficients. Force and moment coefficients and cavitation numbers are tabulated in Appendix B.

RESULTS

The principal variables in this experiment were aspect ratio, angle of attack and cavitation number. The measured and derived parameters were lift, drag and moment coefficients, lift-drag ratio and cavity dimensions. Because of the large number and range of parameters varied and measured in the tests this report consists primarily of a presentation of the data in a readily usable form. No attempt has been made to show variations of all coefficients and cavity measurements with all the variables.

The lift, drag and moment coefficients for the four hydrofoils in noncavitating flow are given in Figs. 5 and 7. Curves of lift, drag and

moment coefficient and lift/drag ratio as a function of cavitation number at constant angle of attack are shown in Figs. 8 through 23 for each aspect ratio. The data points shown in these curves are for cavitation numbers based both on vapor pressure and measured cavity pressure whenever such measurements were possible. In Figs. 24 through 30 lift, drag and moment coefficients and lift-drag ratios are shown as functions of angle of attack for the range of cavitation numbers tested for each aspect ratio hydrofoil. Polar diagrams with cavitation number as a variable are also included for each hydrofoil.

Curves of cavity length as a function of cavitation number for various angles of attack are shown in Figs. 31 and 32 for each model. The effect of aspect ratio on cavity length at constant cavitation number is shown in Figs. 33 and 34 for angles of attack of 8, 10, and 15 degrees. For cavity lengths of 1 and 2 chords the change in cavitation number with aspect ratio at constant attack angles are shown in Fig. 35.

The effect of the three-dimensional flow at the free end of the hydrofoils is to shorten the length of the cavity on the upper surface of the hydrofoils compared with the infinite aspect ratio hydrofoil at the same cavitation number. Thus, a much lower cavitation number was required to obtain the same relative cavity length for the small aspect ratio hydrofoils than for a two-dimensional profile. Because of this, the force and moment coefficients for the four hydrofoils are compared for the same relative extent of cavitation rather than at constant cavitation number. In order to include, where possible, data measured on a two-dimensional hydrofoil for comparison, (Ref. 4), the results have been plotted as a function of the reciprocal of the aspect ratio.

The effect of aspect ratio on the lift, drag and moment coefficients at constant angles of attack are shown in Figs. 40, 43 and 46 for non-cavitating flow and in Figs. 41, 42, 44, 45, 47 and 48 for cavity lengths of one and two times the hydrofoil chord.

Photographs of the cavitating hydrofoils are included together with descriptions of the observed cavity configuration and the effect of the three-dimensional tip flows.

Though some comparisons are made with two- and three-dimensional experimental results in noncavitating flow and with two-dimensional data in cavitating flow, no attempt has been made to compare the results with existing theory. In order to increase the usefulness of this report as a data source, all measured cavitation number and force coefficient data are tabulated in Appendix B.

DISCUSSION OF RESULTS

1. Noncavitating Flow

The lift, drag and moment coefficients for the four wedge-shaped hydrofoils are shown in Figs. 5 and 7 as functions of angle of attack. The zero lift and moment points and minimum drag occur at an angle of attack of 3 degrees instead of zero degrees since the angle was measured from the lower surface of the wedge profile. The characteristic increase in lift slope and linearity with aspect ratio and the shift in maximum lift toward lower angles of attack as aspect ratio is increased can be seen in Fig. 5. All data were taken at a water velocity of 30 fps except for the aspect ratio 4.0 hydrofoil for which the velocity was reduced to 25 and 20 fps for angles of attack of 15 degrees or greater in order to avoid bending of the narrow hydrofoil. The chords of the models varied from 1.5 to 4.4 inches and, therefore, the Reynolds number based on model chord varies from 3.75×10^5 for the aspect ratio 4.0 hydrofoil to 1.12×10^6 for the 0.5 aspect ratio model at a constant velocity of 30 fps.

The aspect ratio 2.0 hydrofoil was tested at Reynolds numbers from 5.0×10^5 to 1.25×10^6 at an angle of attack of 8 degrees. Although there were small differences in the data for noncavitating flow, no significant Reynolds number effects on the coefficients were noted in fully cavitating flow over the limited range of velocities tested.

Figure 6 shows a comparison of the lift coefficient with the results obtained in other experiments for noncavitating flow. The angle of attack for the wedge profiles in Fig. 6 is measured from the midplane of the profile. The curve for the two-dimensional, or infinite aspect ratio, case is from measurements made in the two-dimensional test section of the

High Speed Water Tunnel on a 10-degree wedge section as reported by Parkin (Ref. 4). Data measured at the Langley Towing Basin on flat plate hydrofoils of aspect ratio 1.0 and 0.25 are also included for comparison. These data (Refs. 5 and 6) were measured on flat plate hydrofoils at a submergence of approximately one chord for the aspect ratio 1.0 hydrofoil and one-half chord for the 0.25 aspect ratio hydrofoil.

The data taken in the fully wetted tests are shown in Table I, Appendix B. Here the lift, drag, and moment coefficients and angle of attack are tabulated. Film numbers serve only to identify data groups. Water velocity in all the tests was 30 fps except as shown in the table.

2. Cavitating Flow

The data for cavitating flow were obtained at constant velocity and angle of attack and the test section pressure varied to control cavitation number from fully wetted to full cavity flow. Lift, drag and moment coefficients and lift-drag ratio are plotted in Figs. 8 through 23 and the data are tabulated in Table II, Appendix B. The data are tabulated according to angle of attack for each hydrofoil. The film numbers identify the photographs taken of the cavitating hydrofoil during each data group. The cavitation number based on vapor pressure, defined above, is given for all hydrofoils. For the hydrofoils of aspect ratio 4.0 and 0.5 the cavitation numbers based on measured cavity pressure are given whenever such measurements were obtained. Due to failure of the pressure measuring apparatus, no reliable data on cavity pressures were obtained for the aspect ratio 1.0 and 2.0 hydrofoils. The cavitation numbers based on measured cavity pressure are included in the figures for the aspect ratio 4.0 and 0.5 hydrofoils. These data have been blocked in, whereas the open symbols indicate cavitation numbers based on vapor pressure. The curves were faired through the vapor cavitation number points and this cavitation number has been used in all the curves throughout the report. Cavity pressures could only be obtained when the cavity from the leading edge extended beyond the midchord location of the pressure tap. As seen in the figures and tables, the cavitation number based on measured cavity pressure is always less than that based on vapor pressure. This difference amounts to as much as 0.098 at a σ of approximately 0.6. The difference between σ_v

and σ_k decreases as cavitation number is decreased and becomes approximately 0.02 for cavitation numbers of 0.1 and less. Differences between σ_v and σ_k are discussed more fully in Refs. 2, 4, and 7.

The flat portion at the right in Figs. 8 through 23 is for noncavitating flow or for small amounts of cavitation. The points of incipient cavitation number are connected by dashed curves where possible as are those for cavity lengths of 0.5, 1.0 and 2.0 chords. In Figs. 8 through 23 only the data taken for $\sigma_v \leq 1.5$ are plotted in order to show more clearly the changes due to cavitation number. For the higher angles of attack, therefore, the points of incipient cavitation lie to the right of the figures and cavitation was present over the entire range of σ_v shown. There was negligible change in the coefficients with small amounts of cavitation and the values for $\sigma_v > 1.5$ are included in the tables in the appendix. For small amounts of cavitation there is little change in the lift and drag coefficients. Except for small angles of attack the lift coefficient increases somewhat with increased cavitation until the cavity extends to the trailing edge of the hydrofoil, ($x/c = 1$), (where x is the length of the cavity on the upper surface of the hydrofoil, measured from the profile leading edge) and then decreases sharply and almost linearly. For the aspect ratio 0.5 hydrofoil the increase in lift coefficient between incipient cavitation and $x/c = 1$ is very slight but increases as the aspect ratio is increased. The increase in lift between incipient cavitation and $x/c = 1$ is even more marked on the two-dimensional wedge hydrofoils (Ref. 4).

Similar effects can be noted for the drag coefficient, although to a much lesser degree. Here there is a slight increase in drag between incipient cavitation number and $x/c = 1$, and then a linear decrease in drag as cavitation number is further reduced. The wedge-shaped hydrofoils were not designed for efficient operation in noncavitating flow, and as a result the blunt trailing edges give high drag coefficients and low lift coefficients in fully wetted flow. Consequently, the onset of cavitation provides a more beneficial effect on the lift of these profiles than it would for sharp-edged profiles of clean aerodynamic shape. The drag coefficient on low-drag, sharp-edged profiles would be expected to be more strongly affected by the development of cavitation than the blunt, wedge-shaped profiles of this experiment. As with lift coefficient, the drag coefficient

is less affected by changes in cavitation number at angles of attack of ten degrees or less, particularly for the small aspect ratio hydrofoils.

The effect of cavitation number on the combination of lift and drag are seen in Figs. 11, 15, 19 and 23 which show lift-drag ratio as a function of cavitation number. At angles of attack less than 15 degrees, the onset of cavitation causes an increase in lift-drag ratio to a maximum at $x/c = 1$. The maximum lift-drag ratio shifts toward lower cavitation numbers as the angle of attack is decreased. This effect becomes more marked at smaller aspect ratios. At angles of attack greater than 15 degrees, there is no change in lift-drag ratio from fully wetted to fully cavitating flow. Although the lift-drag ratio does not change with cavitation number at high angles of attack, cavitation does strongly affect the hydrofoil performance. At high angles of attack where the hydrofoils act like stalled airfoils with severe vibration and buffeting in noncavitating flow, the buffeting is apt to increase as cavitation number is decreased until full cavity flow where $x/c > 1$. At this point and for smaller cavitation number, the forces on the hydrofoils are steady. The nature of the water tunnel force balance precludes measurement of these fluctuating forces.

Moment coefficients about the hydrofoil leading edges are shown as functions of cavitation number in Figs. 10, 14, 18, and 22. A positive pitching moment is defined as one tending to increase angle of attack. Between incipient cavitation and $x/c = 1$, the pitching moment becomes more negative and reaches a minimum when $x/c = 1$. Further decrease in cavitation number causes the moment coefficient to increase toward zero. The curves through the moment coefficient data look very much like the reflection of the lift coefficient curves about the horizontal axis. This is to be expected since the origin of the moments is taken at the leading edge of the hydrofoils in these experiments.

The curves faired through the data of Figs. 8 through 23 were used as a basis for crossplots of the coefficients as functions of angle of attack with cavitation number as a parameter which defines the individual members of the various families of curves. In Figs. 24 through 30 the points shown on the curves have been taken from the curves of Figs. 8 through 23 which were faired through the experimental data. They are not experimental points and are included in the crossplots only to facilitate their use.

In these figures each symbol denotes a different cavitation number.

Lift coefficient as a function of angle of attack for constant cavitation number is shown in Figs. 24 and 25 for each hydrofoil. For the larger aspect ratio hydrofoils the lift coefficient reaches a maximum when $x/c = 1$. This is even more marked on the two-dimensional hydrofoils (Ref. 4). In each case the maximum, or knee, in the curve appears when $x/c = 1$. When the cavity extends beyond the trailing edge of the hydrofoil ($x/c \geq 1$), the lift slope is greatly reduced. For $x/c > 1$ the lift coefficient becomes linear with angle of attack as aspect ratio is reduced, and the slope of the lift coefficient versus angle of attack decreases slightly as aspect ratio is decreased.

Drag coefficient curves are shown in Fig. 26. The families of curves of drag coefficient are very similar for the four hydrofoils, although there is less change in drag coefficient with cavitation number for the low aspect ratio profiles for angles of attack less than 20 degrees. Cavitation polar diagrams for the hydrofoils are shown in Figs. 27 and 28. In these figures, angle of attack is shown by dashed curves where possible. The lift-drag ratio as a function of angle of attack at constant cavitation number is given in Fig. 29. The peak in each curve occurs at $x/c = 1$. For high angles of attack and low σ_v the lift-drag ratio data for the aspect ratio 4.0 hydrofoils is a good representation of the cotangent rule. For the smaller aspect ratio hydrofoils the lift-drag ratio follows the cotangent rule for angles of attack greater than 15 degrees where there is little difference with cavitation number. The moment coefficient curves of Fig. 30 resemble reflections of the lift coefficient curves about the horizontal plane as was noted in the curves through the experimental points. As with all the data the knee in the moment coefficient curves occurs when $x/c = 1$. When the cavity extends beyond the trailing edge of the hydrofoil, the moment coefficient is linear with angle of attack with the slope decreasing as aspect ratio is decreased.

Figures 31 and 32 show the dimensionless cavity length as a function of cavitation number at constant angle of attack for the four hydrofoils. Curves have been faired through the measured cavity length data and, in general, consistent families of curves resulted. There are, however, a number of cases wherein the curves cross, particularly at low cavitation

numbers. Overlapping and crossing of the curves at small cavitation numbers is due to the extreme sensitivity of the cavity length to cavitation number at low σ and the fact that the photographs of the cavity were taken during the tests at one or two random points rather than by obtaining an average cavity length over the period required to make the force measurements. The crossings of the curves at higher cavitation numbers are due, in part, to the tip flow effects which cause the outboard end of the cavity to angle sharply toward the hydrofoil root making an accurate determination of the cavity length very difficult. In Figs. 31 and 32 only those cavities originating along the leading edge of the hydrofoil were considered and no measurements were made of tip vortex cavities. It can be seen in the figures that for constant angle of attack and cavitation number the cavity length decreases as aspect ratio is decreased.

The effect of aspect ratio on cavity geometry can be seen more clearly in Figs. 33 and 34 where cavity length is shown as a function of aspect ratio at constant cavitation numbers for angles of attack of 8, 10 and 15 degrees. These figures show that aspect ratio has little effect on cavity length for high cavitation numbers and in fact no consistent differences were noted in incipient cavitation numbers for the four hydrofoils. For smaller cavitation numbers aspect ratio has a very marked effect on cavity length.. For example, at an angle of attack of 15 degrees and $\sigma_v = 0.4$, the dimensionless cavity length is six times larger for the aspect ratio 4.0 hydrofoil than for the 0.5 aspect ratio profile. The cavity length data of Figs. 31 and 32 are plotted as cavitation number versus the reciprocal of the aspect ratio for constant cavity lengths of one and two chords in Figs. 35a and 35b respectively. The data are shown as a function of $1/AR$ in order to include the results on two-dimensional hydrofoils as measured by Parkin (Ref. 4). Parkin did not report cavity dimensions, however, and the cavitation numbers corresponding to the maximums in the lift curves were assumed to correspond to $x/c = 1$. The apparent anomalies in the curves of Fig. 35a for angles of attack of 20 degrees and greater for aspect ratios of 2.0 and 4.0 are due to the fact that at high angles of attack with $x/c \leq 1$ the flow separates and the cavity is not permanently attached to the leading edge of the model. The rapidly fluctuating cavitation makes measurements of cavity length difficult. In Fig. 35a the $1/AR = 0$, or two-dimensional

data, are consistent with that measured on the finite aspect ratio hydrofoils. Since no cavity length measurements were reported on the two-dimensional hydrofoils, no infinite aspect ratio data could be included in the $x/c = 2$ curves of Fig. 35b.

The formation of the tip vortex cavitation was independent of aspect ratio in the tests. In general, for angles of attack of 8 degrees and less, the tip cavity initially attached itself to the trailing edge of the hydrofoil whereas for higher angles of attack the tip vortex cavities originated at the leading edge of the models. Observations and photographs of the cavitating hydrofoils show that for all angles of attack and for cavitation numbers which resulted in steady state cavities attached to the leading edge of the hydrofoil, the tip cavities were conical in shape and remained separate from the main cavity. The effect of end flow on the cavity originating at the hydrofoil leading edge as well as the effect of aspect ratio on cavity length can be seen in Fig. 36. For the smaller aspect ratio hydrofoils in Fig. 36, the cavity on the upper side of the profile can be seen to angle sharply toward the root of the model leaving a triangular, wetted surface near the free end. In these photographs, taken at an angle of attack of 8 degrees and a cavitation number of approximately 0.15, three separate cavities can be seen to exist on all four hydrofoils. One cavity originates along the leading edge of the hydrofoil and extends over the upper surface of the profile. A separate tip cavity is formed on the free end of the hydrofoil and the third cavity originates at the blunt trailing edge. Figure 37 shows top and side photographs of the four hydrofoils at an angle of attack of 15 degrees and a cavitation number of approximately 0.25. In this figure, with more extensive cavitation, the separate conical tip cavity can be readily seen. It can be noted that the relative area of the profiles affected by this tip flow is much greater for the smaller aspect ratio hydrofoils. Figures 38 and 39 show the aspect ratio 1.0 and 2.0 profiles respectively at an angle of attack of 30 degrees for a range of cavitation numbers. For angles of attack of 20 degrees and greater, where strong flow separation occurs and cavitation begins in the separated wake, a separate tip cavity is not established until the cavitation number is reduced to the point where a clear steady-state cavity attaches itself to the leading heads of the hydrofoil. Then, as at smaller angles of attack, the conical tip cavity remains

separated from the main cavity by a film of water.

The effect of aspect ratio on lift, drag and moment coefficients is shown in Figs. 40 through 48. The coefficients are shown for three conditions, fully wetted flow, ($x/c = 0$), $x/c = 1.0$ and $x/c = 2.0$. The curves have been plotted as functions of $1/AR$ in order to include data on two-dimensional hydrofoils (Ref. 4). Each figure consists of a family of curves of constant angle of attack. Curves of constant cavitation number are shown where possible for the cavitating cases. Since cavity length is a sensitive function of aspect ratio at constant cavitation number, the results are shown for the same relative flow and cavity conditions resulting in a more consistent family of curves.

The apparent inconsistency of lower lift at infinite aspect ratio for small angles of attack in Fig. 40 may be due to the configurations of the models. The model for the infinite aspect ratio data had a 10 degree total wedge angle, whereas the models for the finite aspect ratio data had a 6 degree total wedge angle.

The familar effects of aspect ratio on the hydrodynamic coefficients in fully wetted flow ($x/c = 0$) is also noted in fully cavitating flow. Except for small increases in the lift and drag coefficients and decreases in moment coefficients, the curves for $x/c = 1$ are nearly identical to those for fully wetted flow. As noted above, the lift and drag coefficients decrease rapidly as cavitation number is reduced and the cavity extends beyond the trailing edge of the hydrofoil. The sharp reduction in lift and drag coefficient and increase in moment coefficient can be seen in Figs. 42, 45 and 48 for $x/c = 2.0$. Here the effect of aspect ratio is still similar to that for fully wetted flow; however, the slopes of the curves are greatly reduced and the coefficients are much less sensitive to aspect ratio.

CONCLUSIONS

Some general conclusions can be drawn from the results of these tests:

1. The High Speed Water Tunnel provides a valuable means of studying the hydrodynamic characteristics of three-dimensional hydrofoils.

2. The effects of cavitation on the force and moment coefficients

for the low aspect ratio hydrofoils of these tests were essentially the same as on two-dimensional profiles.

3. Because of tip flow effects, aspect ratio has a strong effect on cavity length for equal cavitation numbers.

4. The effect of aspect ratio on the force and moment coefficients in full cavity flow were very similar to that for noncavitating flow. At very low cavitation numbers, the forces and moments were less sensitive to aspect ratio.

5. For angles of attack less than 20 degrees the tip vortex cavity always remained separate from the cavity on the upper surface of the hydrofoil which originates along the leading edge. For angles of attack of 20 degrees and greater the tip cavity was separate at low cavitation numbers where steady-state cavities were established. In full cavity flow the tip cavity always assumed a distinct conical shape.

ACKNOWLEDGEMENT

The author wishes to thank Mrs. Z.L. Harrison for setting up and carrying out the data reduction and for preparation of the figures for this report.

REFERENCES

1. Knapp, R.T., Levy, J., O'Neill, J.P., Brown, F.B., "The Hydrodynamics Laboratory of the California Institute of Technology," Trans. ASME, Vol. 70, No. 5, pp. 437-457, July 1948.

2. Kermeen, R.W., "Water Tunnel Tests of the NACA-4412 and Walchner Profile 7 Hydrofoils in Noncavitating and Cavitating Flows," California Institute of Technology, Hydrodynamics Laboratory, Report No. 47-5, January 1956.

3. Hotz, G.M. and McGraw, J.F., "The High Speed Water Tunnel Three-Component Force Balance," California Institute of Technology, Hydrodynamics Laboratory, Report No. 47-2, December 1954.

4. Parkin, B.R., "Experiments on Circular Arc and Flat Plate Hydrofoils in Noncavitating and Full Cavity Flows," California Institute of Technology, Hydrodynamics Laboratory, Report No. 47-6, February 1956. Published in "Journal of Ship Research," Vol. 1, No. 4, p. 34, March 1958.

5. Vaughan, V.L. Jr. and Ramsen, J.A., "Hydrodynamic Characteristics over a Range of Speeds up to 80 Feet Per Second of a Rectangular Modified Flat Plate Having an Aspect Ratio of 0.25 and Operating at Several Depths of Submersion," NACA, TN 3908, April 1957.

6. Waldin, K.L., Ramsen, J.A. and Vaughan, V.L. Jr., "The Hydrodynamic Characteristics of Modified Rectangular Flat Plates Having Aspect Ratios of 1.00, 0.25 and 0.125 and Operating Near a Free Surface," NACA, Report 1246, 1955.

7. Parkin, B.R. and Kermeen, R.W., "Water Tunnel Techniques for Force Measurements on Cavitating Hydrofoils," Journal of Ship Research, Vol. 1, No. 1, April 1957.

APPENDIX A

TEST SECTION FLOW CALIBRATION

Five static pressure taps were installed along the horizontal centerline of the flat reflection plate and provision was made for making velocity and pressure surveys across the test section at nine points. A rake with 16 static and total head tubes was used in flow calibration experiments. The velocity and pressure calibration tests were made at velocities of 20, 30, 40 and 50 fps. The velocity profile is uniform throughout the entire test section except for the boundary layers on the flat plate and tunnel wall. The boundary layer on the flat plate is approximately 3/8 in. thick at the balance spindle centerline. Figure 49 shows the measured velocity profile at the balance spindle location for velocities of 40 and 50 fps.

Cavitation tests using the flow calibration rake spanning the entire test section were also used to detect any lack of uniformity in the flow or pressure field. Cavity length is a very sensitive function of cavitation number at small cavitation number, therefore, any variations in velocity or pressure across the test section would be noted as differences in the length of the cavities formed along the calibration rake. Variations in cavity length due to differences in static pressure of 1/4 inch of water can easily be detected, however, no variations in the lengths of the cavities across the test section were noted.

A static pressure calibration along the flat reflection plane was made simultaneously with the velocity profile measurements. These tests showed a slight decrease in pressure along the length of the test section amounting to a decrease in pressure coefficient of .006 per foot.

APPENDIX B - DATA TABLES

Table I - Noncavitating Flow

AR = 4.0
V = 30, 25, 20 fps

Film No.	α	C_L	C_D	C_M	V
0140	3°	0.0155	0.0561	-0.0110	30
0150	4°	0.0508	0.0594	-0.0168	30
0160	5°	0.1144	0.0612	-0.0327	30
0170	6°	0.1800	0.0639	-0.0491	30
0180	7°	0.2465	0.0682	-0.0663	30
0190	8°	0.3164	0.0726	-0.0836	30
0200	9°	0.4017	0.0802	-0.1093	30
0210	10°	0.4789	0.0910	-0.1334	30
0220	12°	0.6617	0.1268	-0.2112	30
0230	12°	0.6605	0.1264	-0.211	30
0240	15°	0.8415	0.1963	-0.3150	25
0250	20°	0.8544	0.2939	-0.3853	25
0260	25°	0.7752	0.3629	-0.3592	25
0270	30°	0.7583	0.4415	-0.4096	20
0280	15°	0.8438	0.1975	-0.3160	25
0290	10°	0.4825	0.0917	-0.1312	30
0300	5°	0.1173	0.0609	-0.0330	30
0310	3°	0.0109	0.0542	-0.0053	30
AR = 2.0 V = 30 fps					
005	0°	-0.147	0.056	0.039	
006	1°	-0.102	0.053	0.028	
007	2°	-0.053	0.049	0.015	
008	3°	-0.005	0.050	0.002	
010	4°	0.042	0.050	-0.011	
011	5°	0.088	0.052	-0.023	
012	6°	0.135	0.055	-0.036	
014	8°	0.227	0.067	-0.058	
015	9°	0.276	0.070	-0.070	
016	10°	0.331	0.078	-0.089	
017	12°	0.454	0.104	-0.124	
018	14°	0.582	0.139	-0.174	
019	16°	0.703	0.182	-0.233	
020	18°	0.810	0.232	-0.297	
021	20°	0.906	0.292	-0.367	
022	22°	0.953	0.352	-0.424	
023	24°	0.879	0.377	-0.416	
024	20°	0.905	0.293	-0.365	
025	16°	0.702	0.183	-0.232	
026	12°	0.452	0.103	-0.123	
027	8°	0.227	0.066	-0.059	
028	7°	0.179	0.061	-0.046	
029	3°	-0.008	0.050	-0.006	
030	0°	-0.148	0.057	-0.040	
AR = 1.0 V = 30 fps					
414	3°	0.0020	0.0471	0.0001	
415	4°	0.0310	0.0488	-0.0087	
416	5°	0.0582	0.0499	-0.0160	
417	6°	0.0875	0.0547	-0.0234	
418	7°	0.1137	0.0576	-0.0295	
419	8°	0.1453	0.0623	-0.0379	
420	9°	0.1790	0.0663	-0.0453	
421	10°	0.2118	0.0707	-0.0532	
422	12°	0.2916	0.0892	-0.0771	
423	15°	0.4243	0.1322	-0.1226	
424	20°	0.6362	0.2279	-0.2105	
425	25°	0.8415	0.3754	-0.3139	
426	30°	1.0264	0.5629	-0.4405	
427	15°	0.4209	0.1323	-0.1198	
428	10°	0.2140	0.0713	-0.0528	
429	5°	0.0573	0.0514	-0.0150	
430	3°	0.0008	0.0484	-0.0006	
AR = 0.5 V = 30 fps					
718	3°	-0.003	0.0321	0.0011	
719	4°	0.0161	0.0339	-0.0046	
720	5°	0.0325	0.0335	-0.0085	
721	6°	0.0496	0.0337	-0.0123	
722	7°	0.0687	0.0374	-0.0175	
723	8°	0.0844	0.0408	-0.0202	

Table I - Noncavitating Flow (Cont'd)

AR = 0.5 (Cont'd.)

Film No.	α	C_L	C_D	C_M
724	9°	0.1039	0.0469	-0.0250
725	10°	0.1280	0.0533	-0.0319
726	12°	0.1860	0.0684	-0.0546
727	15°	0.2756	0.0978	-0.0814
728	20°	0.455	0.1698	-0.1499
729	25°	0.625	0.2808	-0.2211
730	30°	0.799	0.4313	-0.3093
731	15°	0.2784	0.0998	-0.0829
732	10°	0.1287	0.0547	-0.0323
733	5°	0.0324	0.0345	-0.0080
734	3°	-0.006	0.0321	0.0014

Table II - Cavitating Flow

Aspect Ratio = 4.0

Film No.	σ_v	σ_k	C_L	C_D	C_M	L/D
			α = 3°, V = 30 fps			
33	6.072		-0.010	0.057	0.005	-0.18
34	3.667		-0.014	0.058	0.009	-0.25
35	1.573		-0.012	0.058	0.009	-0.21
36	1.274		-0.012	0.065	0.009	-0.18
37	1.055		-0.013	0.066	0.009	-0.20
38	0.855		-0.011	0.055	0.008	-0.20
39	0.643		-0.011	0.049	0.008	-0.22
40	0.552		-0.011	0.049	-0.002	-0.22
41	0.334		-0.011	0.033	0.006	-0.32
42	0.230		-0.008	0.027	0.005	-0.31
43	0.129		-0.007	0.020	0.005	-0.36
44	0.075		-0.008	0.014	0.004	-0.53
47	0.064		-0.007	0.014	0.007	-0.54
48	0.553		-0.011	0.047	0.003	-0.24
49	3.680		-0.014	0.059	0.006	-0.23
50	5.563		-0.013	0.058	0.006	-0.22
			α = 4°, V = 30 fps			
52	5.599		0.052	0.059	-0.012	0.87
53	3.648		0.051	0.595	-0.010	0.85
54	1.502		0.049	0.628	-0.007	0.79
55	1.274		0.049	0.067	-0.007	0.72
56	1.067		0.048	0.0688	-0.007	0.70
57	0.855		0.051	0.0566	-0.009	0.80
58	0.645		0.049	0.0509	-0.009	0.96
59	0.543		0.050	0.047	-0.010	1.07
60	0.334		0.054	0.034	-0.010	1.57
61	0.230		0.054	0.028	-0.010	1.92
62	0.128		0.056	0.021	-0.012	2.66
63	0.077		0.056	0.017	-0.011	3.40
64	0.058		0.060	0.014	-0.012	4.32
65	0.548		0.050	0.046	-0.009	1.09
66	3.674		0.050	0.061	-0.010	0.82
67	5.581		0.049	0.059	-0.009	0.84
			α = 6°, V = 30 fps			
69	6.240		0.174	0.063	-0.041	2.78
70	3.686		0.180	0.065	-0.043	2.78
71	1.383		0.181	0.070	-0.040	2.60
72	1.173		0.177	0.076	-0.039	2.34
73	0.988		0.170	0.072	-0.036	2.35
74	0.765		0.176	0.064	-0.039	2.76
75	0.555		0.181	0.056	-0.040	3.25
76	0.452		0.180	0.049	-0.039	3.71
77	0.344		0.188	0.040	-0.040	4.67
78	0.242		0.230	0.032	-0.061	7.17
79	0.136	0.109	0.197	0.024	-0.067	8.36
80	0.084	0.059	0.155	0.018	-0.051	8.69
82	0.559		0.184	0.056	-0.039	3.29
83	3.725		0.180	0.065	-0.044	2.75
84	5.664		0.179	0.063	-0.056	2.84

Table II - Cavitating Flow (Cont'd)

AR = 4.0 (Cont'd)

Film No.	σ_v	σ_k	C_L	C_D	C_M	L/D
			$\alpha = 8^\circ$, V = 30 fps			
86	5.642		0.319	0.075	-0.083	4.22
87	3.751		0.320	0.077	-0.081	4.17
88	1.617		0.313	0.073	-0.076	4.28
89	1.405		0.315	0.075	-0.076	4.18
90	1.203		0.311	0.078	-0.075	3.99
91	0.995		0.312	0.080	-0.075	3.89
92	0.777		0.311	0.077	-0.073	4.04
93	0.570		0.332	0.067	-0.082	5.00
94	0.362	0.340	0.399	0.055	-0.149	7.25
95	0.248	0.226	0.312	0.049	-0.115	7.09
96	0.141	0.115	0.221	0.031	-0.077	7.13
97	0.125	0.103	0.170	0.023	-0.055	7.39
98	0.574		0.343	0.065	-0.087	5.29
99	0.738		0.318	0.073	-0.080	4.38
100	0.718		0.325	0.073	-0.083	4.46
			$\alpha = 10^\circ$, V = 30 fps			
102	5.767		0.480	0.092	-0.131	5.21
103	3.789		0.477	0.092	-0.128	5.19
104	1.672		0.473	0.093	-0.122	5.07
105	1.443		0.471	0.092	-0.121	5.13
106	1.213		0.469	0.095	-0.120	4.94
107	1.017		0.478	0.098	-0.121	4.86
108	0.802		0.492	0.098	-0.132	5.03
109	0.582		0.603	0.095	-0.225	6.38
110	0.358	0.333	0.406	0.073	-0.155	5.57
111	0.250	0.225	0.294	0.053	-0.107	5.55
112	0.140	0.119	0.197	0.036	-0.067	5.53
113	0.161	0.148	0.200	0.037	-0.066	5.36
114	0.595		0.612	0.095	-0.229	6.44
115	3.784		0.488	0.091	-0.129	5.38
116	5.777		0.482	0.092	-0.130	5.21
			$\alpha = 12^\circ$, V = 30 fps			
118	5.905		0.658	0.126	-0.206	5.21
119	3.866		0.661	0.128	-0.205	5.18
120	1.672		0.645	0.126	-0.189	5.14
121	1.464		0.643	0.126	-0.188	5.11
122	1.242		0.643	0.127	-0.188	5.06
123	1.036		0.664	0.139	-0.202	4.97
124	0.802		0.727	0.135	-0.273	5.39
125	0.578	0.483	0.629	0.123	-0.250	5.12
126	0.364	0.334	0.425	0.092	-0.163	4.64
127	0.255	0.222	0.328	0.072	-0.121	4.55
128	0.138	0.123	0.247	0.053	-0.088	4.63
129	0.124	0.107	0.237	0.052	-0.083	4.60
130	0.155	0.120	0.237	0.053	-0.082	4.50
132	0.709	0.677	0.682	0.133	-0.272	5.15
133	3.880		0.654	0.126	-0.205	5.21
134	5.894		0.662	0.127	-0.207	5.21
			$\alpha = 15^\circ$, V = 25 fps			
136	8.612		0.837	0.199	-0.312	4.21
137	5.634		0.821	0.196	-0.305	4.19
138	2.563		0.838	0.196	-0.305	4.28
139	2.291		0.831	0.198	-0.307	4.20
140	1.957		0.830	0.198	-0.302	4.20
141	1.660		0.832	0.198	-0.302	4.19
142	1.349		0.840	0.200	-0.306	4.21
143	1.060		0.856	0.207	-0.330	4.13
144	0.715		0.748	0.193	-0.318	3.89
145	0. 0	0.486	0.591	0.163	-0.241	3.62
146	0.399	0.365	0.455	0.128	-0.177	3.56
147	0.239	0.198	0.346	0.097	-0.131	3.57
148	0.174	0.144	0.298	0.083	-0.110	3.58
149	0.187	0.157	0.299	0.085	-0.111	3.52
151	1.179		0.848	0.206	-0.314	4.12
152	5.864		0.835	0.203	-0.312	4.12
153	8.612		0.823	0.198	-0.307	4.15

Film No.	σ_v	σ_k	C_L	C_D	C_M	L/D
			$\alpha = 20^\circ$, V = 25 fps			
156	8.765		0.860	0.299	-0.382	2.87
157	5.790		0.864	0.300	-0.383	2.88
158	2.303		0.851	0.295	-0.373	2.88
159	2.036		0.883	0.304	-0.385	2.90
160	1.689		0.867	0.297	-0.378	2.92
161	1.374		0.881	0.300	-0.384	2.94
162	1.063		0.895	0.308	-0.394	2.90
163	0.902		0.841	0.294	-0.370	2.86
164	0.739		0.758	0.272	-0.327	2.79
165	0.579		0.648	0.237	-0.273	2.74
166	0.415		0.525	0.194	-0.214	2.71
167	0.344		0.472	0.170	-0.1 0	2.78
168	0.249	0.207	0.402	0.147	-0.157	2.74
169	0.274	0.248	0.416	0.152	-0.164	2.75
170	0.200	0.180	0.374	0.134	-0.145	2.80
171	0.211	0.190	0.369	0.132	-0.143	2.80
172	0.201	0.174	0.369	0.133	-0.140	2.77
174	6.016		0.858	0.293	-0.384	2.93
175	8,786		0.849	0.293	-0.380	2.90
			$\alpha = 25^\circ$, V = 25 fps			
177	8.967		0.770	0.364	-0.352	2.12
178	5.982		0.783	0.371	-0.356	2.11
179	2.429		0.784	0.371	-0.354	2.11
180	2.039		0.785	0.371	-0.358	2.12
181	1.735		0.785	0.369	-0.358	2.13
182	1.428		0.788	0.371	-0.361	2.13
183	1.099		0.828	0.389	-0.384	2.13
184	0.941		0.836	0.394	-0.384	2.12
185	0.772		0.810	0.385	-0.369	2.10
186	0.607		0.713	0.339	-0.318	2.10
187	0.435		0.610	0.289	-0.268	2.11
188	0.296	0.257	0.530	0.251	-0.225	2.11
189	0.216	0.196	0.472	0.225	-0.197	2.10
190	0.139	0.111	0.443	0.208	-0.184	2.13
191	0.167	0.152	0.443	0.207	-0.182	2.14
192	1.291		0.787	0.368	-0.357	2.14
193	6.190		0.781	0.373	-0.357	2.09
194	9.182		0.775	0.365	-0.353	2.12
			$\alpha = 30^\circ$, V = 20 fps			
196	13.501		0.756	0.443	-0.356	1.71
197	8.923		0.749	0.439	-0.351	1.71
198	2.776		0.761	0.443	-0.358	1.72
199	2.285		0.763	0.445	-0.360	1.71
200	1.808		0.761	0.445	-0.358	1.71
201	1.576		0.762	0.447	-0.363	1.70
202	1.346		0.780	0.454	-0.374	1.72
203	1.103		0.801	0.465	-0.387	1.72
204	0.887		0.823	0.477	-0.401	1.73
205	0.634		0.745	0.434	-0.355	1.72
206	0.399		0.626	0.360	-0.293	1.74
207	0.284	0.235	0.563	0.320	-0.258	1.76
208	0.177	0.146	0.499	0.287	-0.225	1.74
209	0.173	0.153	0.501	0.287	-0.226	1.74
210	0.261		0.546	0.315	-0.252	1.73
211	0.333		0.586	0.340	-0.274	1.72
212	4.518		0.752	0.435	-0.357	1.73
213	10.069		0.756	0.438	-0.361	1.73
214	14.071		0.746	0.438	-0.358	1.70

Table II - Cavitating Flow (Cont'd)

Aspect Ratio = 2.0

Film No.	σ_v	C_L	C_D	C_M	L/D
		$\alpha = 3^\circ$, V = 30 fps			
32	6.265	-0.007	0.050	0.003	-0.14
33	4.805	-0.008	0.050	0.004	-0.17
34	3.737	-0.008	0.051	0.003	-0.15
35	2.096	-0.008	0.051	0.004	-0.17
36	1.632	-0.008	0.050	0.003	-0.16
37	1.476	-0.007	0.049	0.003	-0.15
38	1.382	-0.009	0.050	0.004	-0.17
39	1.274	-0.009	0.053	0.004	-0.18
40	1.064	-0.009	0.053	0.004	-0.17
41	0.848	-0.008	0.052	0.003	-0.15
42	0.574	-0.008	0.046	0.003	-0.17
43	0.507	-0.008	0.045	0.003	-0.17
44	0.408	-0.007	0.040	0.002	-0.18
45	0.310	-0.006	0.033	0.002	-0.19
46	0.153	-0.007	0.024	0.002	-0.30
47	0.049	0.010	0.016	0.001	0.62
48	0.633	-0.008	0.050	0.003	-0.16
49	1.642	-0.007	0.051	0.004	-0.15
50	3.776	-0.008	0.052	0.004	-0.16
51	6.352	-0.008	0.051	0.003	-0.16
		$\alpha = 4^\circ$, V = 30 fps			
54	6.323	0.040	0.052	-0.010	0.76
55	2.686	0.038	0.052	-0.008	0.73
56	1.638	0.038	0.053	-0.008	0.72
57	1.437	0.038	0.052	-0.008	0.72
58	1.314	0.040	0.052	-0.008	0.76
59	1.216	0.038	0.053	-0.008	0.72
60	1.107	0.038	0.052	-0.008	0.73
61	1.003	0.037	0.052	-0.008	0.73
62	0.897	0.039	0.052	-0.008	0.74
63	0.790	0.039	0.051	-0.009	0.76
64	0.684	0.038	0.049	-0.008	0.78
65	0.576	0.038	0.047	-0.009	0.80
66	0.471	0.037	0.044	-0.009	0.83
67	0.363	0.039	0.040	-0.009	0.98
68	0.258	0.037	0.032	-0.007	1.15
69	0.152	0.040	0.024	-0.008	1.67
70	0.048	0.057	0.015	-0.009	3.73
71	0.580	0.040	0.048	-0.009	0.84
72	1.654	0.038	0.053	-0.008	0.71
73	2.686	0.038	0.052	-0.008	0.74
74	3.730	0.038	0.051	-0.008	0.75
75	3.743	0.038	0.053	-0.009	0.72
76	6.243	0.038	0.053	-0.009	0.73
		$\alpha = 5^\circ$, V = 30 fps			
78	6.322	0.086	0.054	-0.022	1.60
79	2.734	0.086	0.054	-0.021	1.59
80	1.850	0.084	0.054	-0.020	1.57
81	1.650	0.088	0.056	-0.024	1.49
82	1.442		0.055	-0.020	1.57
83	1.327	0.085	0.055	-0.020	1.54
84	1.207	0.086	0.055	-0.021	1.56
85	1.113	0.087	0.055	-0.020	1.58
86	0.995	0.083	0.053	-0.020	1.55
87	0.902	0.086	0.054	-0.020	1.59
88	0.785	0.084	0.053	-0.021	1.59
89	0.681	0.084	0.051	-0.021	1.65
90	0.586	0.086	0.050	-0.021	1.72
91	0.474	0.085	0.046	-0.020	1.86
92	0.367	0.084	0.039	-0.019	2.14
93	0.254	0.084	0.033	-0.018	2.57
94	0.146	0.083	0.025	-0.016	3.33
95	0.047	0.099	0.015	-0.028	6.57
96	0.783	0.085	0.053	-0.021	1.62
97	2.704	0.087	0.055	-0.020	1.59
98	6.322	0.087	0.054	-0.021	1.60
		$\alpha = 6^\circ$, V = 30 fps			
100	6.422	0.134	0.056	-0.034	2.37
101	2.735	0.135	0.056	-0.034	2.43
102	1.758	0.133	0.056	-0.033	2.39
103	1.437	0.133	0.056	-0.033	2.38
104	1.347	0.134	0.057	-0.033	2.33
105	1.224	0.134	0.058	-0.033	2.30
106	1.126	0.132	0.058	-0.033	2.27
107	1.014	0.131	0.060	-0.033	2.18
108	0.904	0.130	0.058	-0.032	2.24
109	0.807	0.132	0.058	-0.033	2.28
110	0.685	0.131	0.055	-0.032	2.37
111	0.582	0.130	0.053	-0.032	2.43
112	0.464	0.130	0.049	-0.032	2.64
113	0.374	0.131	0.044	-0.030	2.97
114	0.270	0.134	0.038	-0.029	3.51
115	0.168	0.147	0.027	-0.034	5.42
116	0.154	0.155	0.025	-0.041	6.07
117	0.049	0.116	0.018	-0.035	6.61
118	0.043	0.112	0.017	-0.033	6.76
119	0.117	0.151	0.022	-0.048	6.97
120	0.593	0.129	0.053	-0.031	2.45
121	2.771	0.133	0.052	-0.033	2.30
122	6.483	0.133	0.058	-0.034	2.30
		$\alpha = 7^\circ$, V = 30 fps			
124	6.397	0.178	0.059	-0.045	3.03
125	3.858	0.178	0.060	-0.044	2.96
126	2.726	0.178	0.060	-0.044	2.94
127	1.698	0.181	0.062	-0.044	2.91
128	1.592	0.183	0.063	-0.044	2.90
129	1.473	0.189	0.063	-0.044	2.99
130	1.347	0.180	0.064	-0.044	2.80
131	1.226	0.178	0.065	-0.044	2.74
132	1.141	0.176	0.066	-0.044	2.66
133	1.035	0.178	0.068	-0.044	2.62
134	0.911	0.179	0.068	-0.044	2.64
135	0.806	0.171	0.066	-0.044	2.72
136	0.644	0.174	0.059	-0.042	2.97
137	0.574	0.175	0.057	-0.042	3.07
138	0.470	0.177	0.053	-0.041	3.33
139	0.361	0.177	0.046	-0.041	3.81
140	0.251	0.186	0.037	-0.043	4.99
141	0.144	0.188	0.028	-0.065	6.83
142	0.099	0.154	0.023	-0.051	6.83
143	0.059	0.126	0.020	-0.039	6.44
144	0.052	0.123	0.019	-0.038	6.43
146	0.664	0.179	0.063	-0.047	2.87
147	2.839	0.180	0.067	-0.052	2.70
		$\alpha = 8^\circ$, V = 30 fps			
150	6.497	0.228	0.067	-0.058	3.37
151	3.871	0.229	0.068	-0.057	3.38
152	2.761	0.226	0.067	-0.056	3.38
153	1.669	0.225	0.066	-0.086	3.40
154	1.551	0.224	0.070	-0.056	3.20
155	1.612	0.229	0.069	-0.057	3.32
156	1.458	0.225	0.068	-0.057	3.31
157	1.250	0.227	0.072	-0.057	3.18
158	1.037	0.226	0.074	-0.056	2.05
159	0.817	0.223	0.071	-0.054	3.13
160	0.610	0.232	0.064	-0.056	3.63
161	0.382	0.241	0.052	-0.057	4.63
162	0.277	0.291	0.044	-0.101	6.59
163	0.226	0.267	0.039	-0.097	6.79
164	0.163	0.223	0.034	-0.080	6.60
165	0.107	0.183	0.028	-0.063	6.47
166	0.056	0.147	0.021	-0.048	7.14
167	0.076	0.146	0.025	-0.047	5.85
168	0.076	0.144	0.024	-0.046	6.05
169	0.057	0.145	0.023	-0.047	6.29
170	0.726	0.215	0.067	-0.054	3.21
171	2.991	0.229	0.067	-0.057	3.40
172	6.632	0.226	0.068	-0.057	3.34
		$\alpha = 9^\circ$, V = 30 fps			
174	6.659	0.278	0.072	-0.069	3.87
175	3.899	0.273	0.070	-0.067	3.88
176	3.797	0.275	0.071	-0.068	3.90
177	1.719	0.276	0.071	-0.067	3.88
178	1.489	0.277	0.072	-0.068	3.85

Table II - Cavitating Flow (Cont'd)

AR = 2.0 (Cont'd)

Film No.	σ_v	C_L	C_D	C_M	L/D
		$\alpha = 9^o$ (Cont'd)			
179	1.274	0.274	0.074	-0.067	3.71
180	1.035	0.269	0.080	-0.066	3.37
181	0.833	0.269	0.080	-0.064	3.36
182	0.596	0.275	0.069	-0.065	3.99
183	0.495	0.290	0.065	-0.070	4.47
184	0.381	0.312	0.060	-0.087	5.19
185	0.331	0.356	0.057	-0.129	6.25
186	0.278	0.321	0.051	-0.119	6.25
187	0.220	0.285	0.046	-0.105	6.21
188	0.169	0.231	0.039	-0.086	6.12
190	0.114	0.198	0.033	-0.068	5.91
191	0.060	0.168	0.028	-0.055	5.93
192	0.057	0.163	0.029	-0.053	5.69
193	0.052	0.166	0.029	-0.055	5.80
194	0.698	0.276	0.077	-0.065	3.59
195	3.992	0.275	0.072	-0.069	3.83
196	6.578	0.275	0.071	-0.069	3.87
		$\alpha = 10^o$, V = 30 fps			
198	6.608	0.332	0.079	-0.083	4.18
199	3.923	0.333	0.080	-0.083	4.18
200	2.834	0.331	0.079	-0.082	4.17
201	1.733	0.331	0.080	-0.082	4.14
202	1.514	0.332	0.081	-0.083	4.11
203	1.288	0.329	0.081	-0.082	4.04
204	1.066	0.328	0.087	-0.080	3.76
205	0.833	0.321	0.087	-0.077	3.67
206	0.625	0.340	0.080	-0.084	4.22
207	0.526	0.359	0.078	-0.095	4.61
208	0.398	0.428	0.073	-0.161	5.84
209	0.286	0.342	0.061	-0.129	5.60
210	0.173	0.244	0.045	-0.087	5.37
211	0.108	0.199	0.038	-0.067	5.29
212	0.073	0.182	0.035	-0.060	5.25
213	0.079	0.182	0.035	-0.060	5.12
214	0.071	0.181	0.035	-0.059	5.16
215	0.664	0.338	0.082	-0.083	4.13
216	2.866	0.331	0.073	-0.083	4.15
		$\alpha = 12^o$, V = 30 fps			
219	6.658	0.453	0.103	-0.122	4.40
220	2.850	0.456	0.104	-0.122	4.38
221	1.940	0.445	0.101	-0.119	4.39
222	1.744	0.451	0.103	-0.120	4.36
223	1.514	0.451	0.104	-0.120	4.35
224	1.291	0.448	0.104	-0.119	4.31
225	1.083	0.449	0.106	-0.118	4.23
226	0.842	0.449	0.108	-0.119	4.15
227	0.626	0.491	0.107	-0.151	4.60
228	0.510	0.555	0.106	-0.218	5.25
229	0.407	0.484	0.097	-0.194	4.98
230	0.294	0.363	0.077	-0.139	4.71
231	0.230	0.332	0.070	-0.126	4.70
232	0.178	0.270	0.059	-0.098	4.59
233	0.119	0.238	0.052	-0.083	4.57
234	0.097	0.223	0.048	-0.074	4.61
235	0.098	0.219	0.049	-0.075	4.51
236	0.044	0.207	0.045	-0.071	4.54
237	0.726	0.471	0.110	-0.132	4.29
238	2.956	0.454	0.104	-0.122	4.36
239	6.765	0.458	0.104	-0.124	4.40
		$\alpha = 15^o$, V = 30 fps			
241	6.559	0.629	0.157	-0.196	4.00
242	2.872	0.642	0.160	-0.200	4.00
243	2.116	0.646	0.161	-0.200	4.01
244	1.882	0.646	0.161	-0.199	4.01
245	1.635	0.638	0.160	-0.196	3.99
246	1.433	0.642	0.162	-0.196	3.97
247	1.201	0.642	0.164	-0.197	3.92
248	0.987	0.663	0.167	-0.213	3.97
249	0.850	0.677	0.168	-0.232	4.02
250	0.746	0.711	0.174	-0.265	4.09
251	0.640	0.704	0.171	-0.287	4.12
252	0.535	0.616	0.157	-0.254	3.92
253	0.418	0.513	0.136	-0.207	3.76
254	0.370	0.471	0.126	-0.188	3.75
255	0.306	0.416	0.110	-0.162	3.76
256	0.245	0.367	0.098	-0.140	3.75
257	0.192	0.330	0.089	-0.122	3.71
258	0.140	0.287	0.078	-0.103	3.68
259	0.122	0.283	0.076	-0.101	3.74
260	0.128	0.279	0.076	-0.099	3.66
261	0.102	0.268	0.072	-0.095	3.71
262	0.712	0.697	0.170	-0.264	4.09
263	2.996	0.648	0.165	-0.202	3.94
264	4.059	0.643	0.162	-0.201	3.97
265	6.798	0.650	0.163	-0.204	3.98
		$\alpha = 15^o$ (Cont'd)			
		$\alpha = 20^o$, V = 30 fps			
267	6.840	0.912	0.294	-0.366	3.10
268	2.918	0.907	0.292	-0.363	3.10
269	2.373	0.917	0.294	-0.364	3.11
270	2.016	0.900	0.289	-0.356	3.11
271	1.776	0.903	0.291	-0.354	3.10
272	1.546	0.906	0.295	-0.361	3.07
273	1.319	0.917	0.300	-0.371	3.05
274	1.100	0.926	0.300	-0.394	3.03
275	0.863	0.869	0.293	-0.384	2.97
276	0.659	0.736	0.260	-0.321	2.83
277	0.429	0.553	0.200	-0.230	2.76
278	0.317	0.479	0.174	-0.195	2.75
279	0.266	0.440	0.160	-0.175	2.74
280	0.210	0.400	0.148	-0.155	2.91
281	0.177	0.377	0.141	-0.143	2.67
282	0.174	0.377	0.140	-0.143	2.70
283	0.165	0.371	0.137	-0.141	2.71
284	0.163	0.368	0.137	-0.141	2.69
285	0.802	0.035	0.284	-0.368	2.93
286	3.065	0.912	0.294	0.013	3.10
287	6.877	0.910	0.295	-0.004	3.09
		$\alpha = 25^o$, V = 30 fps			
289	7.034	0.846	0.387	-0.402	2.18
290	2.511	0.861	0.393	-0.409	2.19
291	2.049	0.865	0.394	-0.411	2.19
292	1.580	0.898	0.404	-0.428	2.22
293	1.129	0.925	0.415	-0.441	2.23
294	0.790	0.795	0.365	-0.370	2.18
295	0.563	0.661	0.307	-0.293	2.15
296	0.456	0.579	0.277	-0.261	2.16
297	0.341	0.525	0.242	-0.224	2.17
298	0.287	0.492	0.225	-0.205	2.18
299	0.245	0.466	0.218	-0.192	2.14
300	0.240	0.465	0.217	-0.190	2.14
301	0.245	0.468	0.218	-0.192	2.15
303	1.039	0.904	0.409	-0.430	2.21
304	7.228	0.849	0.390	-0.404	2.18
		$\alpha = 30^o$, V = 30 fps			
359	7.151	0.776	0.450	-0.375	1.72
360	4.314	0.777	0.452	-0.376	1.72
361	2.504	0.781	0.451	-0.376	1.73
362	2.024	0.781	0.452	-0.378	1.73
363	1.547	0.785	0.451	-0.380	1.74
364	1.172	0.799	0.459	-0.390	1.74
365	0.936	0.810	0.465	-0.394	1.74
366	0.691	0.742	0.429	-0.353	1.73
367	0.455	0.619	0.356	-0.285	1.73
368	0.410	0.595	0.340	-0.273	1.75
369	0.365	0.575	0.328	-0.262	1.75
370	0.322	0.557	0.318	-0.251	1.75
371	0.301	0.540	0.310	-0.240	1.74
372	0.263	0.515	0.293	-0.229	1.74
373	1.658	0.776	0.447	-0.375	1.73
374	4.348	0.770	0.447	-0.372	1.72
375	6.154	0.765	0.444	-0.370	1.72

Table II - Cavitating Flow (Cont'd)

AR = 2.0 (Cont'd)

Film No.	σ_v	C_L	C_D	C_M	L/D
		$\alpha = 8^o$, V = 20 fps			
306	13.543	0.225	0.066	-0.057	3.43
307	6.321	0.227	0.068	-0.057	3.36
308	3.567	0.228	0.068	-0.059	3.36
309	2.648	0.226	0.067	-0.057	3.36
310	1.745	0.228	0.068	-0.057	3.33
311	1.271	0.227	0.072	-0.057	3.16
312	0.808	0.225	0.074	-0.054	3.06
313	0.372	0.247	0.053	-0.061	4.64
314	0.254	0.280	0.044	-0.100	6.37
315	0.162	0.188	0.030	-0.064	6.24
316	0.746	0.221	0.071	-0.053	3.11
317	2.019	0.215	0.064	-0.052	3.36
318	13.882	0.226	0.065	-0.057	3.47

Film No.	σ_v	σ_k	C_L	C_D	C_M	L/D
			$\alpha = 8^o$, V = 40 fps			
333	0.284	0.250	0.282	0.046	-0.094	6.24
334	0.227	0.197	0.268	0.041	-0.097	6.58
335	0.162	0.133	0.224	0.035	-0.081	6.36
336	0.105	0.077	0.177	0.028	-0.058	6.23
337	0.058	0.031	0.161	0.025	-0.054	6.40
338	0.053	0.025	0.163	0.025	-0.054	6.46
339	0.058	0.020	0.159	0.027	-0.052	5.93
340	0.457		0.234	0.057	-0.055	4.11
341	1.789		0.228	0.068	-0.058	3.35
342	3.287		0.229	0.067	-0.058	3.43
			$\alpha = 8^o$, V = 50 fps			
344	2.223		0.227	0.073	-0.057	3.09
345	1.285		0.225	0.077	-0.057	2.90
346	0.884		0.221	0.076	-0.054	2.93
347	0.679		0.225	0.068	-0.054	3.32
348	0.495		0.232	0.059	-0.054	3.95
349	0.399		0.252	0.047	-0.066	5.30
350	0.230	0.206	0.279	0.042	-0.101	6.60
351	0.194	0.175	0.255	0.039	-0.093	6.50
352	0.152	0.132	0.218	0.034	-0.078	6.38
353	0.108	0.090	0.187	0.030	-0.064	6.30
354	0.072	0.055	0.163	0.026	-0.055	6.18
355	0.060	0.041	0.167	0.026	-0.056	6.39
356	0.488		0.234	0.060	-0.055	3.93
357	2.206		0.230	0.074	-0.058	3.12

Aspect Ratio = 1.0

Film No.	σ_v	C_L	C_D	C_M	L/D
		$\alpha = 3^o$, V = 30 fps			
432	6.194	0.001	0.045	-0.000	0.03
433	3.690	-0.002	0.046	0.001	0.03
434	1.601	0.000	0.047	0.000	0.01
435	0.866	0.003	0.046	-0.001	0.06
436	0.552	0.001	0.045	-0.001	0.02
437	0.442	0.003	0.044	-0.002	0.08
438	0.341	0.002	0.041	-0.002	0.06
439	0.242	0.002	0.034	-0.002	0.06
440	0.137	0.005	0.028	-0.003	0.17
441	0.086	0.005	0.025	-0.003	0.19
442	0.041	0.018	0.020	-0.004	0.91
443	0.555	-0.002	0.046	-0.001	-0.04
444	3.671	0.001	0.048	-0.001	0.01
445	6.185	-0.002	0.048	-0.000	0.03

AR = 1.0 (Cont'd)

Film No.	σ_v	C_L	C_D	C_M	L/D
		$\alpha = 4^o$, V = 30 fps			
447	6.213	0.029	0.047	-0.003	0.61
448	4.290	0.026	0.048	-0.006	0.53
449	1.595	0.026	0.047	-0.005	0.56
450	0.764	0.027	0.048	-0.007	0.56
451	0.561	0.028	0.046	-0.007	0.61
452	0.454	0.028	0.044	-0.007	0.64
453	0.342	0.027	0.040	-0.007	0.69
454	0.242	0.031	0.034	-0.007	0.89
455	0.139	0.027	0.027	-0.006	0.98
456	0.084	0.031	0.024	-0.007	1.32
457	0.037	0.036	0.019	-0.005	1.88
458	0.022	0.033	0.019	-0.003	1.74
459	0.572	0.026	0.046	-0.005	0.56
460	3.702	0.029	0.049	-0.007	0.59
461	6.224	0.029	0.048	-0.007	0.61
		$\alpha = 5^o$, V = 30 fps			
463	6.246	0.057	0.048	-0.014	1.19
464	3.715	0.055	0.046	-0.013	1.21
465	1.626	0.055	0.047	-0.012	1.17
466	0.988	0.054	0.046	-0.012	1.17
467	0.777	0.055	0.047	-0.013	1.17
468	0.563	0.055	0.045	-0.013	1.21
469	0.455	0.056	0.040	-0.013	1.38
470	0.346	0.057	0.033	-0.014	1.71
471	0.249	0.057	0.028	-0.013	2.06
472	0.140	0.058	0.029	-0.012	2.40
473	0.088	0.059	0.018	-0.011	3.34
474	0.036	0.072	0.014	-0.015	5.13
475	0.037	0.066	0.012	-0.015	5.22
476	0.052	0.064	0.017	-0.013	3.67
477	0.611	0.058	0.048	-0.013	1.21
478	3.774	0.056	0.047	-0.013	1.19
		$\alpha = 6^o$, V = 30 fps			
481	6.235	0.088	0.053	-0.023	1.64
482	2.644	0.085	0.052	-0.021	1.63
483	1.638	0.085	0.053	-0.020	1.61
484	0.905	0.086	0.052	-0.020	1.68
485	0.570	0.087	0.050	-0.021	1.74
486	0.464	0.084	0.047	-0.020	1.78
487	0.358	0.084	0.044	-0.020	1.91
488	0.247	0.086	0.038	-0.020	2.27
489	0.142	0.084	0.030	-0.018	2.80
490	0.044	0.090	0.023	-0.029	3.93
491	0.017	0.075	0.022	-0.023	3.44
492	0.576	0.084	0.050	-0.020	1.69
493	3.747	0.087	0.059	-0.022	1.59
494	6.308	0.084	0.053	-0.021	1.58
		$\alpha = 7^o$, V = 30 fps			
496	6.387	0.115	0.056	-0.030	2.05
497	3.813	0.115	0.057	-0.028	2.00
498	1.651	0.113	0.057	-0.028	1.99
499	1.106	0.113	0.056	-0.027	2.01
500	0.791	0.113	0.056	-0.027	2.02
501	0.577	0.114	0.053	-0.027	2.15
502	0.464	0.117	0.051	-0.027	2.28
503	0.363	0.113	0.047	-0.026	2.43
504	0.257	0.117	0.040	-0.026	2.96
505	0.146	0.119	0.030	-0.027	3.95
506	0.102	0.132	0.026	-0.044	5.02
507	0.043	0.100	0.022	-0.033	4.63
508	0.032	0.096	0.018	-0.031	5.17
509	0.049	0.098	0.018	-0.030	5.53
510	0.644	0.113	0.056	-0.027	2.02
511	3.847	0.114	0.058	-0.029	1.97
512	6.408	0.116	0.057	-0.029	2.03
		$\alpha = 8^o$, V = 30 fps			
514	6.410	0.145	0.060	-0.037	2.42
515	3.814	0.140	0.060	-0.034	2.34
516	1.369	0.140	0.060	-0.033	2.35
517	1.122	0.143	0.063	-0.034	2.27

Table II - Cavitating Flow (Cont'd)

AR = 1.0 (Cont'd)

Film No.	σ_v	C_L	C_D	C_M	L/D
		$\alpha = 8^\circ$ (Cont'd)			
518	0.905	0.142	0.061	-0.034	2.33
519	0.703	0.143	0.062	-0.033	2.30
520	0.599	0.142	0.059	-0.033	2.40
521	0.486	0.143	0.056	-0.033	2.55
522	0.375	0.144	0.051	-0.033	2.80
523	0.267	0.147	0.045	-0.033	3.25
524	0.156	0.174	0.037	-0.057	4.70
525	0.098	0.162	0.032	-0.057	5.10
526	0.046	0.117	0.025	-0.041	4.64
527	0.061	0.124	0.026	-0.043	4.70
528	0.029	0.119	0.025	-0.042	4.79
529	0.619	0.145	0.060	-0.033	2.41
530	3.848	0.143	0.061	-0.036	2.32
531	6.453	0.146	0.062	-0.037	2.36
		$\alpha = 9^\circ$, V = 30 fps			
533	6.478	0.176	0.065	-0.043	2.71
534	3.884	0.172	0.064	-0.041	2.69
535	1.680	0.174	0.064	-0.037	2.73
536	1.032	0.172	0.067	-0.040	2.57
537	0.822	0.175	0.070	-0.040	2.51
538	0.595	0.173	0.065	-0.040	2.66
539	0.487	0.174	0.062	-0.040	2.82
540	0.389	0.177	0.058	-0.039	3.07
541	0.275	0.177	0.050	-0.041	3.58
542	0.161	0.210	0.042	-0.077	5.00
543	0.099	0.172	0.036	-0.061	4.73
544	0.052	0.131	0.029	-0.045	4.57
545	0.595	0.167	0.065	-0.037	2.56
546	3.849	0.176	0.064	-0.043	2.75
547	5.478	0.175	0.065	-0.043	2.71
		$\alpha = 10^\circ$, V = 30 fps			
550	6.504	0.212	0.071	-0.052	3.00
551	3.915	0.209	0.070	-0.049	2.98
552	1.707	0.215	0.070	-0.049	3.06
553	1.053	0.208	0.070	-0.050	2.95
554	0.812	0.206	0.072	-0.048	2.87
555	0.603	0.207	0.071	-0.047	2.93
556	0.496	0.213	0.068	-0.048	3.15
557	0.387	0.222	0.067	-0.053	3.29
558	0.282	0.232	0.065	-0.063	3.59
559	0.226	0.269	0.057	-0.100	4.74
560	0.173	0.240	0.055	-0.091	4.36
561	0.111	0.194	0.049	-0.070	3.94
562	0.107	0.190	0.039	-0.068	4.88
563	0.046	0.149	0.040	-0.051	3.73
564	0.034	0.149	0.037	-0.050	4.04
565	0.637	0.207	0.073	-0.048	2.84
566	3.941	0.207	0.076	-0.052	2.73
567	5.494	0.209	0.075	-0.051	2.79
		$\alpha = 12^\circ$, V = 30 fps			
569	6.642	0.292	0.086	-0.076	3.41
570	3.992	0.288	0.085	-0.074	3.38
571	2.190	0.289	0.085	-0.074	3.40
572	1.285	0.285	0.084	-0.073	3.40
573	1.088	0.289	0.089	-0.078	3.26
574	0.844	0.279	0.086	-0.071	3.25
575	0.742	0.284	0.088	-0.072	3.22
576	0.523	0.299	0.087	-0.078	3.45
577	0.409	0.303	0.081	-0.084	3.77
578	0.282	0.343	0.076	-0.137	4.52
579	0.170	0.259	0.058	-0.100	4.45
580	0.114	0.208	0.049	-0.076	4.23
581	0.058	0.180	0.044	-0.063	4.06
582	0.049	0.179	0.044	-0.063	4.08
583	0.054	0.182	0.043	-0.063	4.24
584	0.660	0.289	0.091	-0.073	3.19
585	4.059	0.292	0.090	-0.076	3.25
586	6.760	0.286	0.089	-0.075	3.20

Film No.	σ_v	C_L	C_D	C_M	L/D
		$\alpha = 15^\circ$, V = 30 fps			
588	6.943	0.423	0.132	-0.122	3.20
589	4.089	0.415	0.130	-0.118	3.19
590	1.924	0.418	0.129	-0.118	3.24
591	1.771	0.417	0.126	-0.118	3.30
592	1.444	0.420	0.129	-0.119	3.25
593	1.211	0.413	0.128	-0.117	3.23
594	0.954	0.405	0.127	-0.113	3.19
595	0.629	0.424	0.131	-0.126	3.24
596	0.534	0.437	0.129	-0.140	3.39
597	0.405	0.487	0.132	-0.204	3.69
598	0.291	0.385	0.105	-0.157	3.68
599	0.236	0.338	0.094	-0.136	3.61
600	0.171	0.286	0.080	-0.111	3.59
601	0.111	0.257	0.071	-0.097	3.60
602	0.068	0.220	0.063	-0.080	3.47
603	0.068	0.221	0.063	-0.081	3.50
604	0.058	0.216	0.063	-0.078	3.43
605	0.084	0.219	0.062	-0.079	3.52
607	0.800	0.392	0.123	-0.109	3.17
608	4.223	0.417	0.131	-0.119	3.19
609	6.887	0.417	0.129	-0.119	3.22
		$\alpha = 20^\circ$, V = 30 fps			
611	6.610	0.640	0.228	-0.211	2.80
612	3.991	0.635	0.227	-0.208	2.80
613	2.380	0.640	0.228	-0.209	2.81
614	1.994	0.639	0.226	-0.209	2.82
615	1.655	0.639	0.227	-0.209	2.82
616	1.413	0.632	0.225	-0.206	2.81
617	1.187	0.630	0.225	-0.208	2.80
618	1.075	0.629	0.226	-0.210	2.79
619	0.970	0.648	0.233	-0.223	2.78
620	0.853	0.654	0.234	-0.236	2.79
621	0.745	0.680	0.240	-0.264	2.83
622	0.622	0.714	0.249	-0.318	2.86
623	0.509	0.623	0.224	-0.276	2.78
624	0.425	0.539	0.198	-0.232	2.72
625	0.361	0.486	0.182	-0.206	2.68
626	0.308	0.437	0.165	-0.182	2.65
627	0.252	0.402	0.153	-0.165	2.64
628	0.193	0.352	0.135	-0.141	2.61
629	0.138	0.319	0.123	-0.124	2.59
631	0.637	0.714	0.251	-0.310	2.85
632	1.768	0.634	0.226	-0.208	2.80
633	6.758	0.642	0.218	-0.191	2.94
		$\alpha = 25^\circ$, V = 30 fps			
635	6.718	0.845	0.379	-0.315	2.23
636	4.035	0.848	0.381	-0.315	2.22
637	2.925	0.856	0.382	-0.317	2.24
638	2.494	0.859	0.381	-0.319	2.25
639	2.025	0.850	0.379	-0.313	2.25
640	1.767	0.858	0.376	-0.314	2.28
641	1.541	0.860	0.383	-0.322	2.25
642	1.323	0.880	0.388	-0.340	2.26
643	1.088	0.881	0.406	-0.367	2.17
644	0.964	0.916	0.395	-0.400	2.32
645	0.848	0.941	0.412	-0.442	2.28
646	0.740	0.850	0.384	-0.404	2.21
647	0.628	0.747	0.349	-0.350	2.17
648	0.539	0.669	0.311	-0.309	2.15
649	0.417	0.557	0.264	-0.251	2.11
650	0.304	0.489	0.234	-0.214	2.09
651	0.194	0.402	0.194	-0.171	2.08
652	0.135	0.370	0.176	-0.154	2.10
653	0.087	0.341	0.163	-0.141	2.09
654	0.640	0.773	0.355	-0.364	2.18
655	4.088	0.852	0.381	-0.315	2.24
656	6.778	0.847	0.379	-0.316	2.24

Table II - Cavitating Flow (Cont'd)

AR = 1.0 (Cont'd)

Film No.	σ_v	C_L	C_D	C_M	L/D
		$\alpha = 30^o$, V = 30 fps			
658	6.877	1.019	0.558	-0.440	1.83
659	4.086	1.025	0.563	-0.443	1.82
660	3.507	1.028	0.564	-0.443	1.82
661	2.904	1.026	0.563	-0.440	1.82
662	2.373	1.020	0.559	-0.436	1.83
663	2.020	1.019	0.558	-0.456	1.83
664	1.799	1.020	0.560	-0.438	1.82
665	1.562	1.026	0.564	-0.448	1.82
666	1.328	1.047	0.577	-0.476	1.81
667	1.118	1.107	0.605	-0.558	1.83
668	0.874	0.972	0.542	-0.488	1.79
669	0.648	0.779	0.440	-0.381	1.77
670	0.538	0.682	0.394	-0.329	1.73
671	0.442	0.614	0.359	-0.291	1.71
672	0.382	0.567	0.332	-0.267	1.71
673	0.306	0.521	0.304	-0.243	1.71
674	0.257	0.486	0.284	-0.224	1.71
675	0.209	0.453	0.265	-0.206	1.71
676	0.163	0.429	0.251	-0.192	1.71
677	0.171	0.431	0.251	-0.193	1.72
678	1.379	1.034	0.570	-0.464	1.81
679	4.204	1.041	0.571	-0.452	1.82
680	6.864	1.023	0.560	-0.443	1.83

Aspect Ratio = 0.5

Film No.	σ_v	σ_k	C_L	C_D	C_M	L/D
			$\alpha = 3^o$, V = 30 fps			
737	6.139		-0.005	0.031	0.002	-0.16
738	3.677		0.000	0.031	0.001	-0.01
739	1.598		-0.001	0.031	0.000	-0.02
740	0.658		0.001	0.032	0.008	0.03
741	0.555		0.001	0.033	-0.001	0.04
742	0.452		0.001	0.034	0.000	0.02
743	0.347		0.002	0.035	-0.002	0.05
744	0.242		0.004	0.029	-0.003	0.14
745	0.137		0.003	0.022	-0.002	0.13
746	0.084		0.003	0.017	-0.002	0.17
747	0.034		0.011	0.011	-0.002	1.08
748	0.560		0.000	0.031	0.000	0.01
749	3.692		-0.002	0.031	0.000	-0.06
750	6.261		-0.003	0.031	0.001	-0.10
			$\alpha = 4^o$, V = 30 fps			
752	6.261		0.014	0.032	-0.003	0.43
753	3.683		0.014	0.031	-0.003	0.44
754	1.598		0.014	0.029	-0.002	0.47
755	0.974		0.015	0.029	-0.003	0.51
756	0.660		0.016	0.029	-0.004	0.54
757	0.558		0.016	0.029	-0.004	0.56
758	0.452		0.017	0.031	-0.005	0.54
759	0.350		0.018	0.032	-0.005	0.56
760	0.243		0.019	0.026	-0.005	0.75
761	0.137		0.021	0.019	-0.005	1.13
762	0.085		0.019	0.016	-0.005	1.21
763	0.034		0.023	0.010	-0.007	2.28
764	0.555		0.017	0.030	-0.004	0.56
765	3.690		0.014	0.032	-0.003	0.44
			$\alpha = 6^o$, V = 30 fps			
773	0.452		0.050	0.036	-0.011	1.38
774	0.345		0.048	0.035	-0.012	1.36
775	0.251		0.051	0.031	-0.013	1.64
776	0.144		0.052	0.022	-0.012	2.39
777	0.090		0.054	0.018	-0.012	3.10
778	0.038		0.060	0.016	-0.015	3.82
779	0.567		0.048	0.036	-0.011	1.33
780	3.752		0.048	0.035	-0.011	1.37
781	6.386		0.050	0.035	-0.012	1.44

AR = 0.5 (Cont'd)

Film No.	σ_v	σ_k	C_L	C_D	C_M	L/D
			$\alpha = 8^o$, V = 30 fps			
783	6.408		0.087	0.042	-0.020	2.06
784	3.819		0.084	0.042	-0.019	2.00
785	1.656		0.083	0.030	-0.017	2.76
786	0.903		0.081	0.041	-0.018	2.00
787	0.688		0.083	0.041	-0.019	2.03
788	0.582		0.082	0.041	-0.019	1.99
789	0.469		0.082	0.041	-0.019	1.99
790	0.356		0.082	0.039	-0.017	2.09
791	0.250		0.086	0.033	-0.018	2.62
792	0.145		0.088	0.027	-0.019	3.25
793	0.097		0.098	0.021	-0.022	4.74
794	0.041	0.019	0.102	0.015	-0.035	6.93
795	0.029	0.014	0.095	0.014	-0.031	6.96
796	0.602		0.089	0.042	-0.018	2.13
797	3.720		0.084	0.037	-0.017	2.25
798	6.291		0.086	0.042	-0.019	2.06
			$\alpha = 10^o$, V = 30 fps			
800	5.802		0.128	0.055	-0.031	2.34
801	3.848		0.125	0.054	-0.029	2.33
802	1.696		0.125	0.054	-0.028	2.34
803	1.258		0.125	0.054	-0.028	2.31
804	0.930		0.122	0.055	-0.027	2.21
805	0.715		0.121	0.054	-0.027	2.26
806	0.492		0.122	0.051	-0.027	2.40
807	0.384		0.121	0.050	-0.028	2.41
808	0.274		0.129	0.042	-0.030	3.05
809	0.162		0.142	0.033	-0.036	4.34
810	0.111	0.091	0.164	0.029	-0.062	5.62
811	0.053	0.037	0.123	0.018	-0.042	6.81
812	0.045	0.026	0.123	0.019	-0.042	6.56
813	0.166	0.093	0.143	0.034	-0.037	4.23
814	0.717		0.123	0.052	-0.032	2.35
815	3.883		0.126	0.052	-0.032	2.44
816	6.512		0.127	0.054	-0.032	2.38
			$\alpha = 15^o$, V = 30 fps			
836	6.630		0.271	0.097	-0.076	2.81
837	4.026		0.272	0.098	-0.075	2.78
838	1.647		0.274	0.096	-0.075	2.84
839	1.400		0.274	0.096	-0.075	2.86
840	1.195		0.272	0.096	-0.075	2.83
841	0.863		0.272	0.096	-0.075	2.83
842	0.627		0.270	0.095	-0.072	2.85
843	0.417		0.280	0.093	-0.081	3.01
844	0.282	0.257	0.304	0.081	-0.111	3.78
845	0.227	0.211	0.301	0.083	-0.122	3.63
846	0.174	0.160	0.275	0.076	-0.109	3.61
847	0.119	0.106	0.217	0.058	-0.082	3.74
848	0.059	0.041	0.181	0.048	-0.066	3.73
849	0.061	0.044	0.184	0.049	-0.067	3.73
850	0.074	0.054	0.182	0.049	-0.065	3.70
851	0.103	0.074	0.185	0.054	-0.066	3.45
852	0.733		0.266	0.094	-0.072	2.82
853	4.142		0.273	0.099	-0.075	2.76
854	6.885		0.276	0.099	-0.077	2.80
			$\alpha = 20^o$, V = 30 fps			
856	6.746		0.452	0.169	-0.147	2.67
857	3.982		0.450	0.168	-0.146	2.68
858	2.317		0.449	0.167	-0.145	2.69
859	1.992		0.446	0.167	-0.144	2.67
860	1.635		0.450	0.169	-0.146	2.66
861	1.405		0.445	0.167	-0.145	2.66
862	1.200		0.444	0.167	-0.145	2.66
863	0.974		0.446	0.168	-0.145	2.65
864	0.752		0.444	0.167	-0.148	2.66
865	0.519	0.453	0.450	0.169	-0.163	2.66
866	0.402	0.360	0.464	0.173	-0.202	2.68
867	0.290	0.266	0.398	0.150	-0.173	2.65
868	0.231	0.201	0.341	0.130	-0.145	2.63
869	0.173	0.151	0.312	0.120	-0.131	2.61
870	0.122	0.108	0.270	0.105	-0.111	2.56
871	0.095	0.073	0.246	0.096	-0.099	2.56

Table II - Cavitating Flow (Cont'd)

AR = 0.5 (Cont'd)

Film No.	σ_v	σ_k	C_L	C_D	C_M	L/D
			$\alpha = 20^o$ (Cont'd)			
872	0.109	0.091	0.249	0.098	-0.100	2.54
873	0.097	0.075	0.242	0.095	-0.096	2.54
874	0.732		0.445	0.170	-0.152	2.62
875	4.048		0.442	0.166	-0.145	2.67
876	6.807		0.446	0.166	-0.146	2.68
			$\alpha = 25^o$, V = 30 fps			
878	6.757		0.626	0.280		2.24
879	4.033		0.636	0.282		2.25
880	2.799		0.626	0.275		2.28
881	2.439		0.628	0.274		2.29
882	1.996		0.621	0.276		2.25
883	1.546		0.624	0.276		2.26
884	1.208		0.628	0.277		2.27
885	0.979		0.620	0.277		2.23
886	0.866		0.615	0.274		2.24
887	0.756	0.658	0.611	0.273		2.24
888	0.639	0.588	0.616	0.272		2.26
889	0.525	0.492	0.605	0.276	-0.278	2.20
890	0.408	0.378	0.517	0.238	-0.236	2.18
891	0.291	0.260	0.433	0.198	-0.192	2.19
892	0.192	0.168	0.364	0.168	-0.157	2.17
893	0.132	0.106	0.320	0.150	-0.134	2.13
894	0.104	0.104	0.320	0.146	-0.133	2.19
895	1.082		0.611	0.268	-0.238	2.28
896	3.337		0.630	0.271	-0.221	2.33
897	6.770		0.626	0.270	-0.220	2.32
			$\alpha = 30^o$, V = 30 fps			
900	6.865		0.801	0.434		1.85
901	4.094		0.796	0.433	-0.308	1.84
902	3.386		0.799	0.433	-0.309	1.85
903	2.935		0.802	0.430	-0.309	1.86
904	2.358		0.794	0.435	-0.306	1.82
905	2.020		0.796	0.435	-0.307	1.83
906	1.573		0.811	0.439	-0.319	1.85
907	1.228		0.795	0.431	-0.322	1.84
908	0.887	0.808	0.762	0.417	-0.330	1.83
909	0.655	0.621	0.724	0.423	-0.359	1.71
910	0.422	0.389	0.550	0.328	-0.265	1.68
911	0.314	0.274	0.477	0.286	-0.225	1.67
912	0.198	0.172	0.401	0.244	-0.184	1.64
913	0.174	0.153	0.376	0.236	-0.171	1.59
914	0.179	0.137	0.385	0.237	-0.176	1.62
915	1.881		0.801	0.437		1.83
916	4.063		0.796	0.430	-0.307	1.85
917	6.903		0.803	0.433	-0.310	1.86

Film No.	σ_v	σ_k	C_L	C_D	C_M	L/D
			$\alpha = 25^o$, V = 20 fps			
919	13.850		0.601	0.269	-0.214	2.23
920	8.795		0.614	0.277	-0.217	2.22
921	2.937		0.612	0.274	-0.216	2.24
922	2.468		0.611	0.272	-0.214	2.25
923	2.042		0.611	0.278	-0.220	2.19
924	1.558		0.617	0.275	-0.219	2.24
925	1.196		0.618	0.277	-0.224	2.23
926	1.073		0.618	0.276	-0.227	2.23
927	0.845		0.616	0.276	-0.236	2.23
928	0.734	0.624	0.611	0.273	-0.250	2.23
929	0.622	0.545	0.609	0.282	-0.276	2.16
930	0.560	0.475	0.605	0.283	-0.282	2.14
931	0.425	0.367	0.541	0.257	-0.252	2.11
932	0.373	0.314	0.518	0.248	-0.239	2.09
933	8.731		0.606	0.274	-0.216	2.21
934	13.753		0.606	0.272	-0.215	2.23
			$\alpha = 30^o$, V = 20 fps			
936	13.967		0.771	0.415	-0.299	1.86
937	8.890		0.773	0.418	-0.298	1.85
938	3.194		0.777	0.417	-0.298	1.87
939	2.486		0.776	0.419	-0.299	1.85
940	1.989		0.775	0.419	-0.297	1.85
941	1.283		0.772	0.416	-0.311	1.86
942	1.050		0.739	0.398	-0.316	1.86
943	0.817		0.726	0.403	-0.325	1.80
944	0.609		0.695	0.405	-0.346	1.72
945	0.506		0.615	0.361	-0.304	1.71
946	0.396		0.530	0.315	-0.251	1.68
947			0.533	0.316	-0.258	1.69
948	2.410		0.776	0.420	-0.298	1.85
949	9.264		0.778	0.420	-0.302	1.85
950	14.109		0.765	0.413	-0.295	1.85

TABLE I

Hydrofoil Models

AR	Chord c Nominal	Chord c Measured	Half Span b Nominal	Half Span b Measured
4.0	1.5 in.	1.503 in.	3.0 in.	3.005 in.
2.0	3.0	2.987	3.0	3.000
1.0	3.0	2.990	1.5	1.500
0.5	4.5	4.412	1.125	1.125

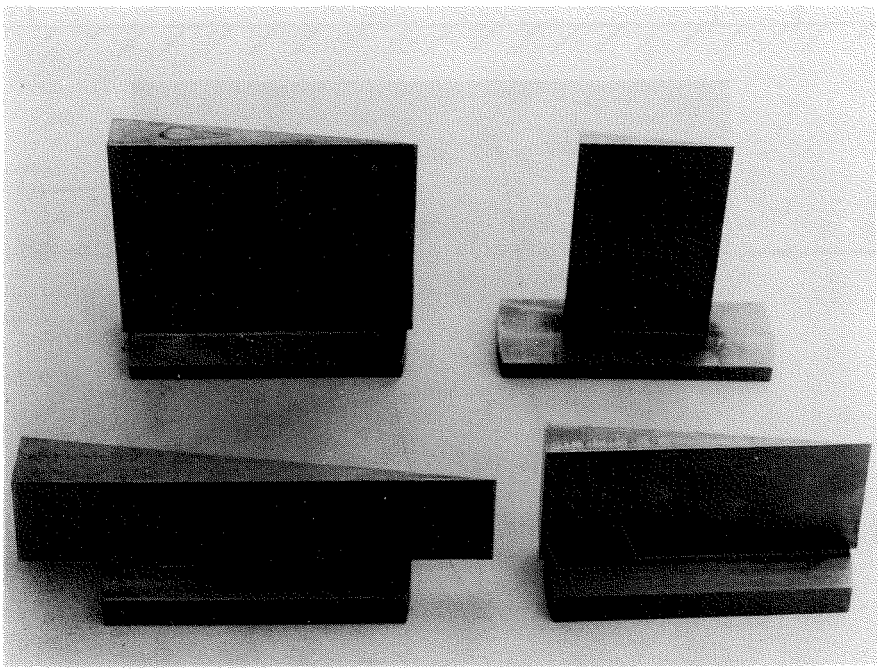

Fig. 1. Wedge Hydrofoil Models.

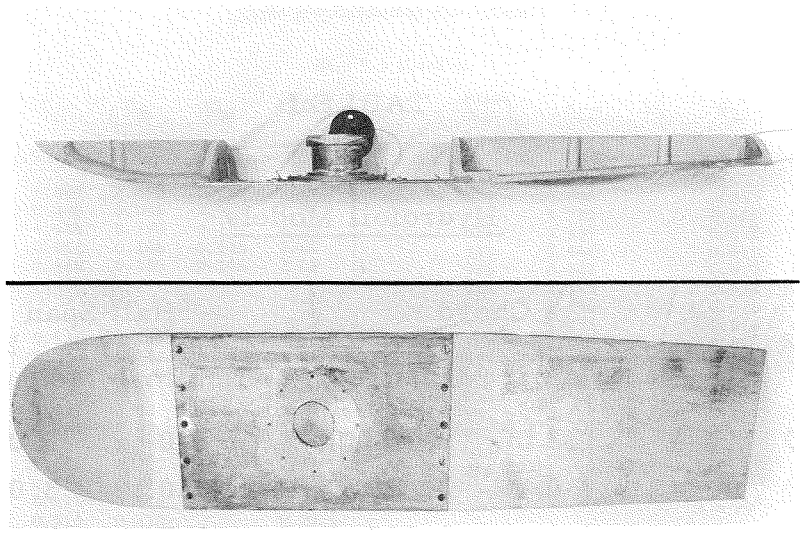

Fig. 2. Assembled Reflection Plate, Nozzle, and Diffuser Blocks.

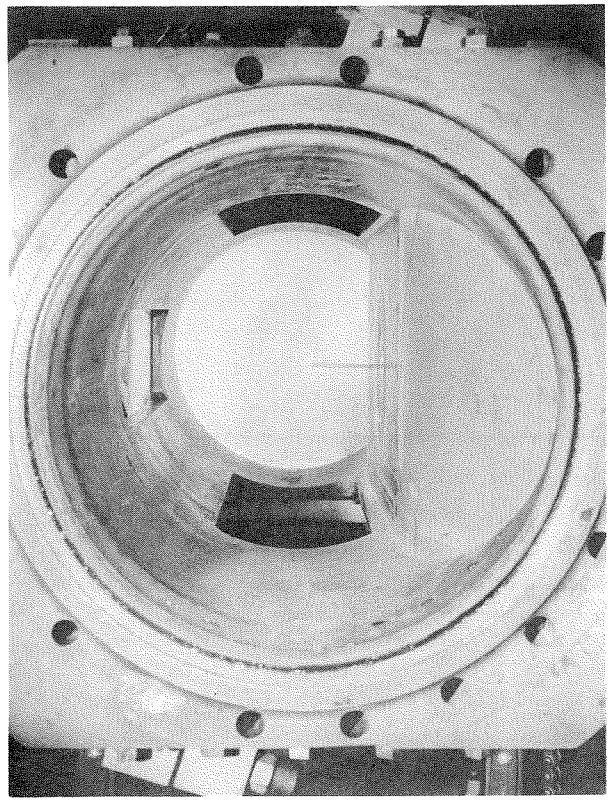

Fig. 3. Reflection Plane Setup in Water Tunnel, Looking Downstream.

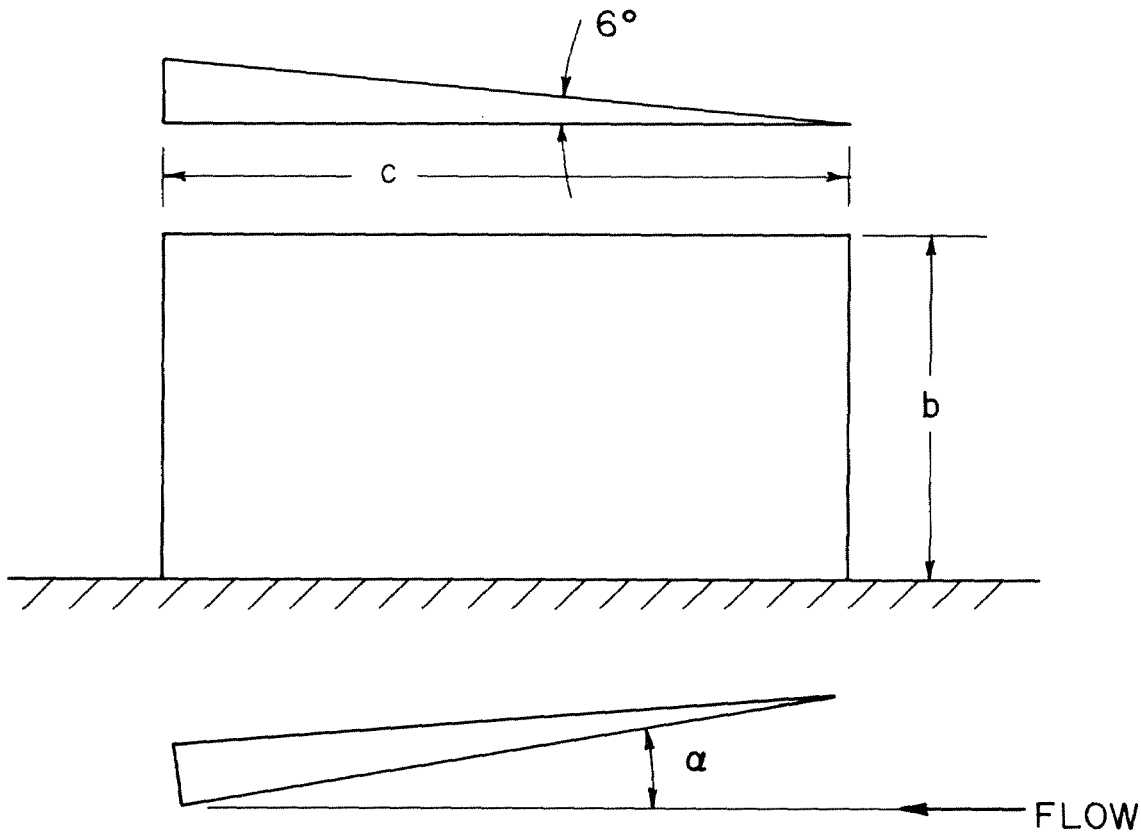

$$AR = \frac{2b}{c} = \frac{2S}{c^2}$$

b = HALF SPAN

c = CHORD

S = PLAN AREA

Fig. 4. Sketch of Wedge Hydrofoil, Showing Angle of Attack Convention.

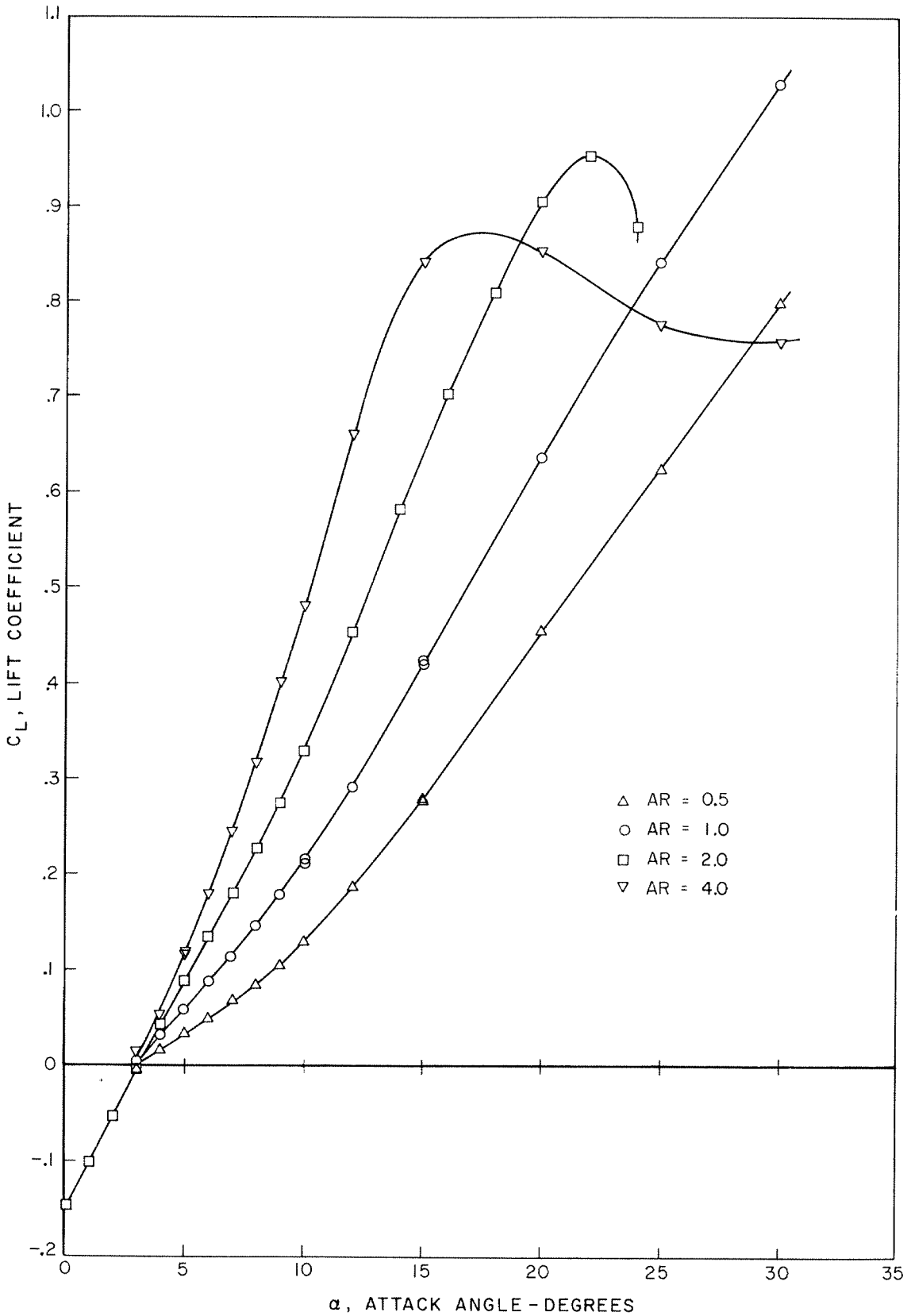

Fig. 5. Lift Coefficient as a Function of Angle of Attack in Noncavitating Flow.

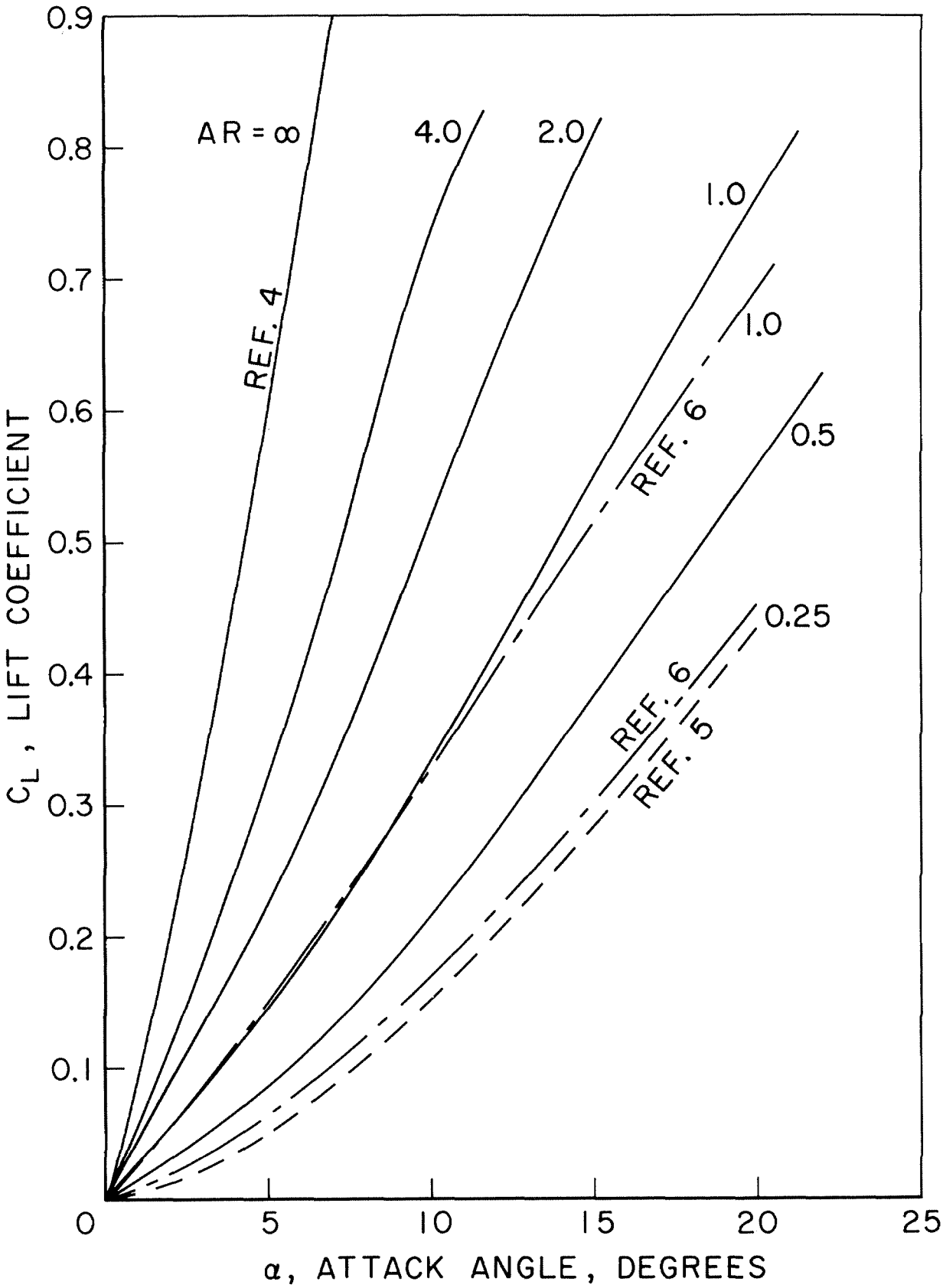

Fig. 6. Comparison of Results for Noncavitating Flow with Towing Tank and Two-dimensional Data

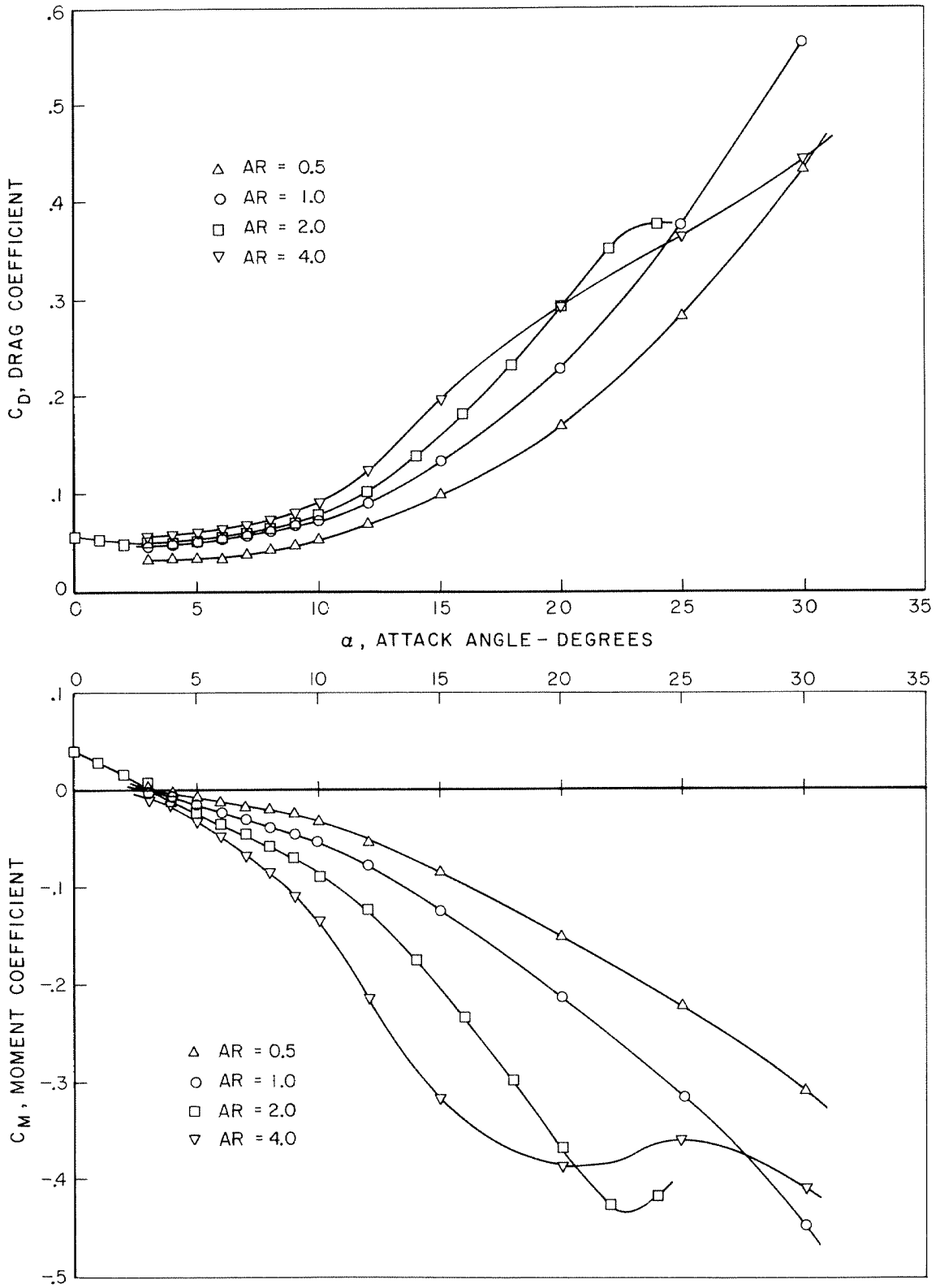

Fig. 7. Drag and Moment Coefficients as a Function of Angle of Attack in Noncavitating Flow.

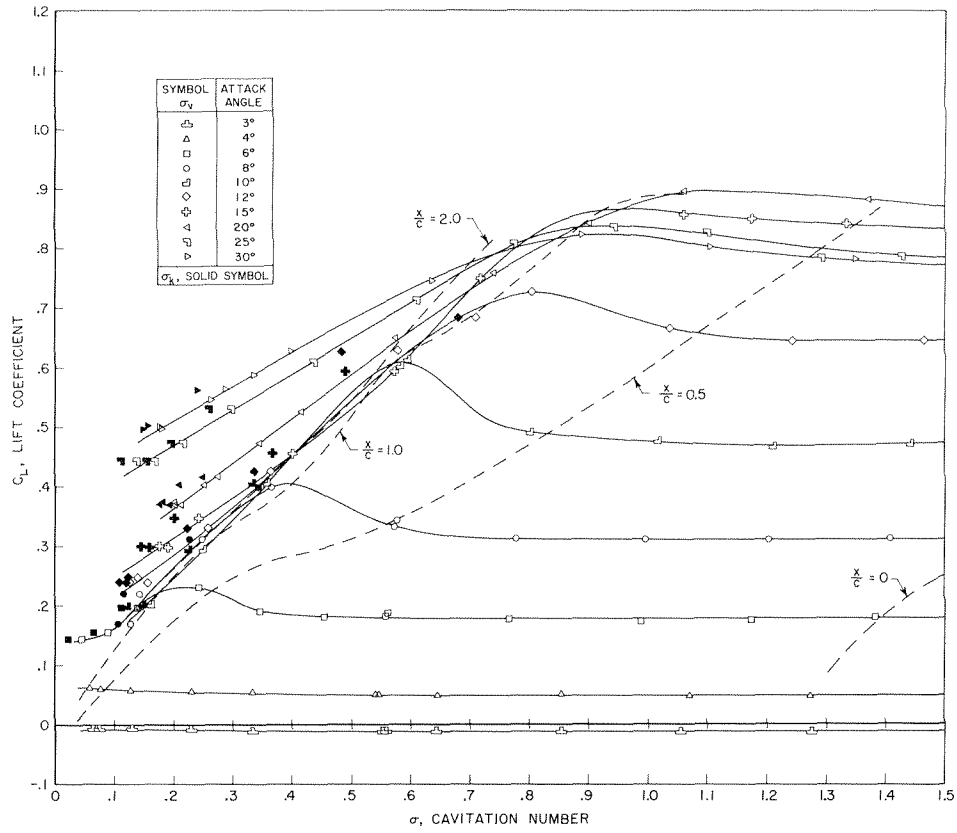

Fig. 8. Lift Coefficient as a Function of Cavitation Number at Constant Angle of Attack, AR = 4.0.

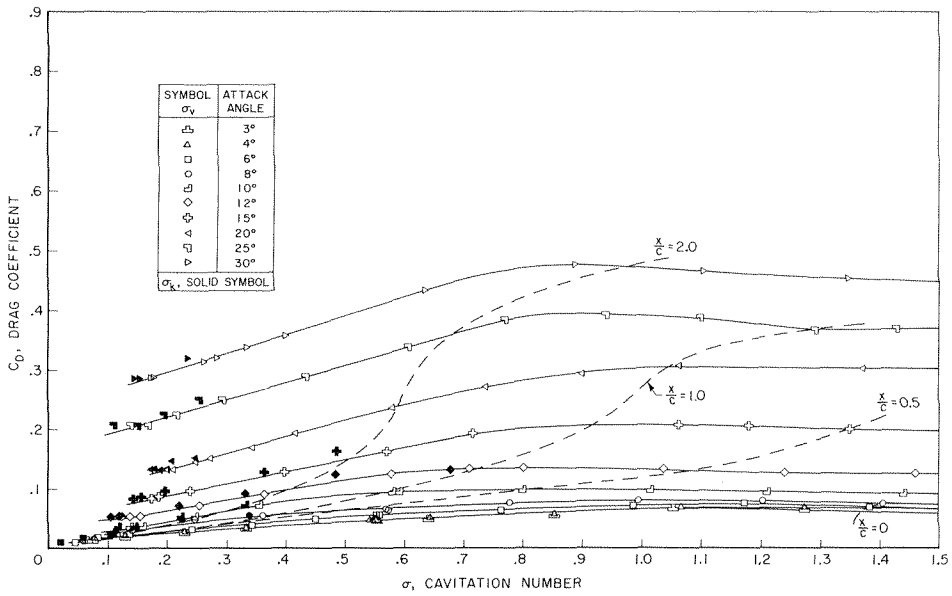

Fig. 9. Drag Coefficient as a Function of Cavitation Number at Constant Angle of Attack, AR = 4.0.

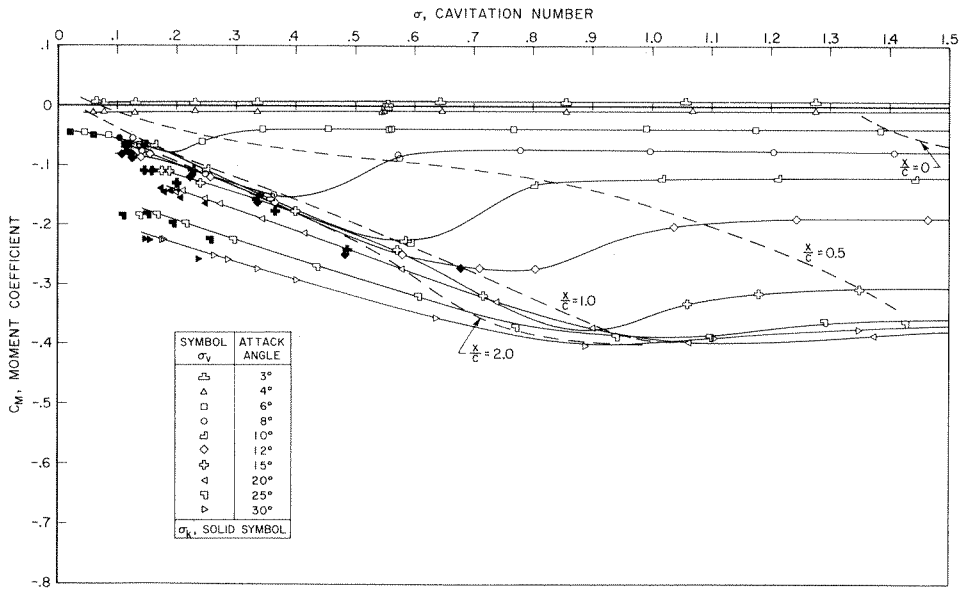

Fig. 10. Moment Coefficient as a Function of Cavitation Number at Constant Angle of Attack, AR = 4.0.

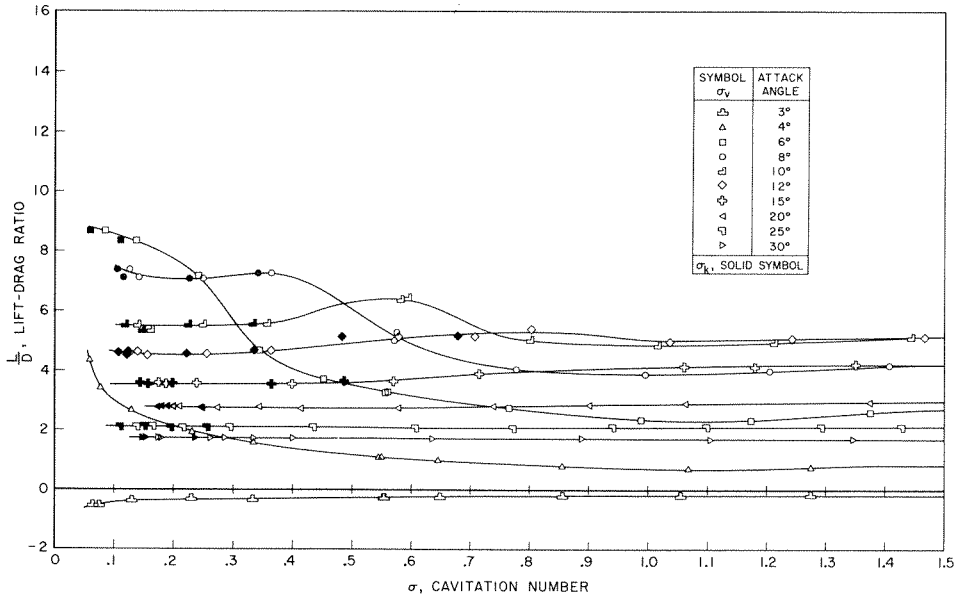

Fig. 11. Lift-Drag Ratio as a Function of Cavitation Number at Constant Angle of Attack, AR = 4.0.

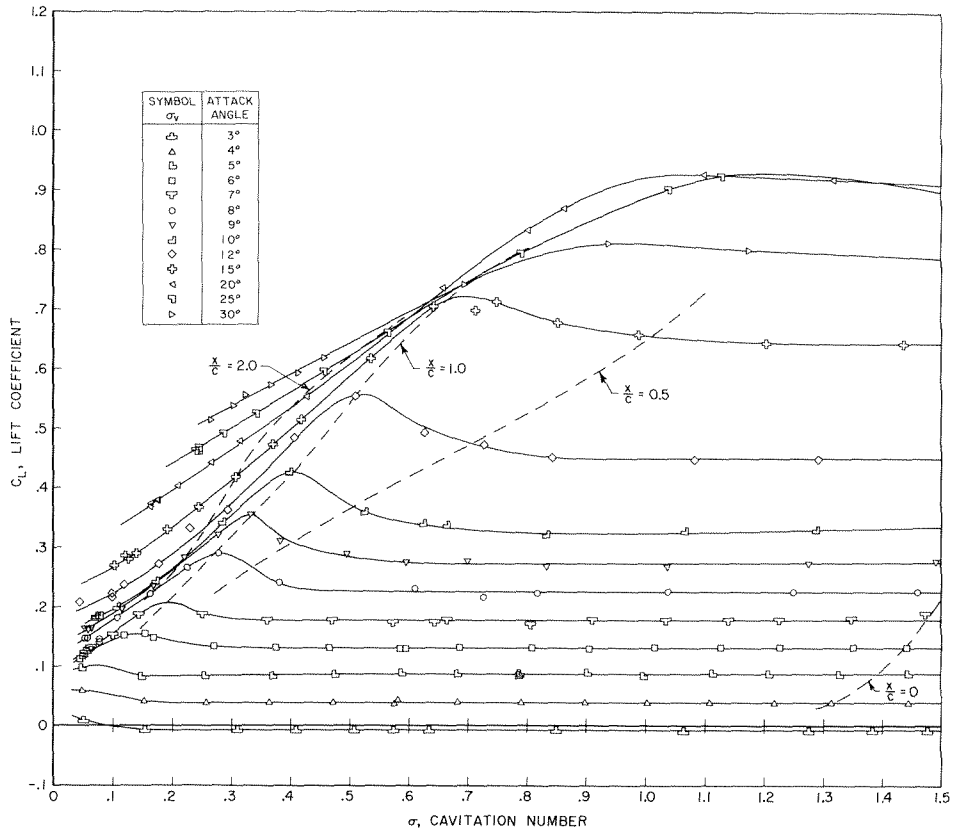

Fig. 12. Lift Coefficient as a Function of Cavitation Number at Constant Angle of Attack, AR = 2.0.

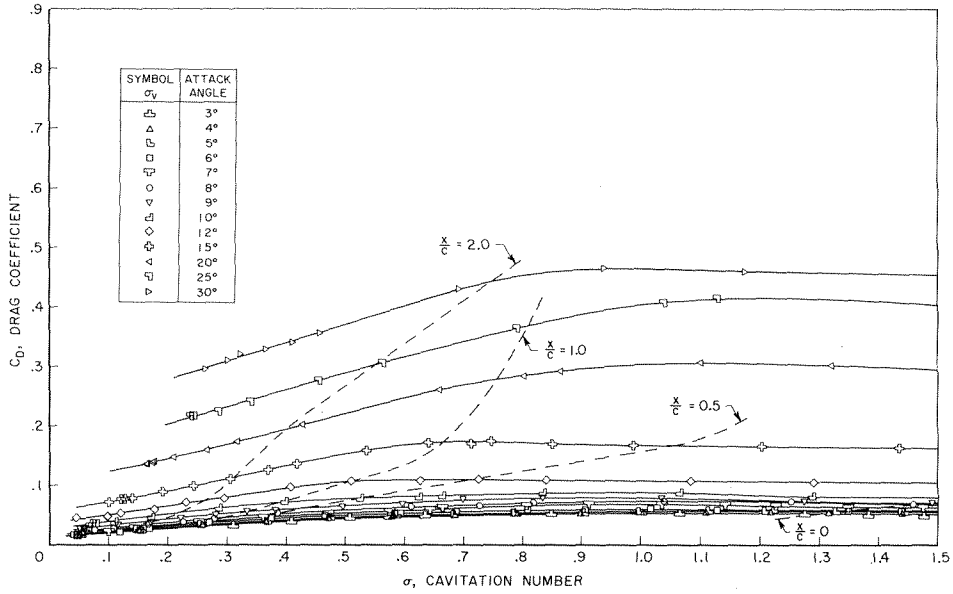

Fig. 13. Drag Coefficient as a Function of Cavitation Number at Constant Angle of Attack, AR = 2.0.

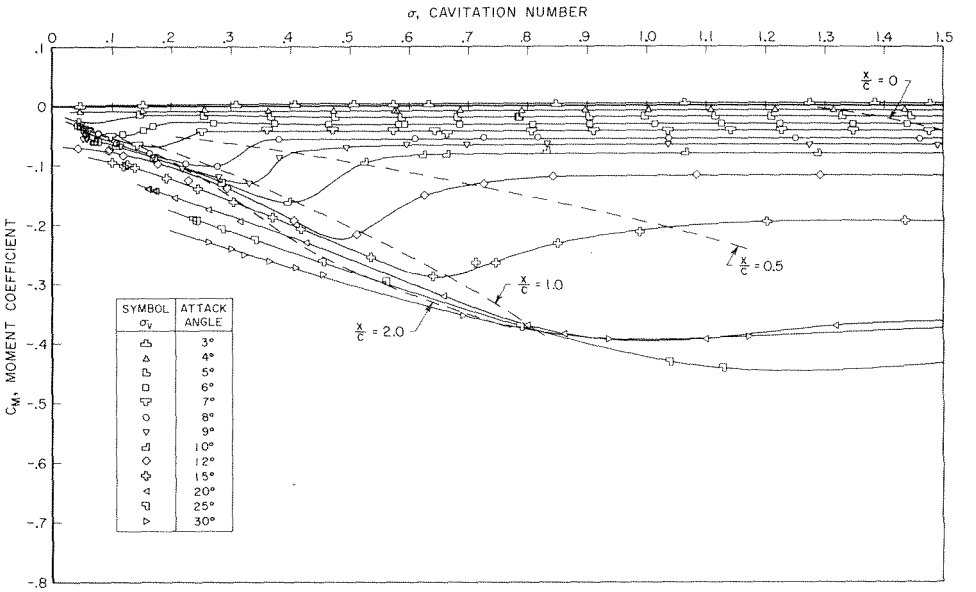

Fig. 14. Moment Coefficient as a Function of Cavitation Number at Constant Angle of Attack, AR = 2.0.

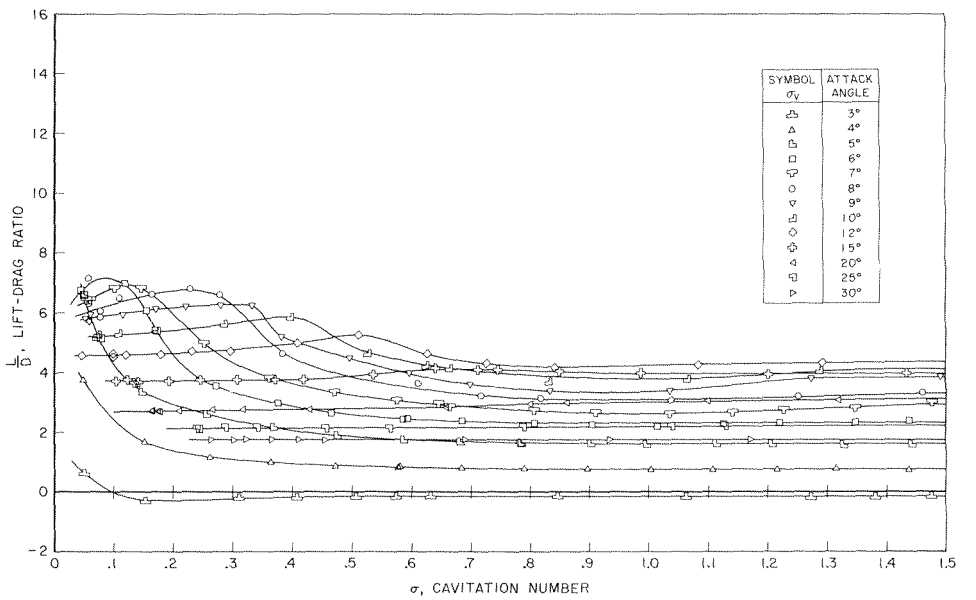

Fig. 15. Lift-Drag Ratio as a Function of Cavitation Number at Constant Angle of Attack, AR = 2.0

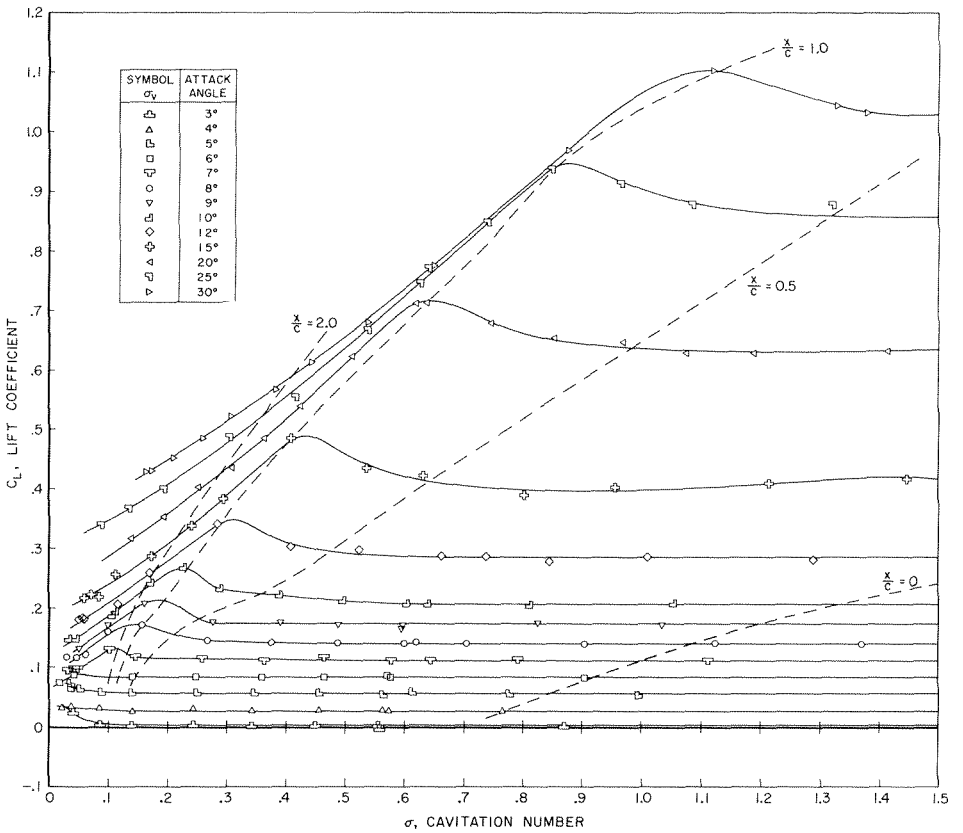

Fig. 16. Lift Coefficient as a Function of Cavitation Number at Constant Angle of Attack, AR = 1.0.

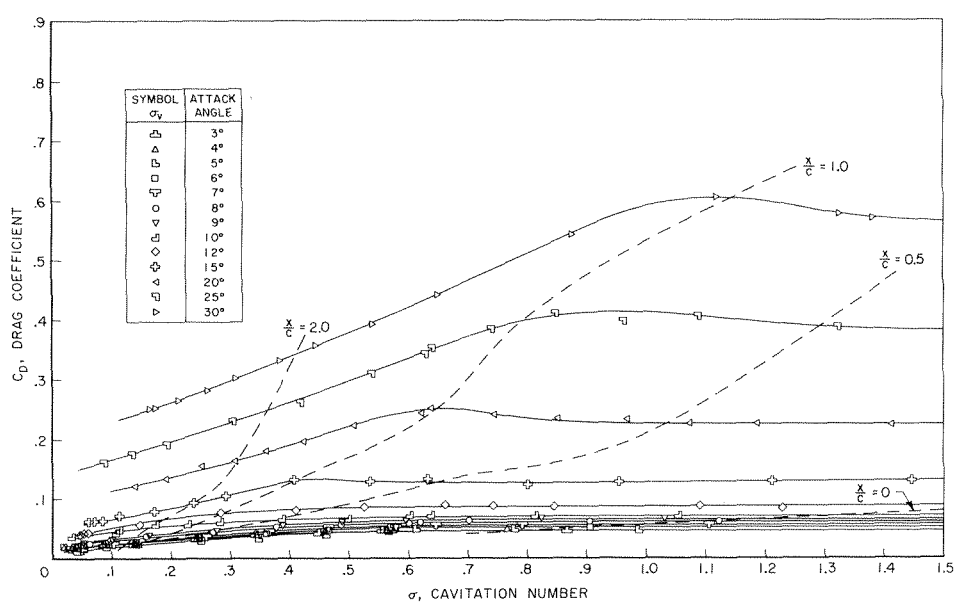

Fig. 17. Drag Coefficient as a Function of Cavitation Number at Constant Angle of Attack, AR = 1.0.

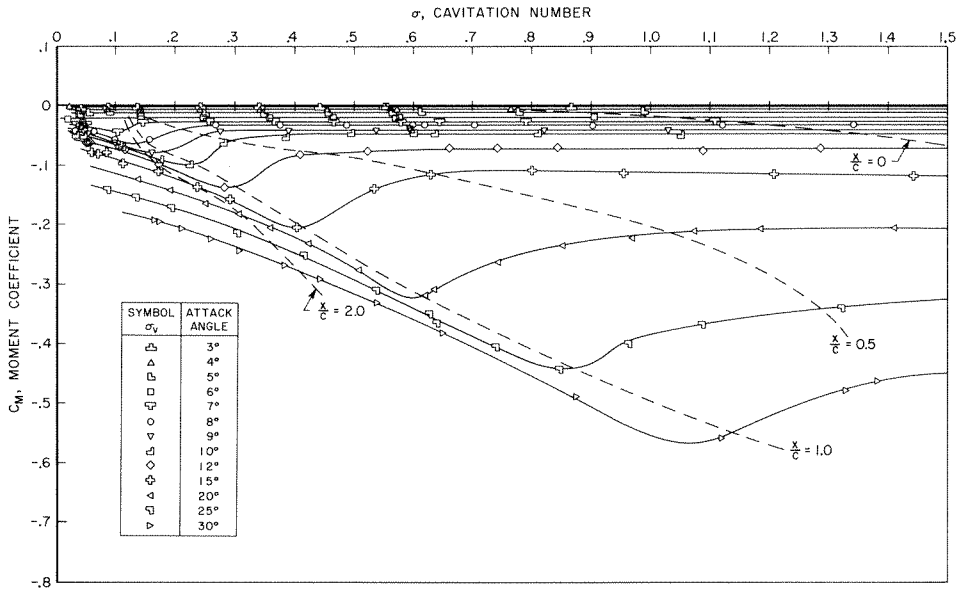

Fig. 18. Moment Coefficient as a Function of Cavitation Number at Constant Angle of Attack, AR = 1.0.

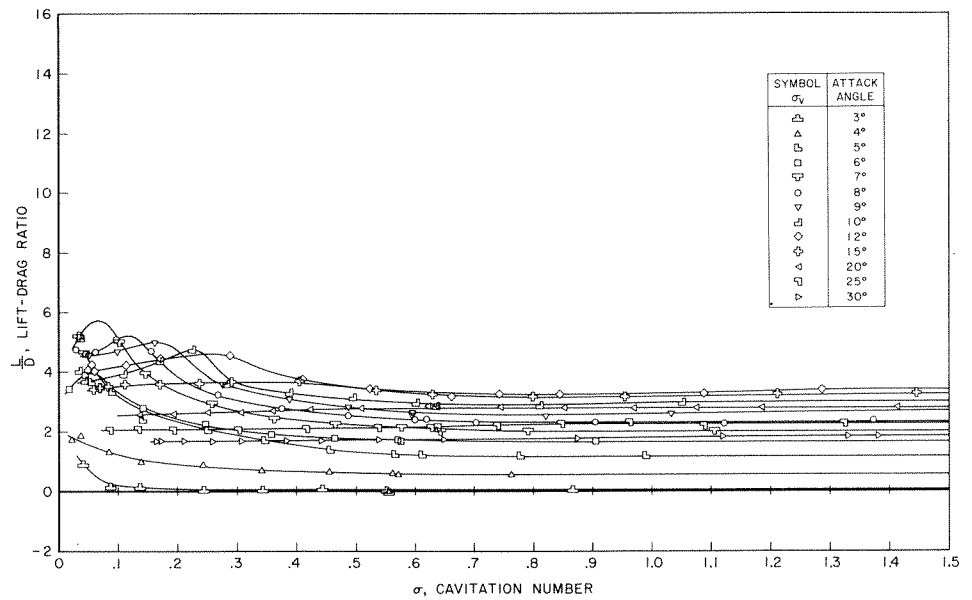

Fig. 19. Lift-Drag Ratio as a Function of Cavitation Number at Constant Angle of Attack, AR = 1.0.

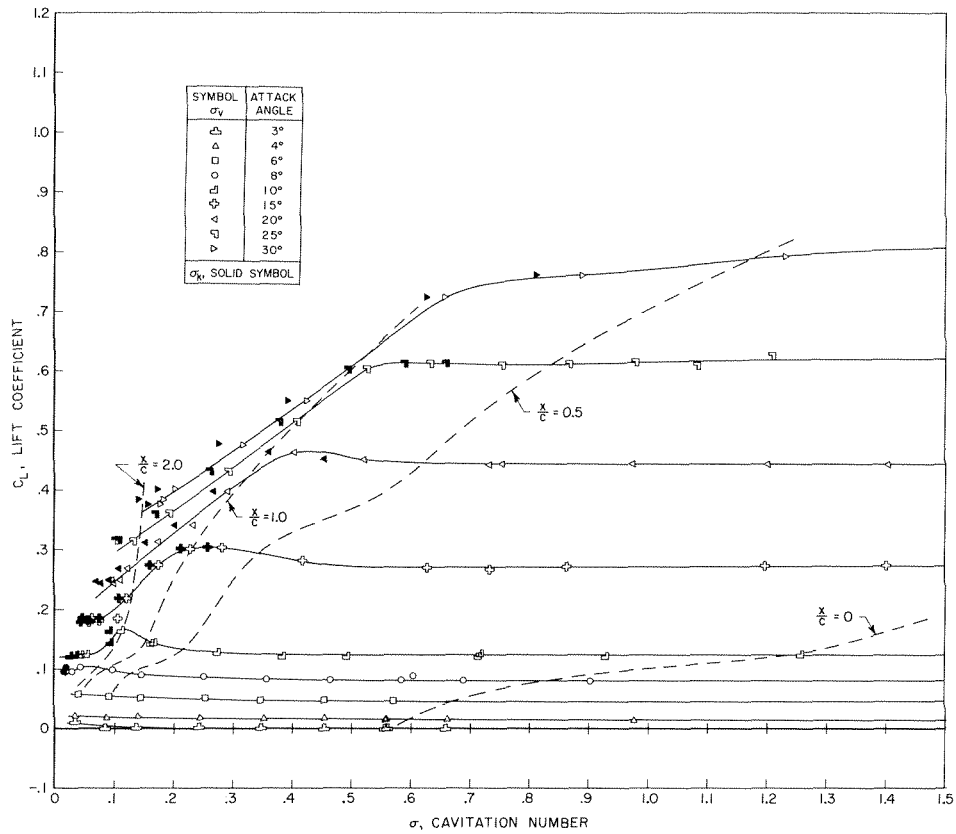

Fig. 20. Lift Coefficient as a Function of Cavitation Number at Constant Angle of Attack, AR = 0.5.

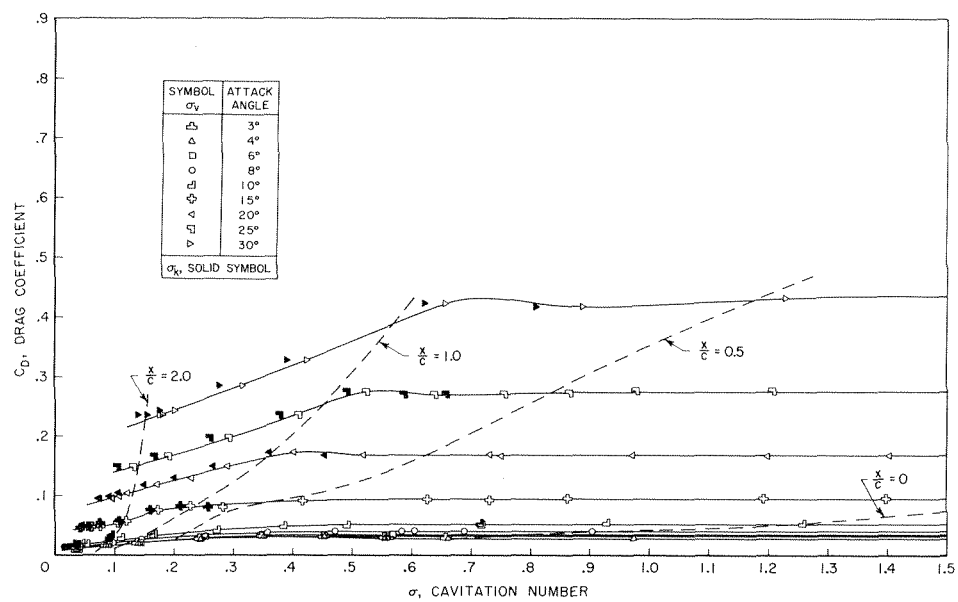

Fig. 21. Drag Coefficient as a Function of Cavitation Number at Constant Angle of Attack, AR = 0.5.

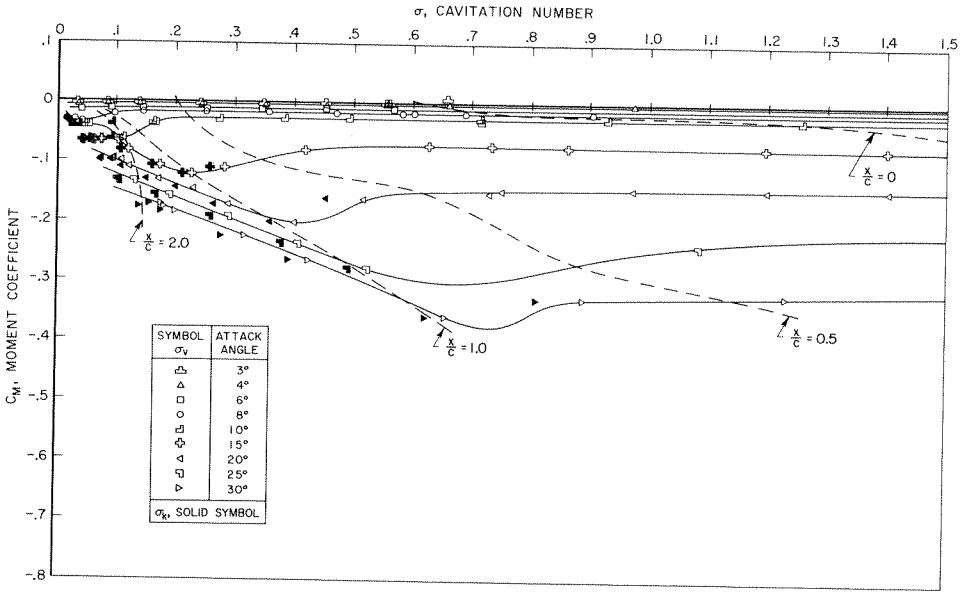

Fig. 22. Moment Coefficient as a Function of Cavitation Number at Constant Angle of Attack, AR = 0.5.

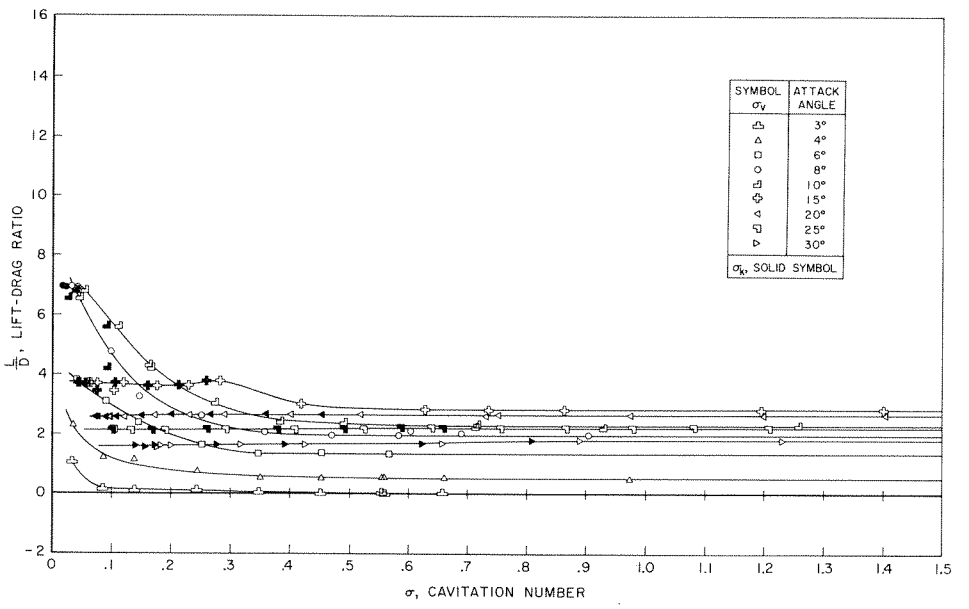

Fig. 23. Lift-Drag Ratio as a Function of Cavitation Number at Constant Angle of Attack, AR = 0.5.

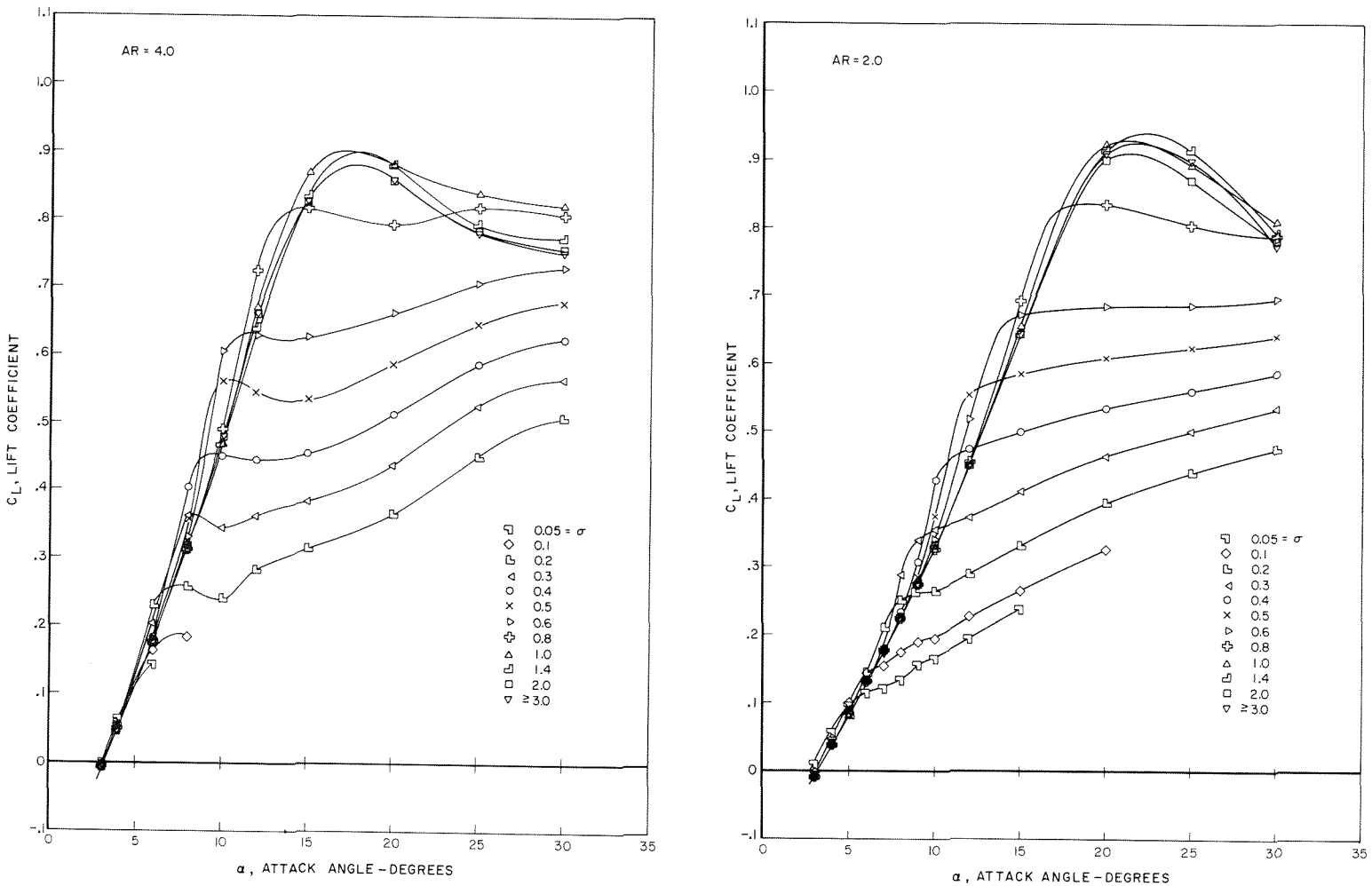

Fig. 24. Lift Coefficient as a Function of Angle of Attack at Constant Cavitation Number, AR = 4.0, 2.0.

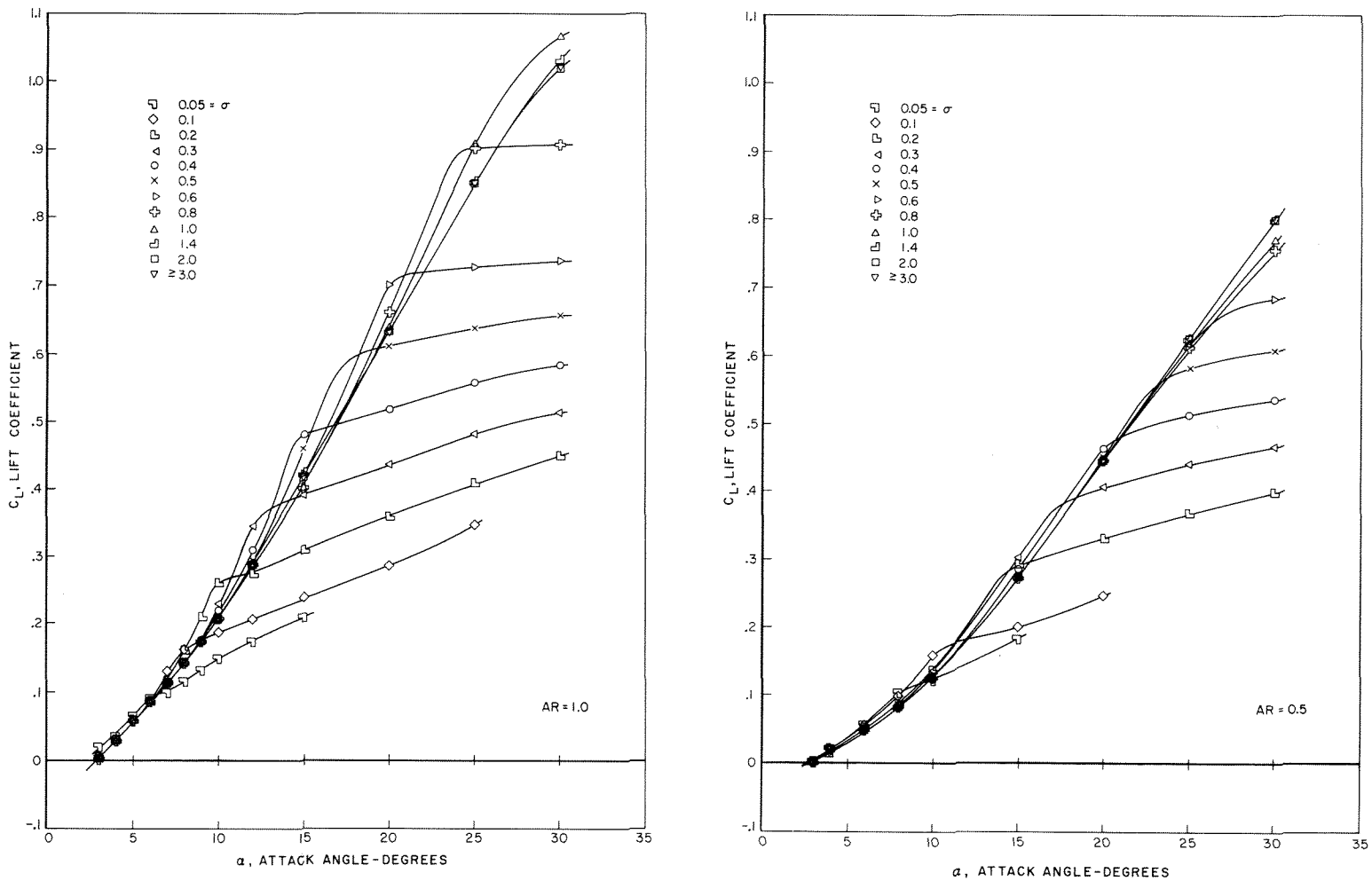

Fig. 25. Lift Coefficient as a Function of Angle of Attack at Constant Cavitation Number, AR = 1.0, 0.5.

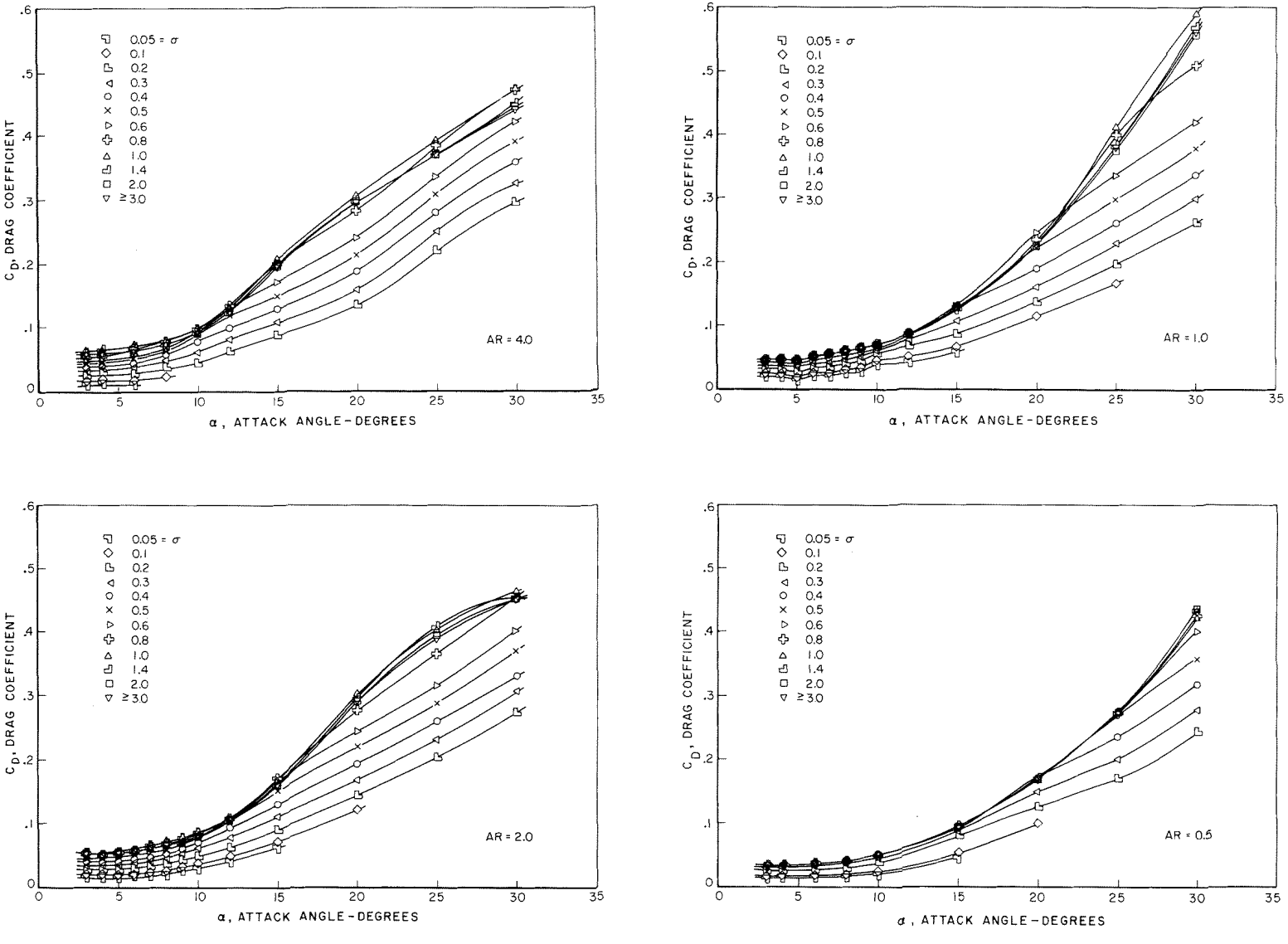

Fig. 26. Drag Coefficient as a Function of Angle of Attack at Constant Cavitation Number, AR = 4.0, 2.0, 1.0, 0.5.

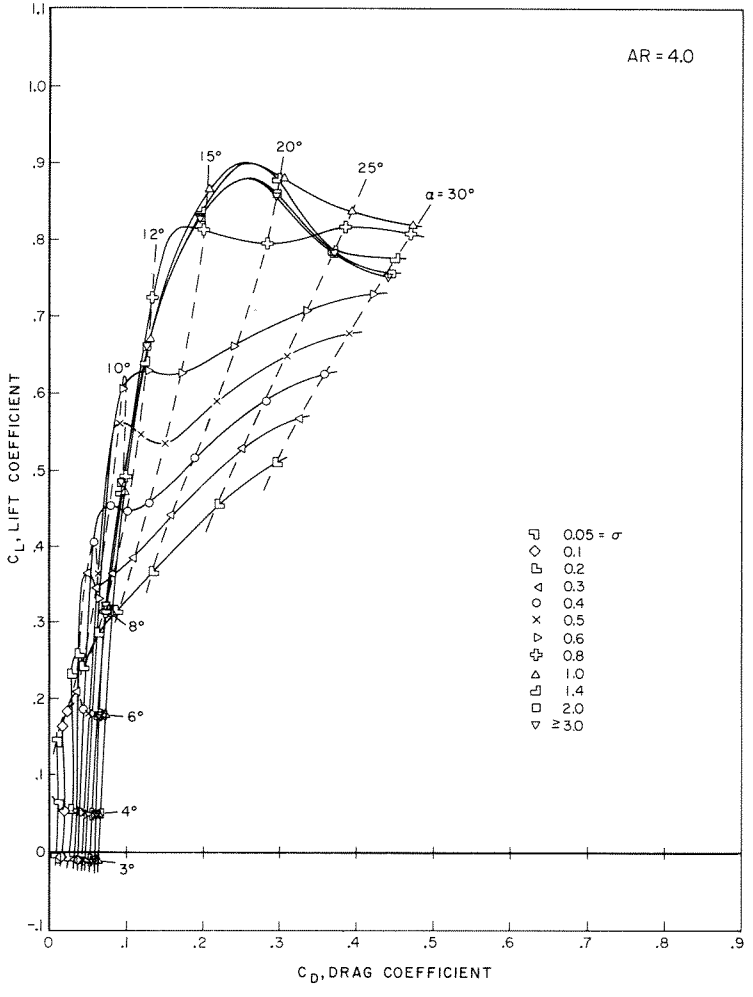

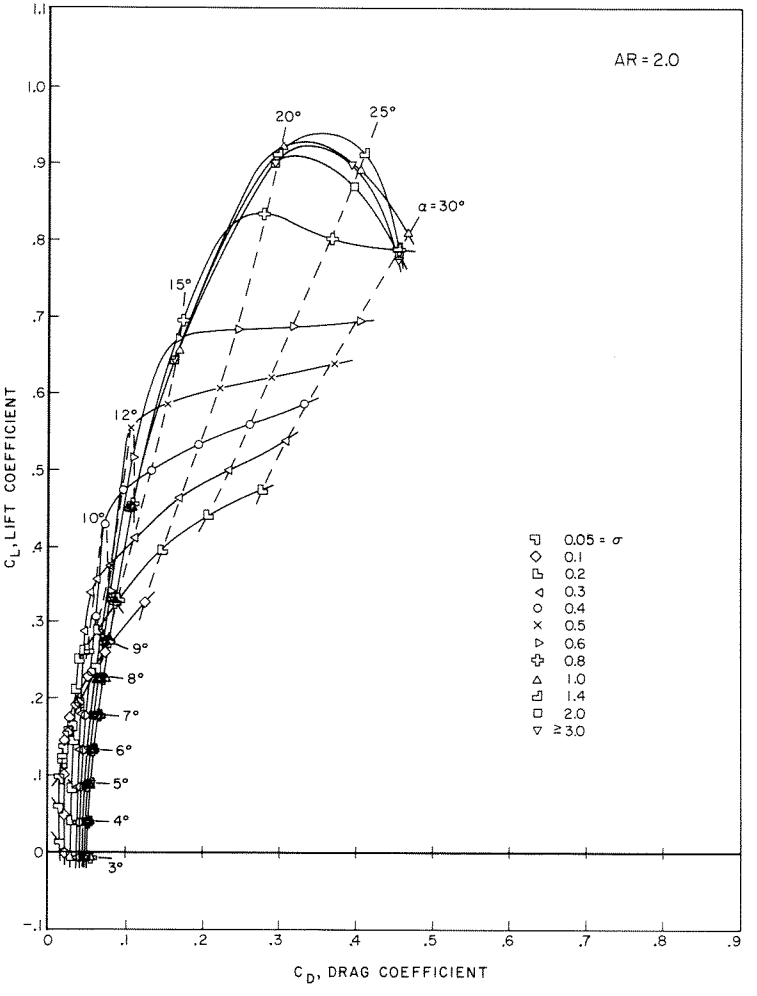

Fig. 27. Cavitation Polar Diagrams, AR = 4.0, 2.0.

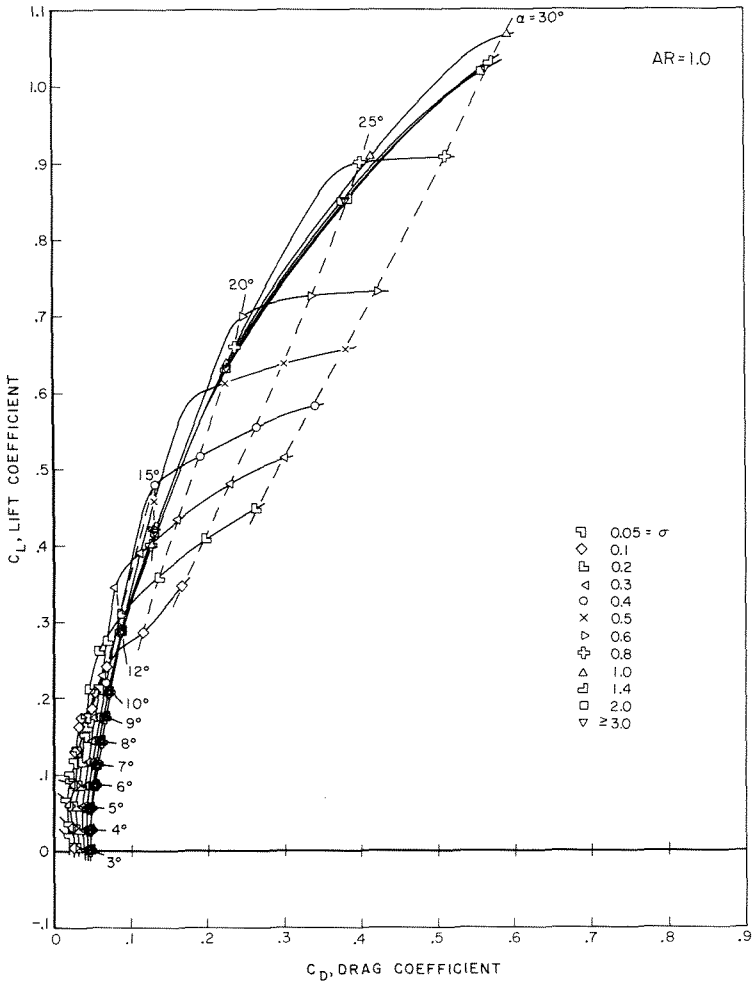

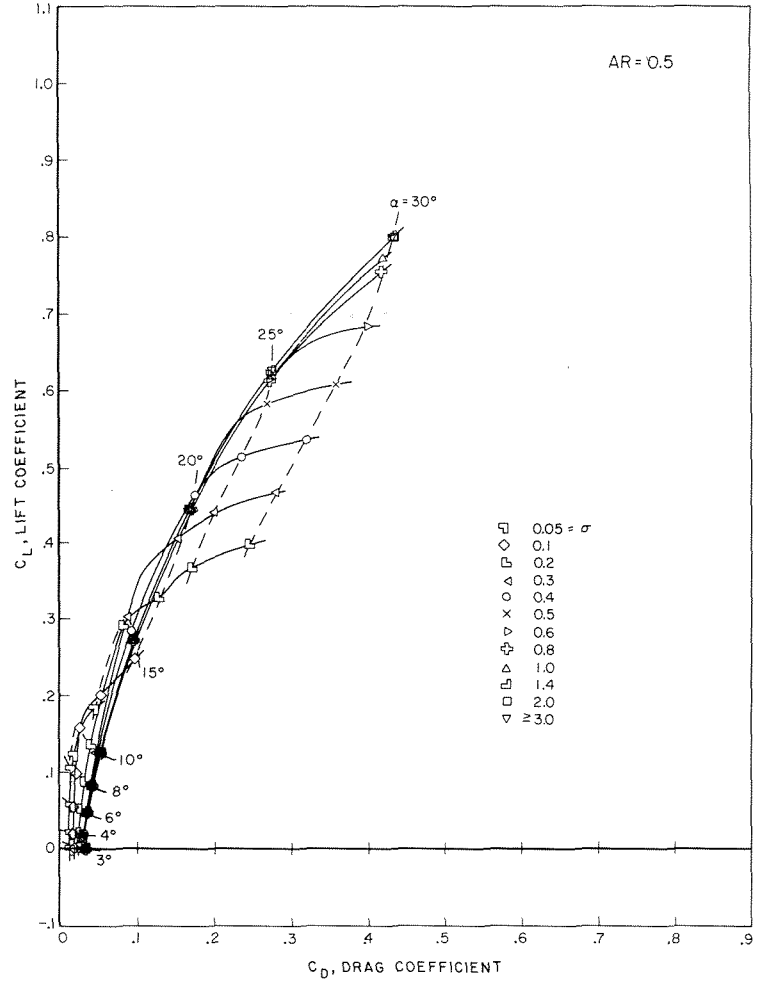

Fig. 28. Cavitation Polar Diagrams, AR = 1.0, 0.5.

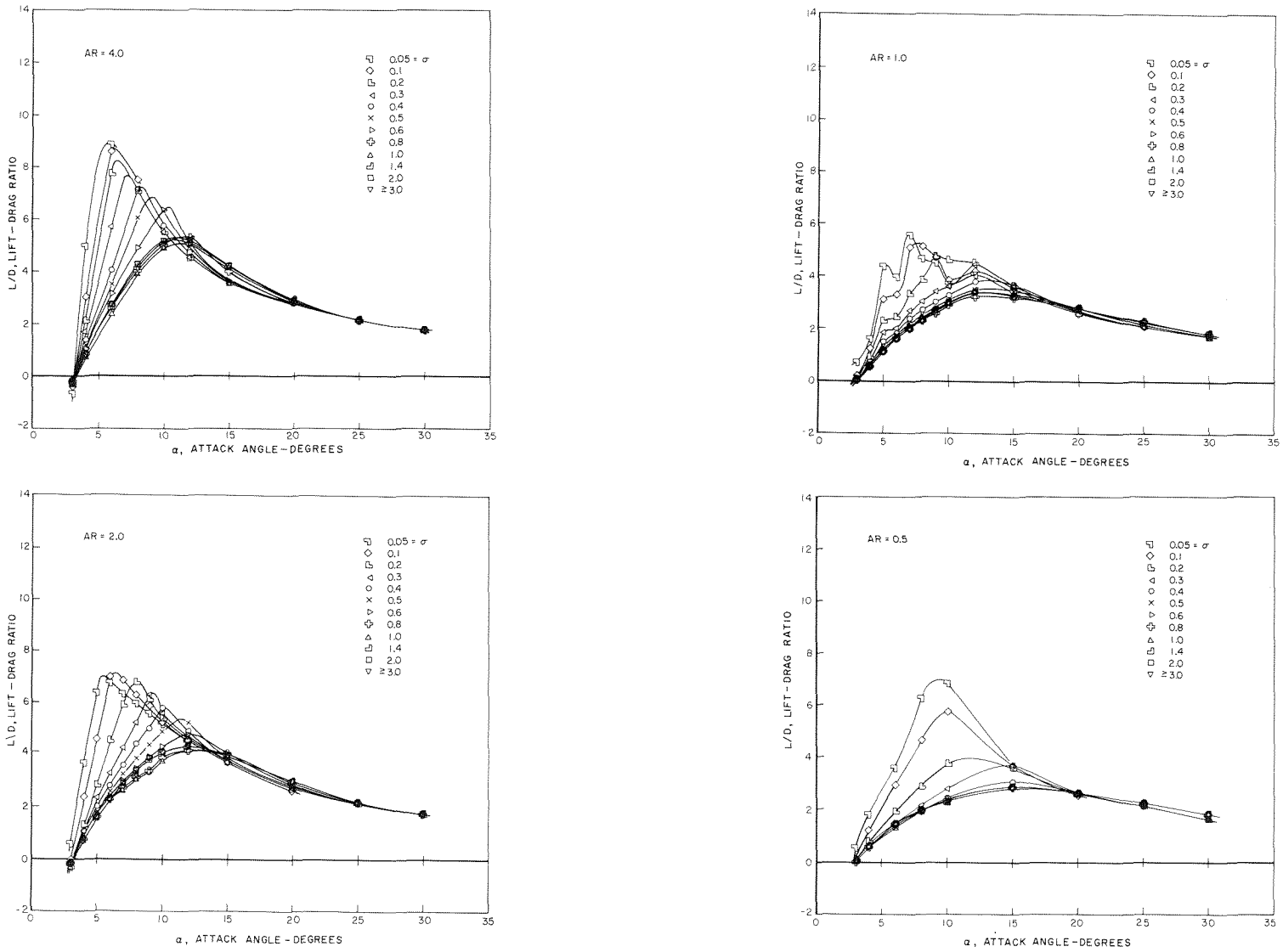

Fig. 29. Lift-Drag Ratio as a Function of Angle of Attack at Constant Cavitation Number, AR = 4.0, 2.0, 1.0, 0.5.

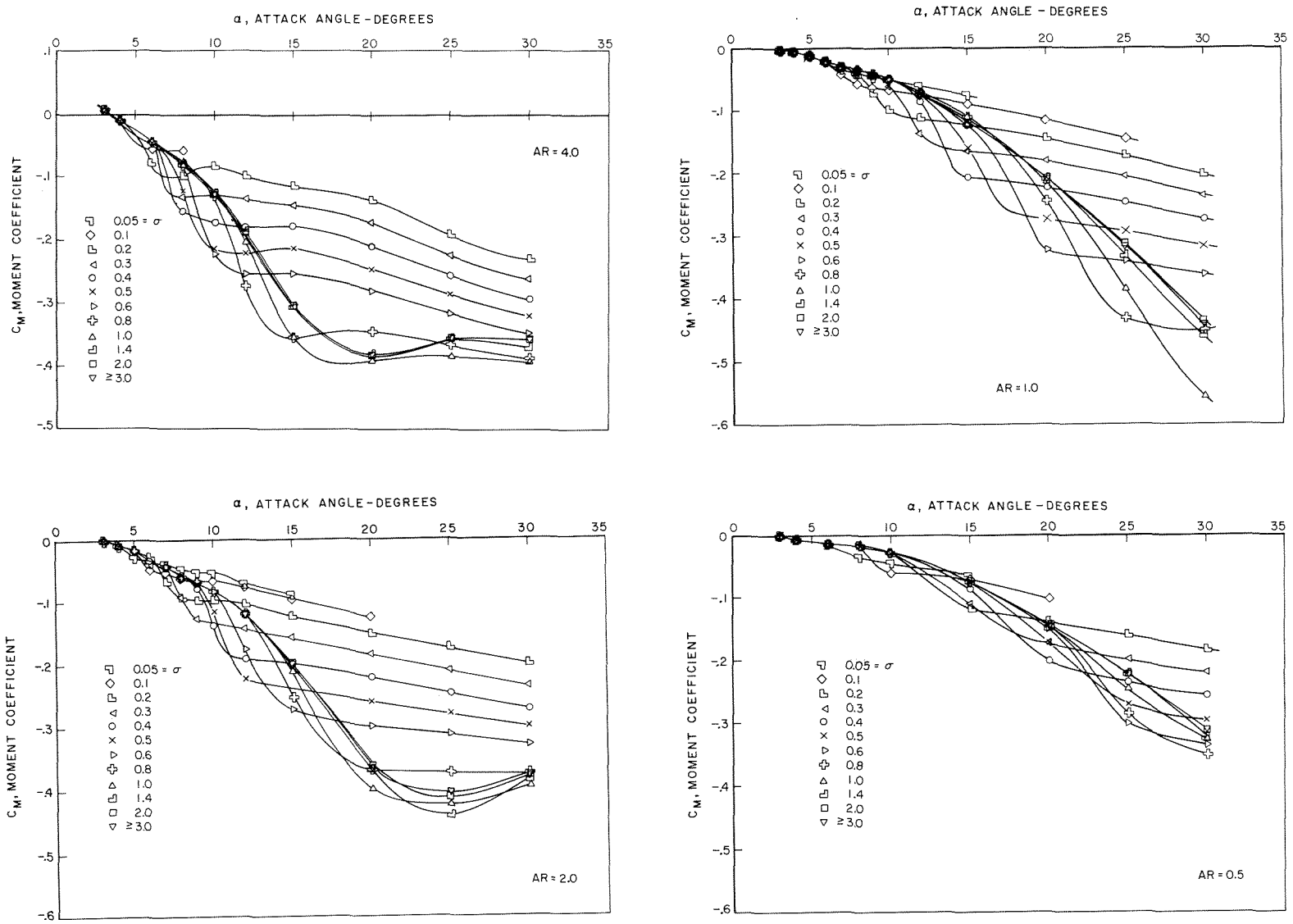

Fig. 30. Moment Coefficient as a Function of Angle of Attack at Constant Cavitation Number, AR = 4.0, 2.0, 1.0, 0.5.

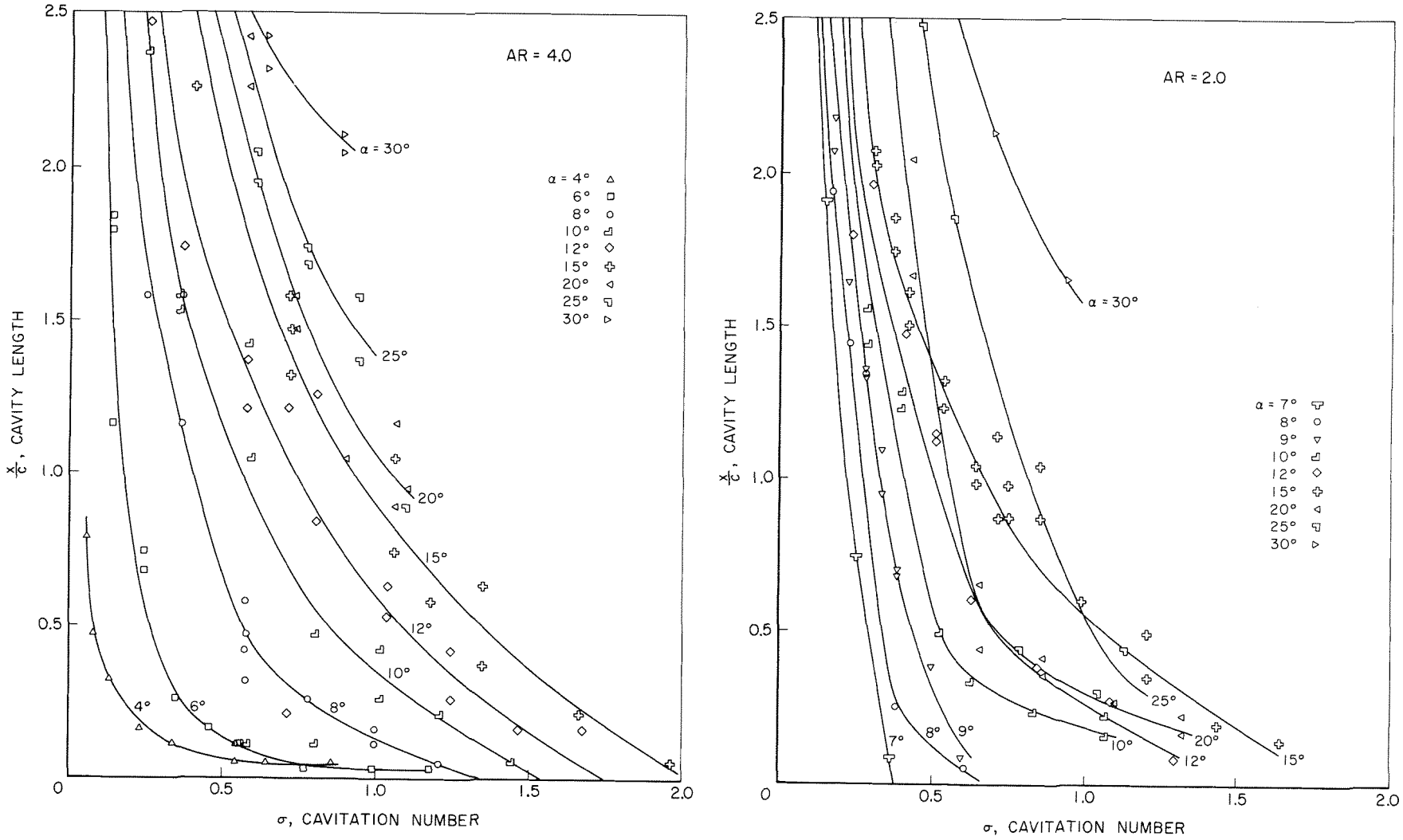

Fig. 31. Dimensionless Cavity Length as a Function of Cavitation Number AR = 4.0, 2.0.

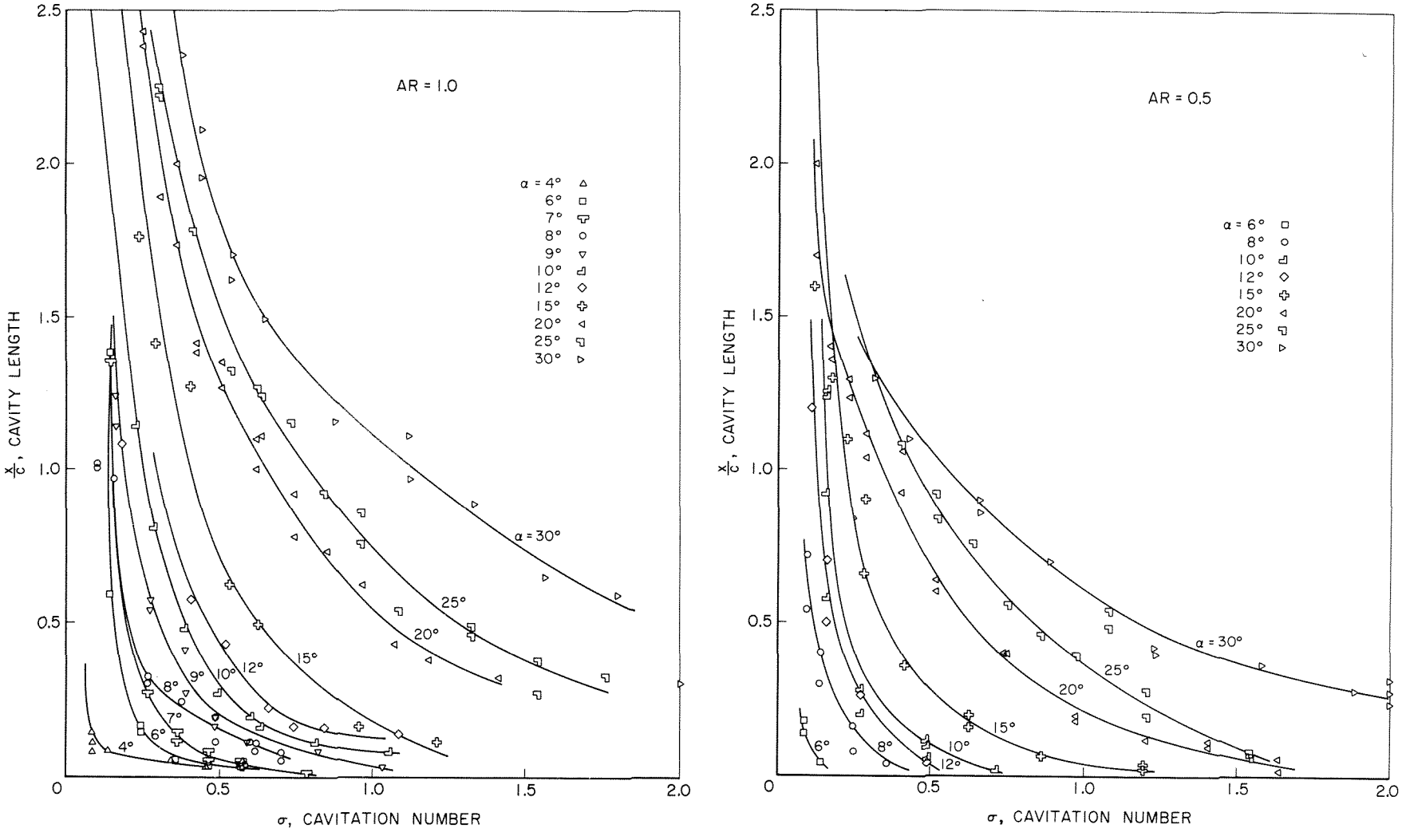

Fig. 32. Dimensionless Cavity Length as a Function of Cavitation Number
AR = 1.0, 0.5

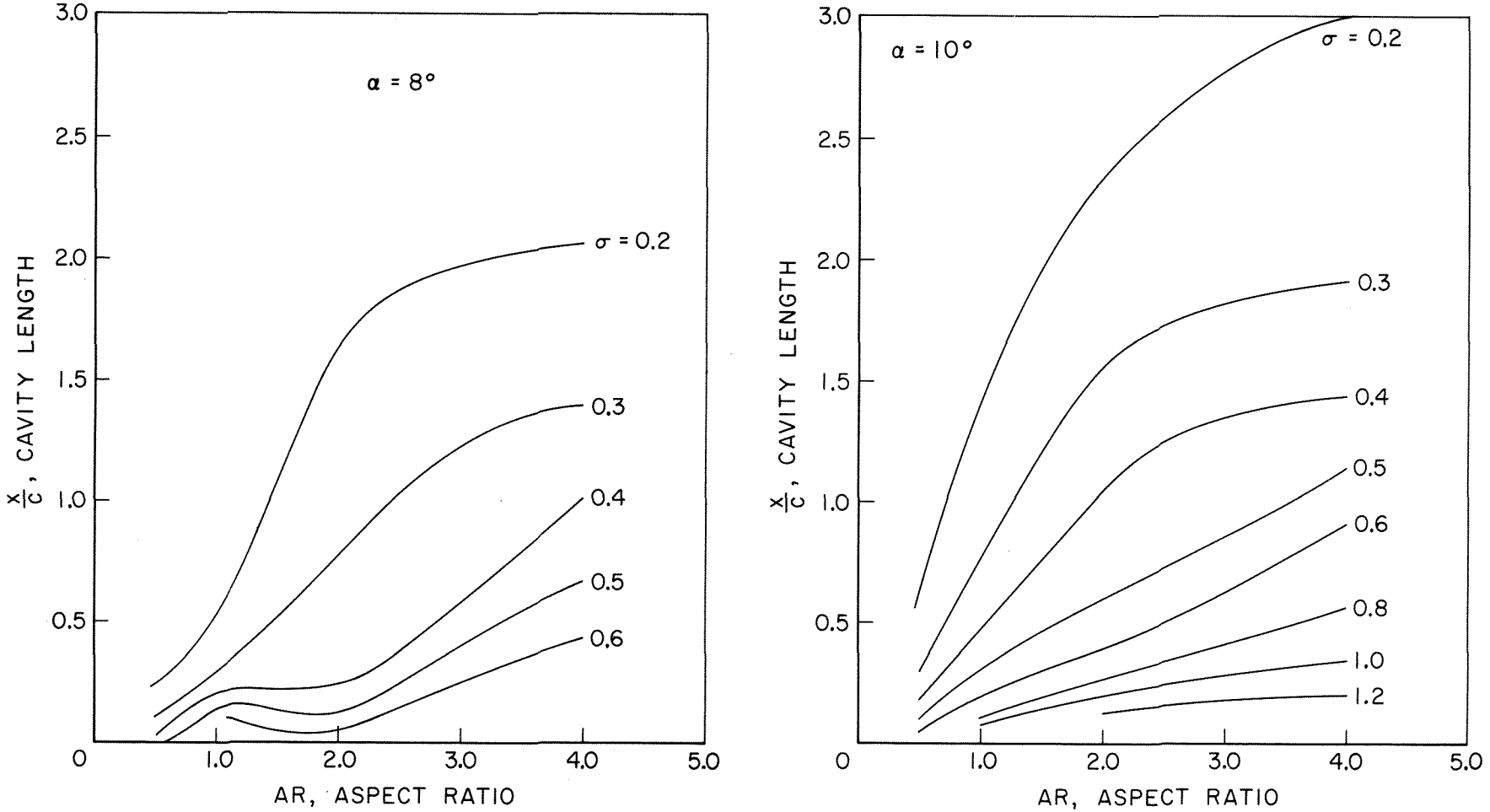

Fig. 33. Cavity Length as a Function of Aspect Ratio and Cavitation Number for Angles of Attack of 8^{o}, 10^{o}.

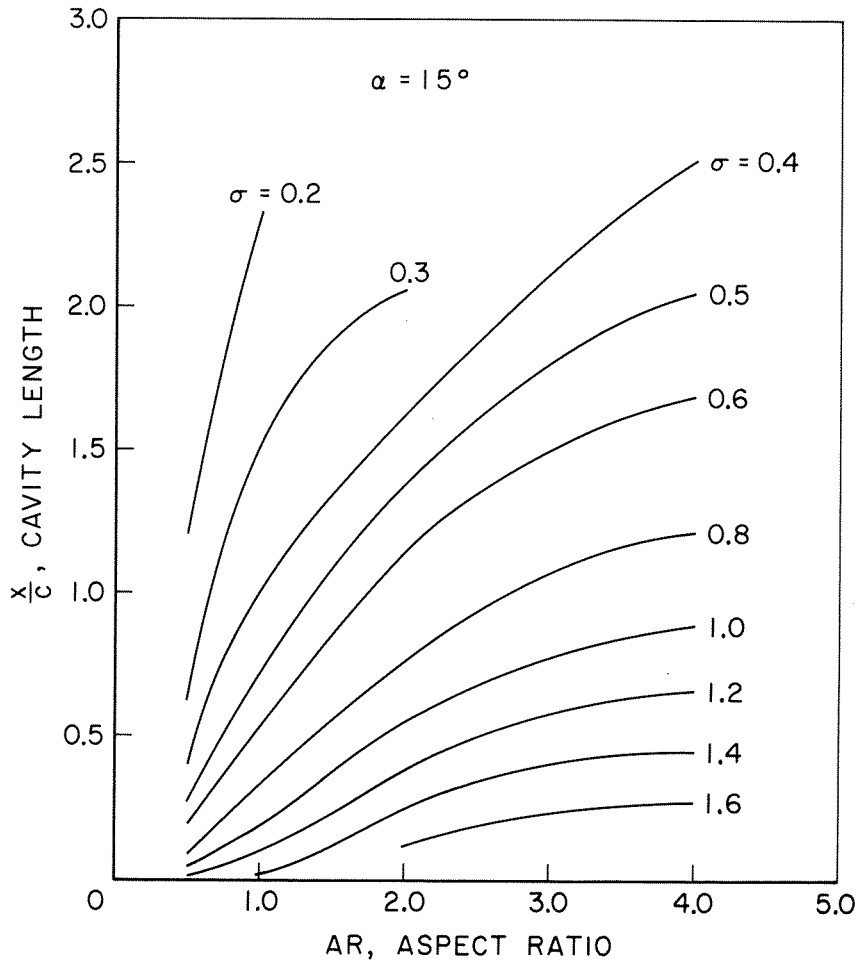

Fig. 34. Cavity Length as a Function of Aspect Ratio and Cavitation Number for an Angle of Attack of 15°.

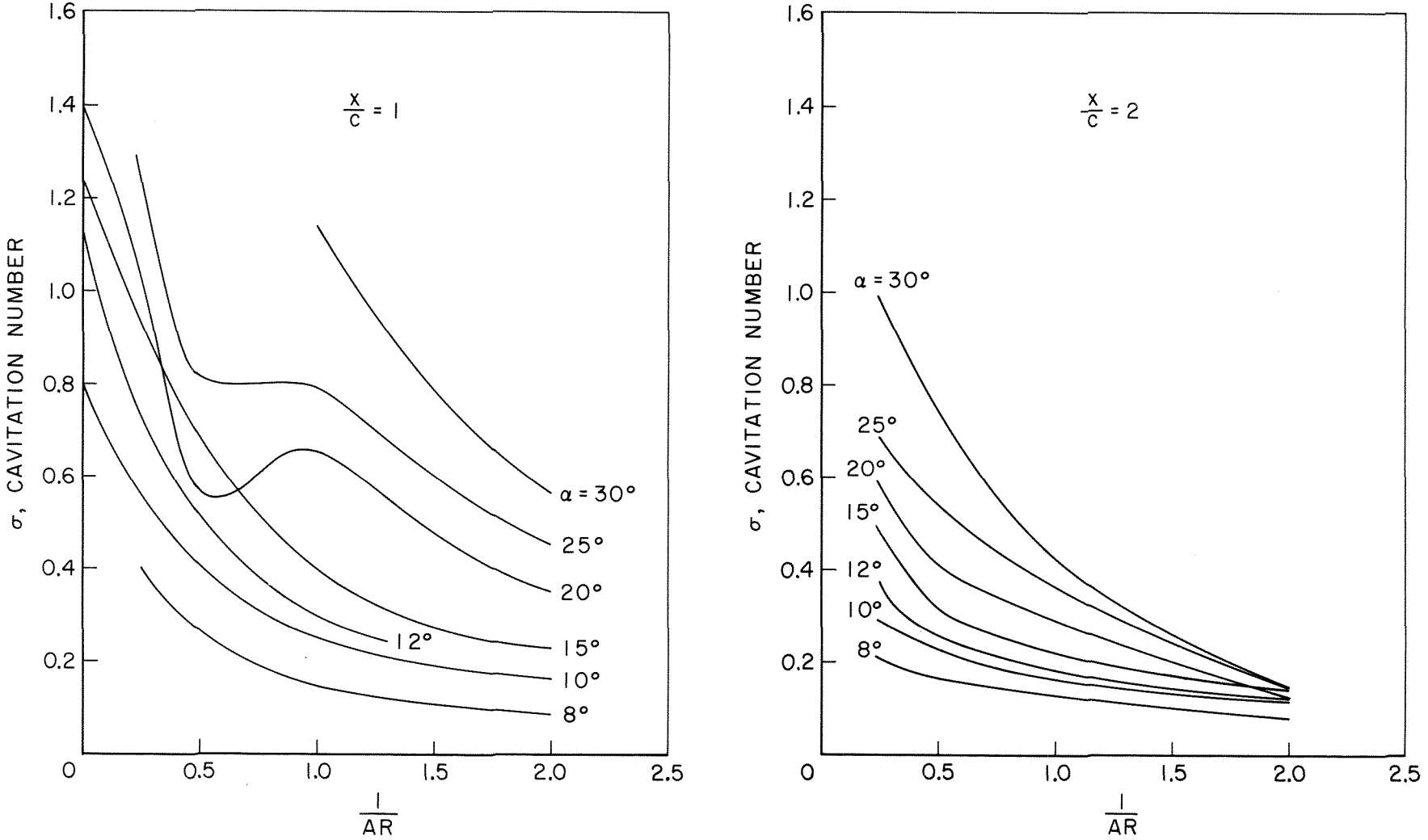

Fig. 35. a) The Effect of Aspect Ratio on the Cavitation Number for $x/c = 1$.
b) The Effect of Aspect Ratio on the Cavitation Number for $x/c = 2$.

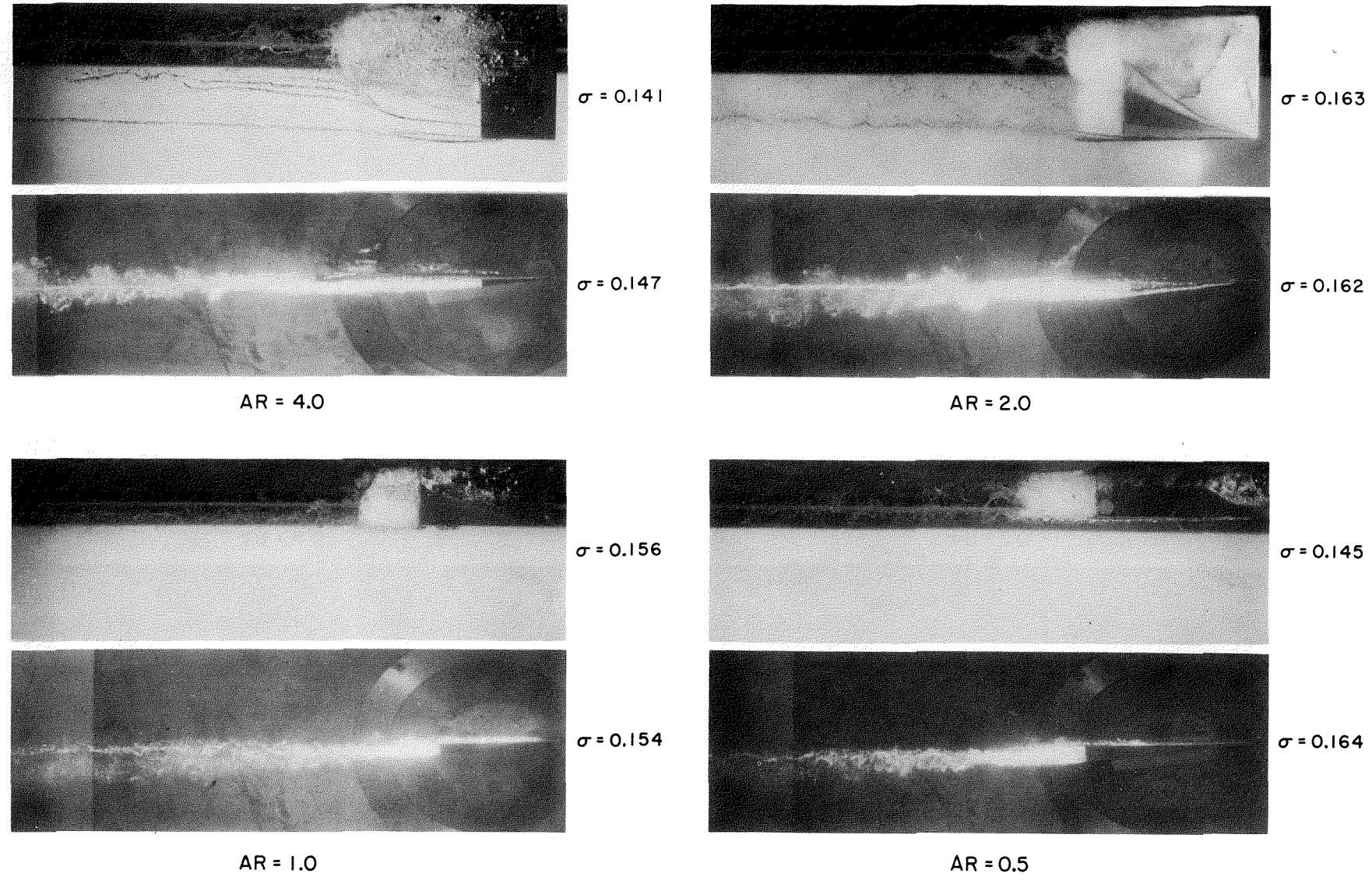

Fig. 36. Top and Side Views of the Cavitating Hydrofoils at an Angle of Attack of 8^{o}.

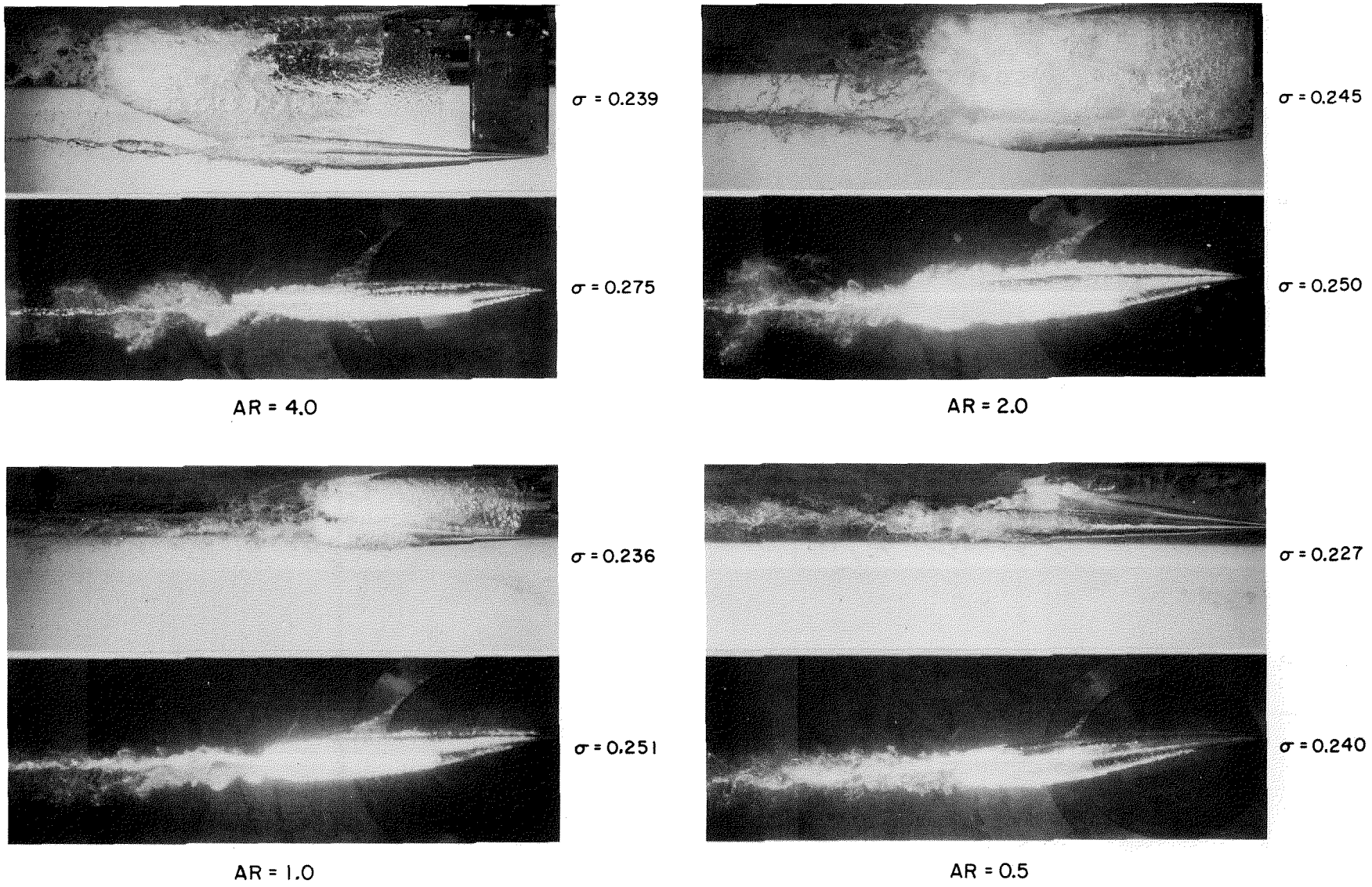

Fig. 37. Top and Side Views of the Cavitating Hydrofoils at an Angle of Attack of 15^{o}.

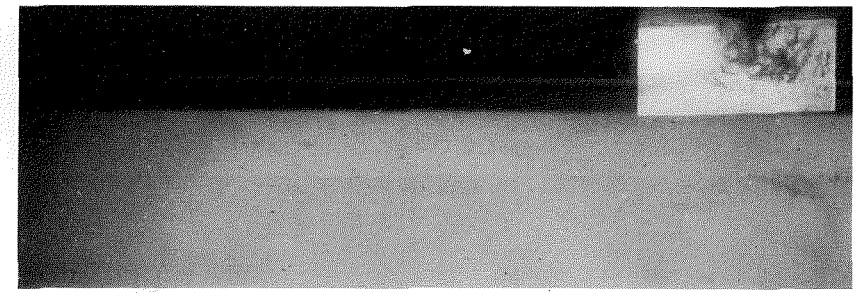

σ = 1.80

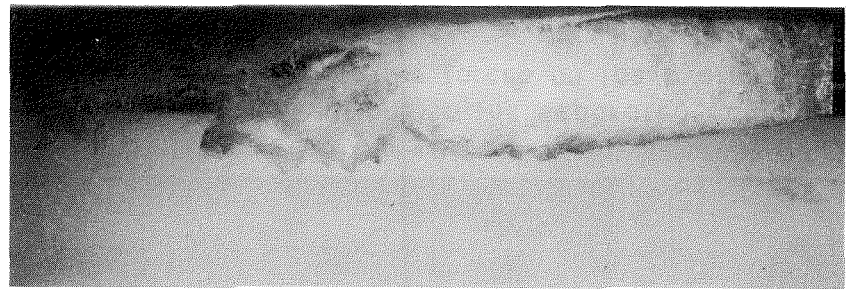

σ = 0.38

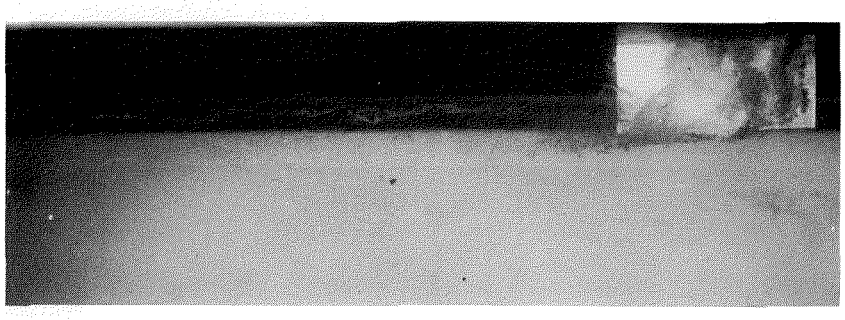

σ = 1.33

σ = 0.26

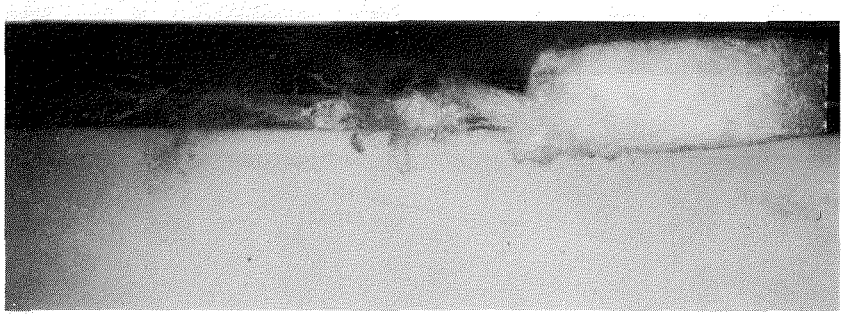

σ = 0.65

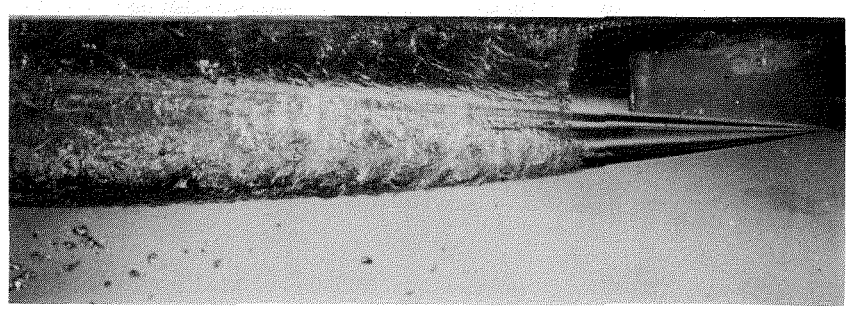

σ = 0.17

(Note development of separate, conical, tip cavity)

Fig. 38. Cavitation on the AR = 1.0 Hydrofoil at an Angle of Attack of 30^{o}.

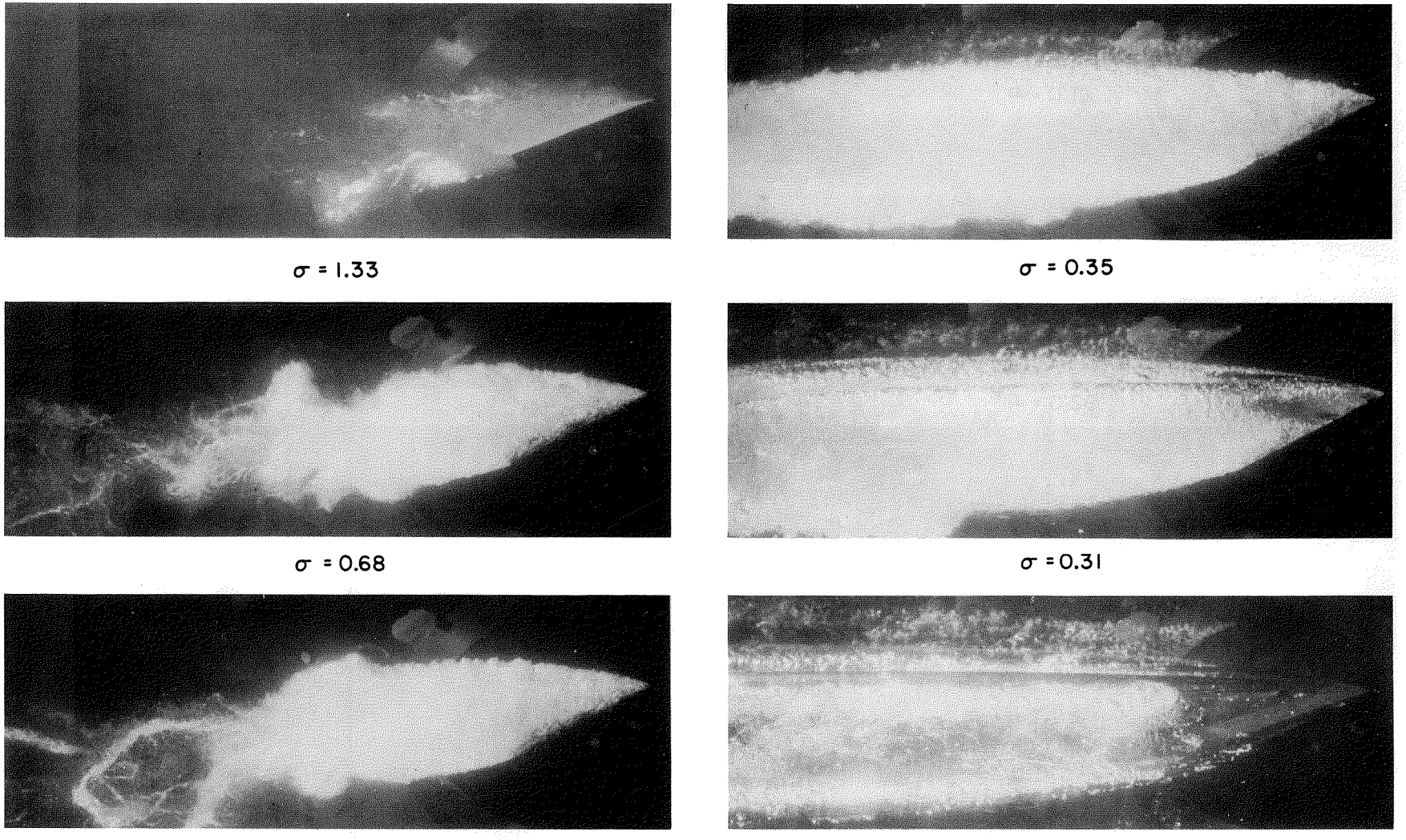

Fig. 39. Development of Cavitation on the AR = 2.0 Hydrofoil at an Angle of Attack of 30^{o}.

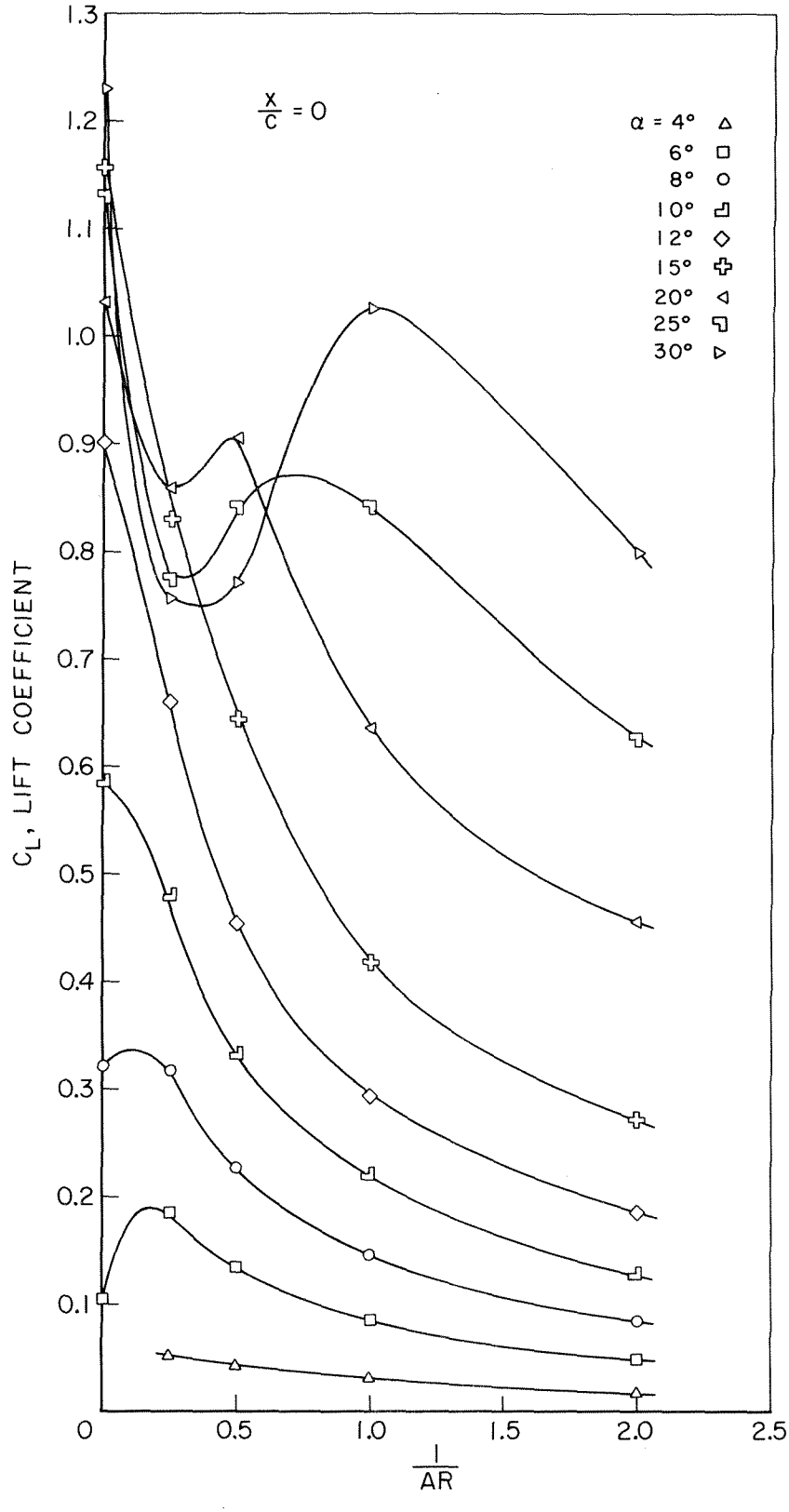

Fig. 40. The Effect of Aspect Ratio on Lift Coefficient in Noncavitating Flow.

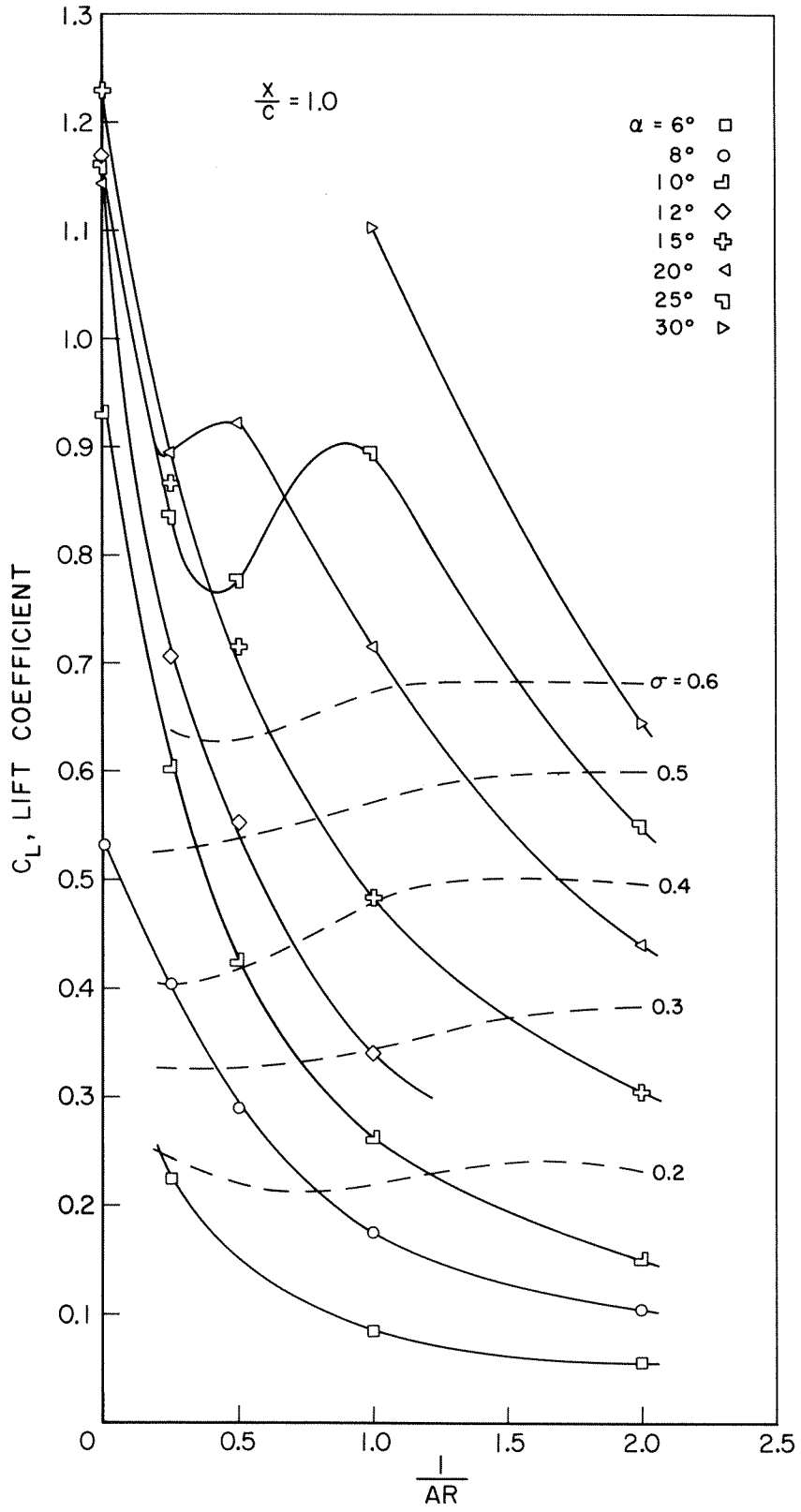

Fig. 41. The Effect of Aspect Ratio on Lift Coefficient in Full Cavity Flow, x/c = 1.0.

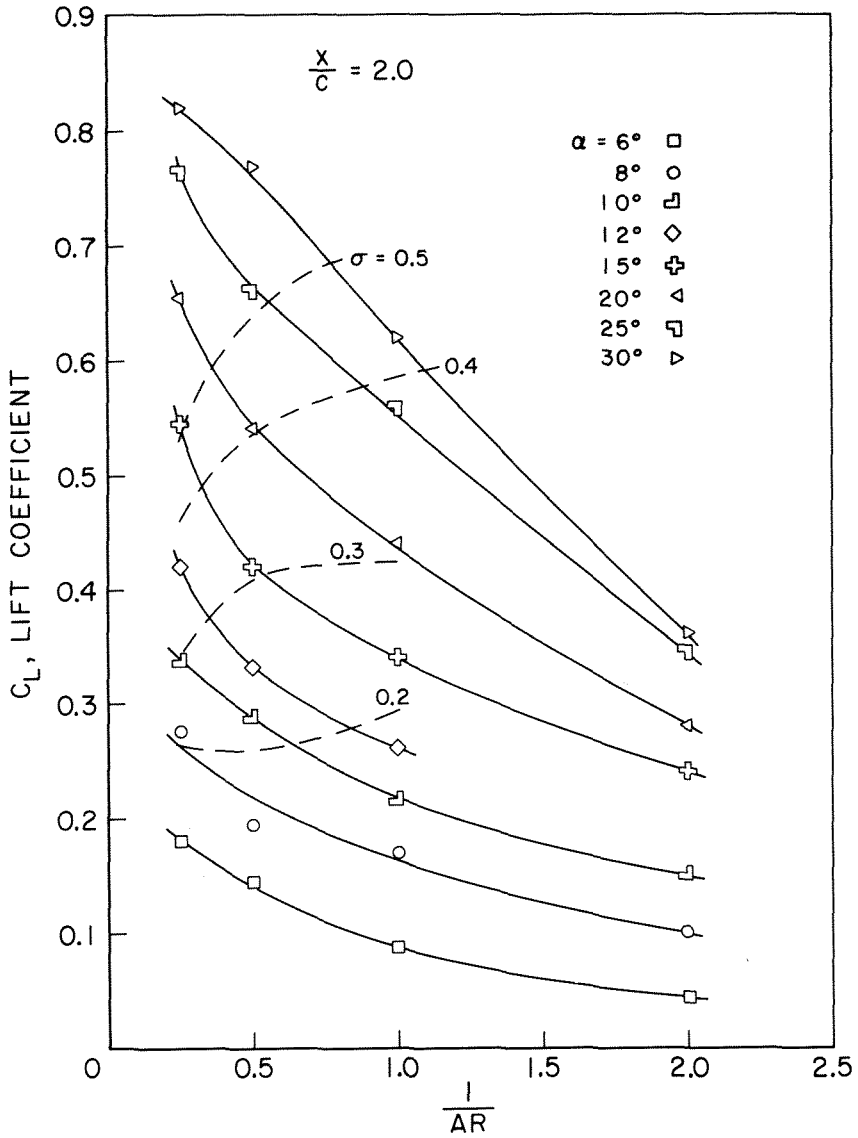

Fig. 42. The Effect of Aspect Ratio on Lift Coefficient in Full Cavity Flow, x/c = 2.0.

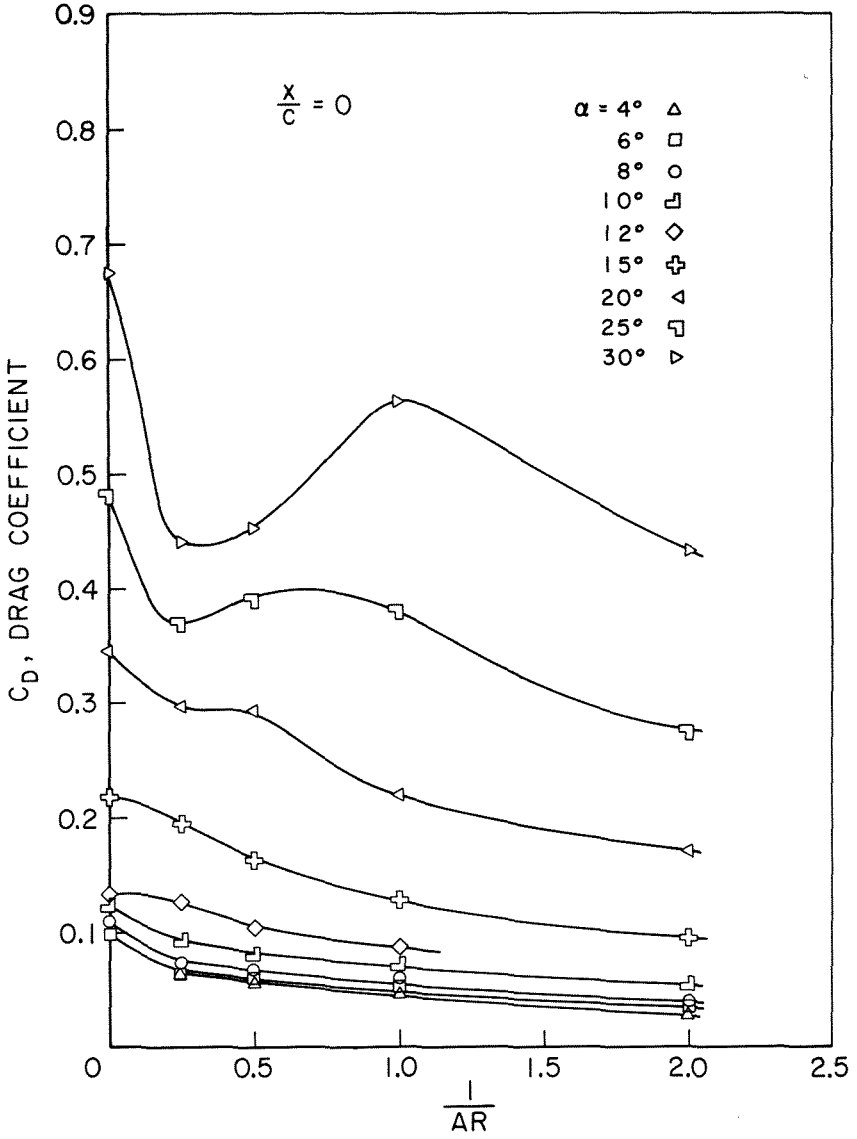

Fig. 43. The Effect of Aspect Ratio on Drag Coefficient in Noncavitating Flow.

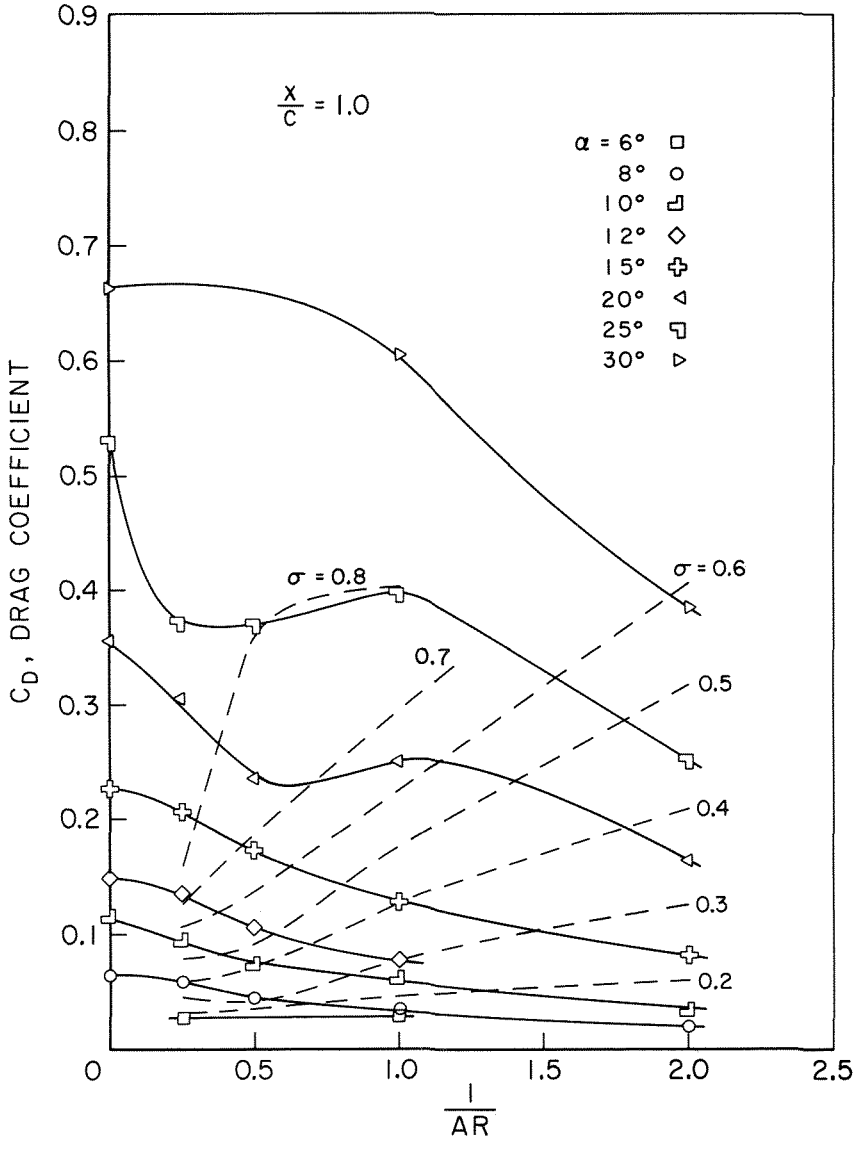

Fig. 44. The Effect of Aspect Ratio on Drag Coefficient in Full Cavity Flow, x/c = 1.0.

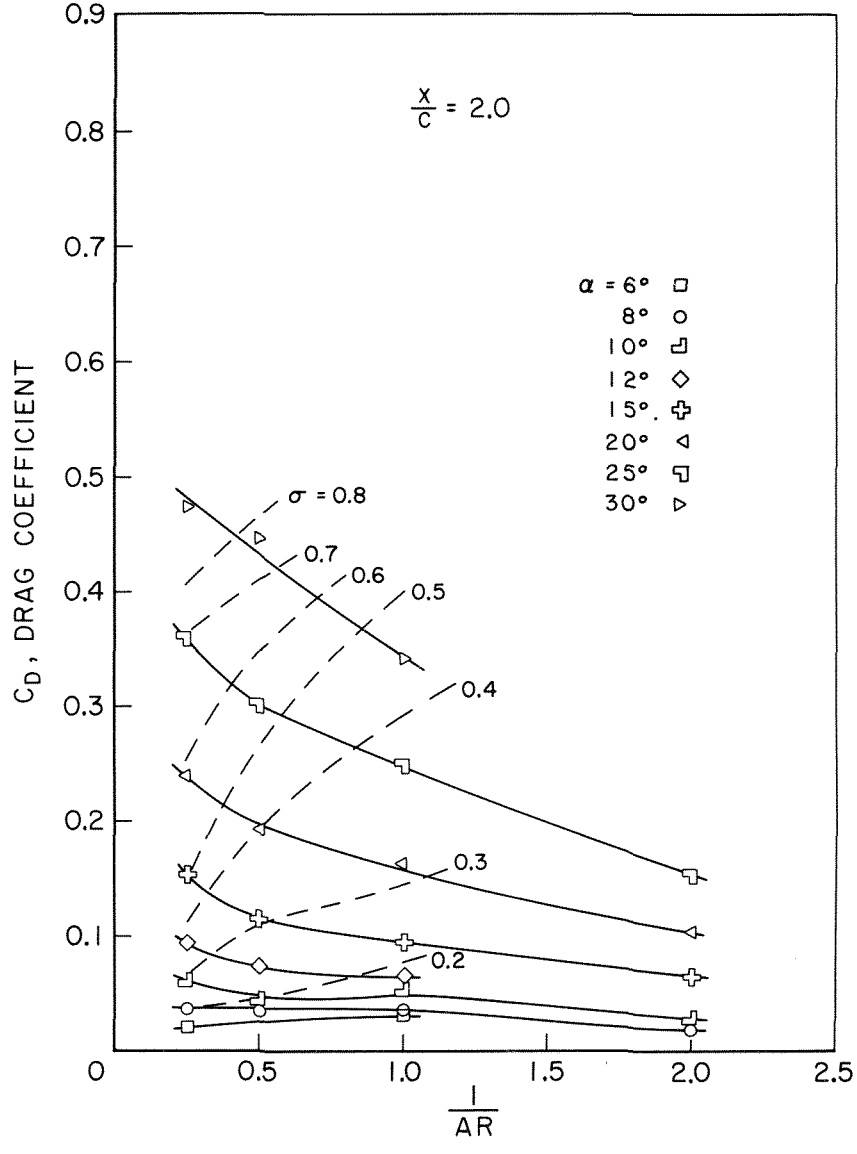

Fig. 45. The Effect of Aspect Ratio on Drag Coefficient in Full Cavity Flow, x/c = 2.0.

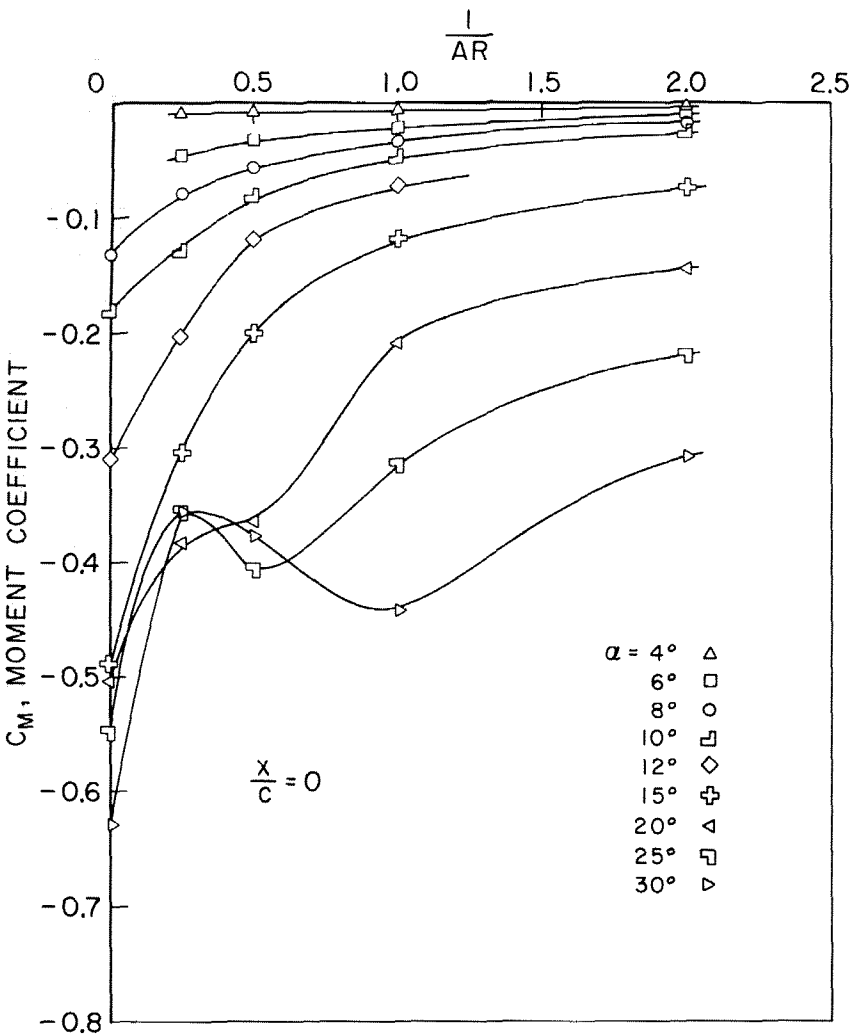

Fig. 46. The Effect of Aspect Ratio on Moment Coefficient in Noncavitating Flow.

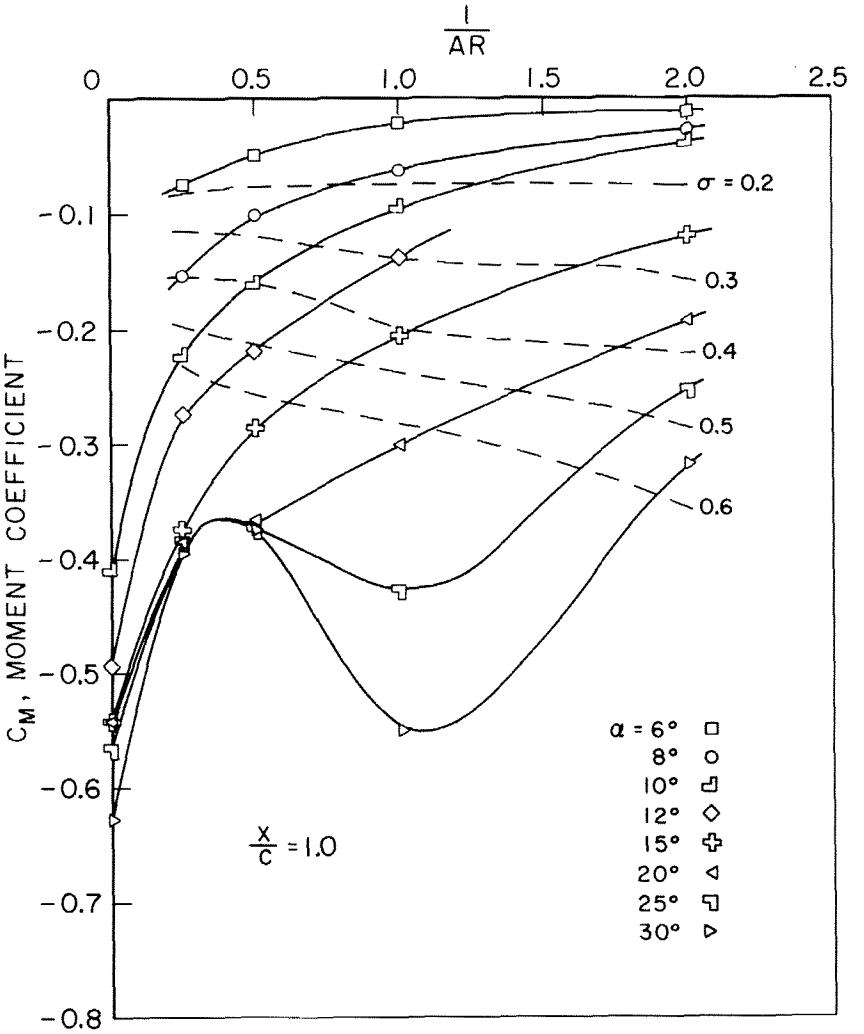

Fig. 47. The Effect of Aspect Ratio on Moment Coefficient in Full Cavity Flow, x/c = 1.0.

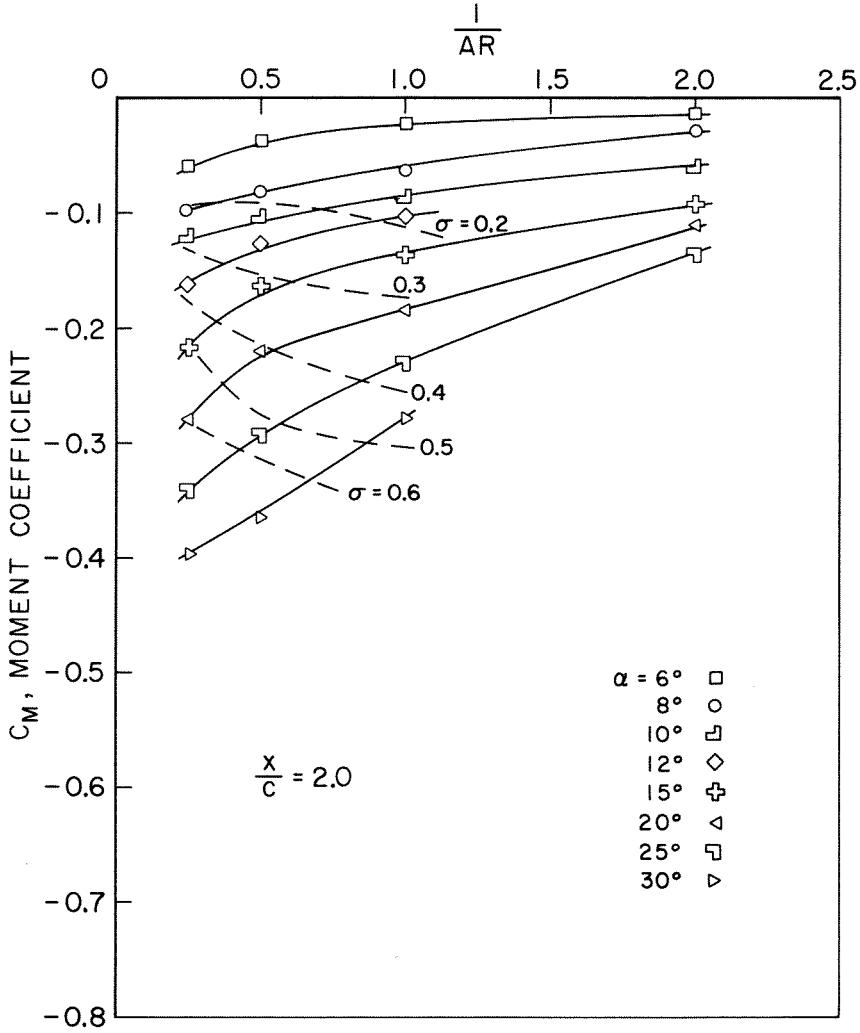

Fig. 48. The Effect of Aspect Ratio on Moment Coefficient in Full Cavity Flow, x/c = 2.0.

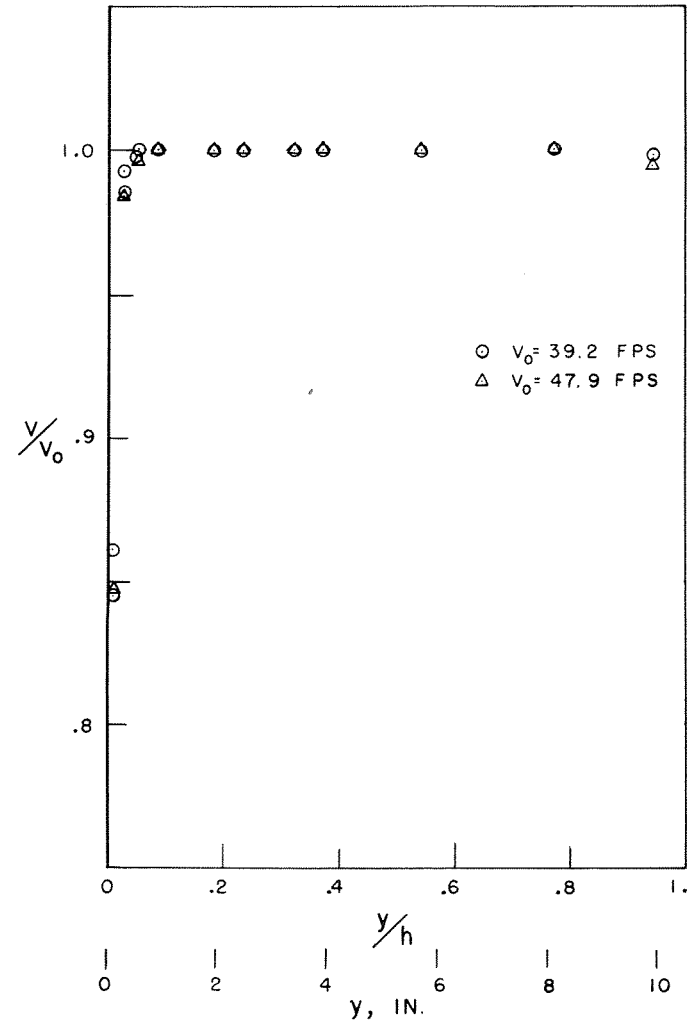

Fig. 49. Transverse Velocity Profile at the Spindle Axis.

Distribution List for Unclassified Reports on Hydrofoils
Issued under Contract Nonr-220(12)

Item	Address	No. Copies
1	Commanding Officer and Director, David Taylor Model Basin, Washington 7, D.C., Attn: Code 513	87
2	Chief of Naval Research, Dept. of the Navy, Washington 25, D.C., Attn: Fluid Dynamics Branch (Code 438)	6
3	Commanding Officer, Office of Naval Research, Branch Office, 495 Summer St., Boston 10, Mass.	1
4	Commanding Officer, Office of Naval Research, Branch Office, 346 Broadway, New York 13, N.Y.	1
5	Commanding Officer, Office of Naval Research, Branch Office, The John Crerar Library Bldg., 10th Floor, 86 E. Randolph St., Chicago 1, Ill.	1
6	Commanding Officer, Office of Naval Research, Branch Office, 1000 Geary St., San Francisco 9, California	1
7	Commanding Officer, Office of Naval Research, Branch Office, 1030 E. Green St., Pasadena 1, California	2
8	Commanding Officer, Office of Naval Research, Branch Office, London, Navy 100, F.P.O. New York, N.Y.	2
9	Director, U.S. Naval Research Laboratory, Attn: Tech. Information Division, Washington 25, D.C.	6
10	Bureau of Weapons, Dept. of the Navy, Washington 25, D.C., Attn: Aero and Hydro Branch (Code RAAD-3)	2
11	Bureau of Weapons, Dept. of the Navy, Washington 25, D.C., Attn: Code RRRE	2
12	Commander, U.S. Naval Ordnance Laboratory, White Oak, Silver Spring 19, Maryland	2
13	Commander, U.S. Naval Ordnance Test Station, Underwater Ordnance Dept., 3202 E. Foothill Boulevard, Pasadena, California, Attn: Pasadena Annex Library (Code P 5507)	3
14	Chief, Bureau of Ships, Dept. of the Navy, Washington 25, D.C., Technical Information (Code 335)	3
	Ship Design (Code 410)	1
	Preliminary Design (Code 420)	1
	Hull Design (Code 440)	1
	Scientific and Research (Code 442)	1
	Propeller Shafting and Bearing (Code 644)	1
15	Commanding General, Aberdeen Proving Ground, Md., Attn: Mr. R. H. Kent, Ballistic Research Laboratories	1

Distribution List (continued)

Item	Address	No. Copies
16	Director, National Aeronautics and Space Administration, 1512 H St., N.W., Washington 25, D.C.	1
17	Director, Langley Research Center, National Aeronautics and Space Administration, Langley Field, Virginia	1
18	Commander, U.S. Naval Ordnance Test Station, China Lake, California, Attn: Library (Code 5507)	1
19	Dr. John Breslin, Director, Davidson Laboratory, Stevens Institute of Technology, Hoboken, N. J.	1
20	Dr. J. H. McMillen, National Science Foundation, 1520 H St., N.W., Washington 25, D.C.	1
21	Dr. H. Rouse, Director, Iowa Institute of Hydraulic Research, State University of Iowa, Iowa City, Iowa	1
22	Engineering Research Institute, University of Michigan, East Engineering Building, Ann Arbor, Mich.	1
23	Dr. V. L. Streeter, Civil Engineering Dept., University of Michigan, Ann Arbor, Michigan	1
24	Dr. G. F. Wislicenus, Pennsylvania State University, Ordnance Research Laboratory, University Park, Pa.	1
25	Dr. A. T. Ippen, Dept. of Civil and Sanitary Engineering, Massachusetts Institute of Technology, Cambridge 39, Mass.	1
26	Dr. L. G. Straub, Director, St. Anthony Falls Hydraulic Laboratory, University of Minnesota, Minneapolis 14, Minn.	1
27	Dean, College of Engineering, University of Notre Dame, Notre Dame, Indiana	1
28	Society of Naval Architects and Marine Engineers, 74 Trinity Place, New York 6, N.Y.	1
29	Professor J. K. Vennard, Stanford University, Dept. of Civil Engineering, Stanford, California	1
30	Professor L. J. Hooper, Director, Worcester Polytechnic Institute, Alden Hydraulic Laboratory, Worcester 6, Mass.	1
31	Dr. J. M. Robertson, Dept. of Theoretical and Applied Mechanics, University of Illinois, Urbana, Ill.	1
32	Dr. A. B. Kinzel, Vice President, Research, Union Carbide and Carbon Corp., 30 E. 42nd St., New York 12, N.Y.	1
33	Goodyear Aircraft Corporation, Akron 15, Ohio Attn: Security Officer	1

Distribution List (continued)

Item	Address	No. Copies
34	Professor H. R. Henry, Hydraulics Laboratory, Michigan State College, East Lansing, Michigan	1
35	Commander, Submarine Development Group TWO, F.P.O. New York, N.Y.	1
36	Commanding Officer and Director, U.S. Naval Engineering Experiment Station, Annapolis, Maryland	1
37	Dr. P. R. Garabedian, Stanford University, Applied Math. and Statistics Laboratory, Stanford, California	1
38	Commander, Armed Services Technical Information Agency, Arlington Hall Station, Arlington 12, Virginia	10
39	Mr. J. G. Baker, President, Baker Manufacturing Co., Evansville, Wisconsin	1
40	Mr. T. M. Buerman, Gibbs and Cox, Inc., 21 West St., New York 6, N.Y.	1
41	Dynamic Developments, Inc., Midway Ave., Babylon, Long Island, New York. Attn: Mr. W. P. Carl, Jr.	1
42	Hydrodynamics Research Laboratory, CONVAIR, San Diego 12, California	1
43	Mr. R. K. Johnston, Miami Shipbuilding Corporation, 615 S.W. Second Avenue, Miami 36, Florida	1
44	Mr. J. D. Pierson, Structural Dept., The Martin Co., Baltimore 3, Maryland	1
45	Mr. W. R. Ryan, Vice President in charge of Engineering, Edo Corporation, College Point 56, Long Island, N. Y.	1
46	Dr. Robert C. Seamans, Radio Corporation of America, Waltham, Mass.	1
47	Dr. A. G. Strandhagen, Head, Dept. of Engineering Mechanics, University of Notre Dame, Notre Dame, Ind.	1
48	Dr. H. W. Lerbs, Hamburgische Schiffbau-Versuchsanstalt Hamburg 33, Bramfelderstrasse 164, Germany	1
49	Commander, Air Research and Development Command, Andrews Air Force Base, Washington 25, D.C.	1
50	Avco Manufacturing Corporation, Advanced Development Division, 2385 Revere Beach Parkway, Everett 49, Mass. Attn: Technical Librarian	1
51	Dr. L. Landweber, Iowa Institute of Hydraulic Research, State University of Iowa, Iowa City, Iowa	1

Distribution List (continued)

Item	Address	No. Copies
52	Max Planck Institut Fur Stromungsforschung, Gottingen, Germany	1
53	Dr. M. St. Denis, Weapons System Evaluation Group, Institute for Defense Analysis, The Pentagon, Washington 25, D.C.	1
54	Technical Research Group, 2 Aerial Way, Syosset, L.I., New York, Attn: Dr. Paul Kaplan	1
55	Editor, Engineering Index, Inc., 29 West 39th St., New York, N. Y.	1
56	Editor, Applied Mechanics Reviews, Southwest Research Institute, 8500 Culebra Road, San Antonio 6, Texas	1
57	Librarian, Institute of the Aeronautical Sciences, 2 East 64th Street, New York 21, N. Y.	1